ACTIVE PHOTONIC DEVICES BASED ON LIQUID CRYSTAL ELASTOMERS

JEAN-CHRISTOPHE LAVOCAT

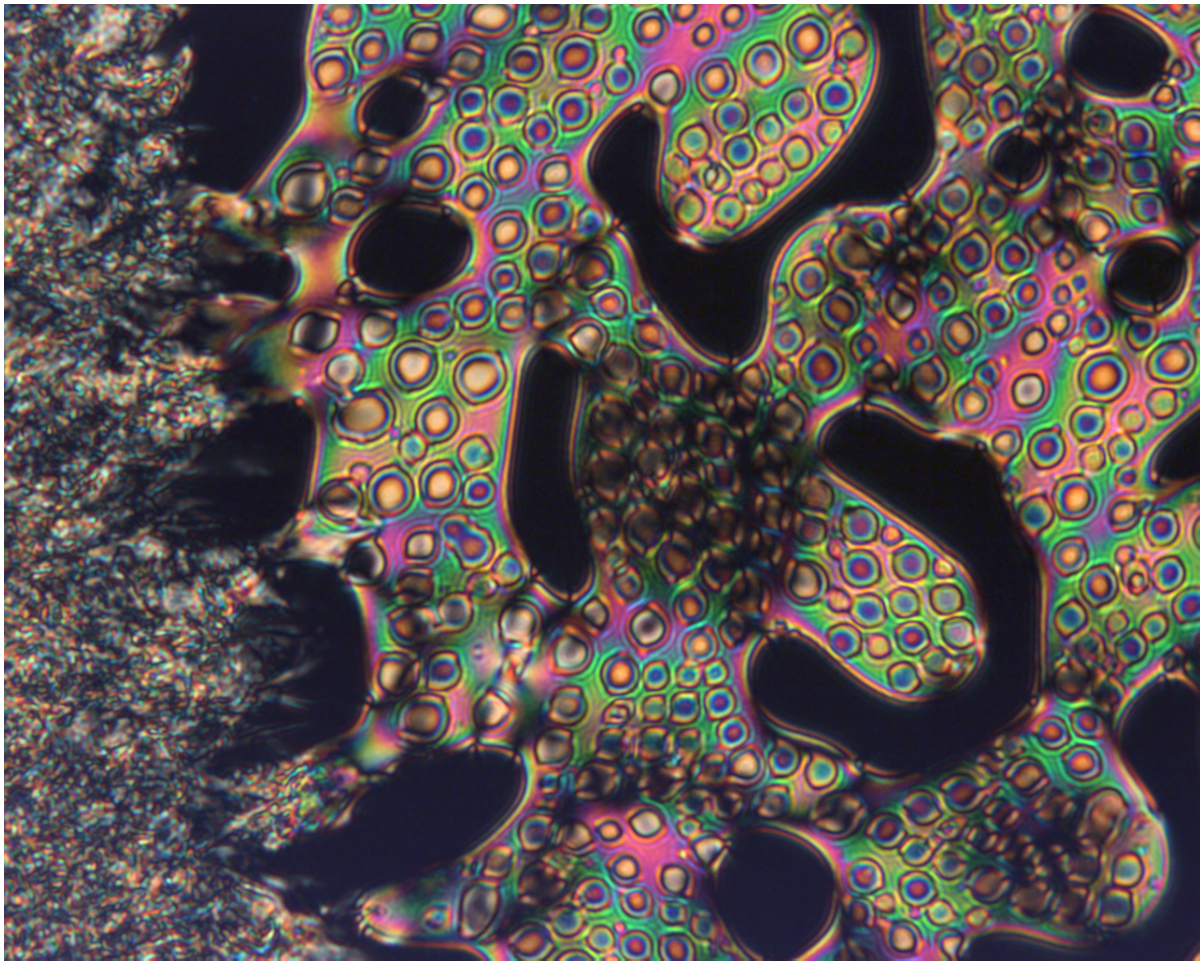

Fabrication and applications

Ph.D. in Photonic Science
Physics Department

Under the supervision of
Diederik Wiersma – Niek Van Hulst
LENS – ICFO

December 2013 – version 1.3

Jean-Christophe Lavocat: *Active photonic devices based on liquid crystal elastomers,* Fabrication and applications, © December 2013

Dedicated to the loving memory of Albert Lavocat

1924 – 2013

You may encounter many defeats,
but you must not be defeated.
In fact, it may be necessary
to encounter the defeats,
so you can know who you are,
what you can rise from,
how you can still come out of it.

— Maya Angelou

PREFACE

This thesis represents the culmination of almost four years (2010 - 2014) spent between LENS (Italy) and ICFO (Spain). The project initially involved a limited group of people in LENS (basically a chemist and myself) and very few specific equipments were available. However, thanks to the determination of Diederik Wiersma, my supervisor, things evolved nicely and several motivated colleagues joined the project from 2011 onwards.

Within this enthusiastic team we had to rediscover processes and recipes that many groups have already been using since some years prior our interest in the field. None of us had practical knowledge on liquid crystal elastomers and we had to strengthen interactions between our various disciplines of expertise (mechanics, photonics, chemistry, modeling). Understanding each other was a challenge that we ultimately (and mostly peacefully) met.

Discovering the friendly atmosphere surrounding this branch of research was also a constant revitalization for my motivation. I am really glad to have or exchanged emails with numerous researchers, always delighted to answer a question about physics or chemistry. Our project could not be where it is at this stage without the help of various teams from SISSA (Italy), Liquid Crystal Institute - KENT (USA), Institut Curie (France), Florida State University (USA), Kyoto University (Japan), University of Ljubljana (Slovenia) and Air Force Research Lab (USA).

As time and budget increased, our Italian team managed to get access to better facilities and newer equipment. The first concrete results appeared in February 2011 and June 2011: first the fabrication of an azobenzene-doped LCE micro structure via DLW; then, four months later, the activation of a similar micro structure by a laser excitation.

The reproducibility of our first achievement was really weak and we had been unable to produce new moving samples in almost a year. It was at the time I had to move to my other institution in Spain, that the most promising results appeared. The (now) big Italian team successfully determined the correct parameters to fabricate a micro

sized liquid crystal elastomer containing light sensitive azo-benzene molecule. Congratulations to all of you dear friends.

It does not matter how slowly you go as long as you do not stop.
— Confucius

Joining ICFO (Spain) for the second part of my thesis had been another really interesting step for me. I have been faced with the issue of discovering a new work environment while trying to keep a continuity within my project. I must admit that ICFO's administration is particularly efficient to integrate newcomers. But this aside, trying to fit an unfamiliar material and a dedicated technology into a group specialized in single molecules observation and near field optics revealed not to be easy at all.

I feel particularly indebted toward my supervisor Niek van Hulst for the help, attention and experience he provided me during my stay in his group. Together we started to plan the creation of a tunable nano antenna set on a LCE layer. An pioneering idea which is definitely worth investigating in the future but which was too ambitious for one year time frame.

I was offered the opportunity to extend the duration of my project, but decided not to accept this extra time for personal reasons. Hence, it was decided to restrict the scope of the research about LCE at the nanoscale to a "simpler" plasmonic grating tuning via a LCE substrate.

Fabricating a metallic grating embedded in an elastomer was finally a riveting theme. It was at the crossroads between nanofabrication, plasmonics and material sciences while being a basic problem to tackle. I only scratched the surface of a combination (LCE with plasmonics) that could lead the way to active plasmonic elements. Think of an optical switch that you could activate directly through your circuit by using the proper wavelength.

Last but not least, the concept of photonic or plasmonic bistability often orbited around my mind. Due to the kinetics involved in azobenzene isomerization, one can easily imagine a photonic crystal made of LCE: it initially absorbs light and contracts, but this contraction changes the lattice and prevents the light confinement which is followed by a consequent relaxation to the initial state. From there the sequence repeats. Many similar scenarios could be envisioned, but none have yet been investigated.

By converting light into a mechanical cycle, many new applications would be accessible at the micro and nano-scale. One could soon have the gumption to develop a mechanical motor at the microscale, powered by a continuous beam of light.

ABSTRACT

Through this thesis I try to give a glimpse of the potential applications a rigorous fabrication of Liquid Crystal Elastomers (LCE) could lead to. Producing structures made of LCE with sub micro-metric resolution and containing azobenzene molecules could open the way to 4D nano-printing. A buzzword that however hides a dormant breakthrough if the community manages to understand how to couple efficiently the chemistry and the physics behind this material.

After a theoretical presentation of the elastomer (chapter 2) some basic properties involving light interaction have been modeled and explained (chapter 3). Most of the content is then dedicated to the description of two specific fabrication techniques which are illustrated by two different applications. The first one is a micro swimmer whose appendages could be made of LCE by Direct Laser Writing and remotely activated by light (chapters 4 and 5). The second one is a plasmonic grating embedded via nanotransfer printing into a LCE layer (chapters 6).

RÉSUMÉ

Au travers de cette thèse, j'ai essayé de donner un aperçu des applications potentielles qu'une fabrication attentive des Elastomères à Cristaux Liquides (ECL) pourrait permettre. Produire des structures à base d'ECL avec une résolution sub micrometrique et qui contiennt des molécules d'azobenzène pourrait ouvrir la route à la nano-impression 4D. Un mot clé à la mode, mais qui reflète une révolution larvée si la communauté arrive à comprendre comment coupler efficacement la chimie et la physique qui caractérisent ce matériau.

Après une présentation théorique de l'elastomère (chapitre 2), des propriétés basiques d'intéractions avec la lumière ont été modélisées et expliquées (chapitre 3). Le reste du contenu est dédié à deux techniques de fabrication illustrées par deux applications différentes. La première est un "micro-nageur" dont l'appendice peut être fabriqué avec de l'ECL grâce une méthode nommée Direct Laser Writing (chapitres 4 et 5). La seconde application est un réseau plasmonique accordable déposé à la surface d'un film d'ECL par nanotransfer printing (chapitre 6).

ASTRATTO

Lo scopo di questa tesi è di mostrare le potenziali applicazioni che possono derivare da una rigorosa elaborazione di Elastomeri di Cristalli Liquidi (ECL). La produzione di strutture composte di ECL, con risoluzione inferiore al micron e contenenti molecole di azobenzene, può aprire la strada a tecniche di nano-printing 4D. Parola, quest'ultima, che comunque nasconde un latente potenziale che potrebbe essere sfruttato se si capisse a fondo come accoppiare efficientemente la chimica e la fisica di questo materiale.

Dopo aver mostrato a livello teorico le qualità degli elastomeri (Capitolo 2), alcune proprietà basiche che coinvolgono l'interazione con la luce sono state modellate e sono spiegate (Capitolo 3). La maggior parte del contenuto di questo lavoro è quindi dedicato alla descrizione di due specifiche tecniche di produzione che sono illustrate da due differenti applicazioni. La prima è quella di un micro-nuotatore le cui appendici potrebbero essere fatte di ECL tramite il Direct Laser Writing e successivamente attivate a distanza attraverso l'uso della luce (Capitoli 4 e 5). La seconda è relativa ad un reticolo plasmonico incorporato in uno strato di ECL tramite il nanotransfer printing (Capitolo 6).

ABSTRACTO

A través de esta tesis, intento dar una visión de las posibles aplicaciones a las que una rigurosa fabricación de Elastómeros de Cristal Líquido (ECL) podría llevar. La producción de estructuras hechas de ECL con resolución sub micrométrica que contienen moléculas de amino benceno podría abrir el camino a la nano-impresión 4D. Una palabra de moda que sin embargo esconde un descubrimiento latente si la comunidad logra entender cómo acoplar eficientemente la química y la física que se esconde tras este material.

Después de una presentación teórica del elastómero (capítulo 2) algunas propiedades básicas de interacción de la luz han sido modeladas y explicadas (capítulo 3) La mayoría del contenido está dedicado a la descripción de dos técnicas de fabricación que son ilustradas por dos aplicaciones diferentes: la primera es un micro swimmer cuyos apéndices podrían estar hechos de ECL con Direct Laser Writing y activada remotamente por luz (capítulos 4 y 5). La segunda es un red plasmónico integrado por nanotransfer printing a una capa de ECL. (capítulo 6).

Soyons reconnaissants aux personnes qui nous rendent heureux,
ils sont les charmants jardiniers par qui nos âmes sont fleuries.

— Marcel Proust

ACKNOWLEDGMENTS

Taking part in this project proved to be extensively rewarding in terms of human relationships. Many people had a great influence on the positive outcome of my experiments and I want to particularly thank all of those who have offered their support.

First of all, I would like to warmly express my gratitude to Diederik Wiersma (LENS) and Niek van Hulst (ICFO) my two supervisors. Without them, I would not have learned perseverance and autonomy as much as I did. Under their supervision I had the opportunity to try different ways of solving problems but also to cultivate a sense of creativity. Thank you both for that.

Most of the work presented in this thesis is not the result of my mere effort. Instead, many people participated directly to these outcomes (sometimes collectively, sometimes independently). In chronological order, I would like to thank Camilla Parmeggiani for her chemistry skills, Kevin Vynck for his knowledge about modeling and simulations, Giacomo Cerretti first for the time spent in front of Comsol and then together with Hao Zeng in the lab checking the different LCE recipes and finally Daniele Martella for all the molecules he synthesized. I would also like to thank deeply Alberto Curto for his knowledge about nano antenna and Jan Renger for his essential help for fabricating plasmonic structures and for his guidance.

Some of the ideas and resources being used to tackle our issues have been provided by LCE experts. My full recognition goes to Luciano Teresi, Antonio DeSimone, Patrick Keller, William S. Oates, Kenji Urayama, Martin Čopič and Michael McConney for fruitful discussions.

Another special attention goes to Romolo Savo, Rajeshkumar Mupparapu, Matteo Burresi, Lorenzo Cortese, Filippo Pratesi, Francesco Riboli, Tomas Svensson, Sara Nocentini, Ho Chih Hua and Sepideh Zakeri for the really fun moments we had together in Italy; to Emilie Wientje, Nicolò Accanto, Anshuman Singh, Ion Hancu, Marta Castro López, Lukasz Piatkowski, Gaëtan Calbris, James Huggal, Richard Lane, Jana Nieder, Klaas-Jan Tielrooij, Pablo de Roque, Nikos Fayard, Florian Sterl and many others ICFOnian futbalin players.

Additionally I cannot forget to mention the different management and technological units from both institutions: NanoLab, Purchase,

Mechanical and Electronic Workshops, Human resources, Frontdesk, IT. Their impressive support has always been quick and valuable.

Without really noticing it, I have been sharing offices, optical tables and clean room equipment with people from dozens of nationalities, spanning over Europe, Africa, Asia, America and Australia. I obviously cannot name you all (otherwise it would be a boring list of names that does not reflect the great time we spent together), but if we ever met in a lab either in Italy, Spain or France, be sure that I remember you and that I am really grateful for shared moments.

Finally, I would like to communicate my deepest gratitude to my mother who have always been supporting me over the distances along my life, and to Marie-George Clouet, my life partner, for the patience she demonstrated during my long moments of doubt and hesitation.

CONTENTS

i INTRODUCTION 1

1 INTRODUCTION 3

2 LIQUID CRYSTAL ELASTOMERS 7
2.1 Historical Development 7
2.2 Chemistry 8

ii SIMULATION OF LIQUID CRYSTAL ELASTOMERS AT THE NANOSCALE 13

3 LCE SIMULATIONS 15
3.1 Introduction 15
3.2 Governing equations 16
3.2.1 Structural Mechanics: Finite Strain Theory 16
3.2.2 Stress and Linear Elastic deformations 17
3.2.3 Hyperlastic materials 18
3.3 Exponential approximation limits 22
3.4 Dynamical deformation 25

iii LASER WRITING ON LIQUID CRYSTAL ELASTOMERS 29

4 DIRECT LASER WRITING 31
4.1 Principles of laser writing 31
4.1.1 Photolithography 31
4.1.2 Two-photon absorption 33
4.1.3 Two-photon lithography 34
4.2 Laser writing issues in LCEs 36
4.2.1 Problems due to the LC 37
4.2.2 Problems due to the azobenzene 38
4.3 Laser Writing of LCEs 40
4.3.1 LCE preparation 40
4.3.2 Transition temperature 41
4.3.3 Cell preparation 42
4.3.4 Direct Laser Writing parameters 43
4.3.5 Direct Laser Writing evolution 43
4.3.6 LCE development 45
4.3.7 Experimental Results 46

iv LIQUID CRYSTAL ELASTOMER AND MICRO FLUIDIC 49

5 MICROFLUIDICS OF MEMS 51
5.1 Introduction 51
5.2 Fluid Mechanisms at small scale 51
5.2.1 General Properties 51
5.2.2 Navier-Stokes Equation 55
5.2.3 The Stokes Equations 55

5.2.4 Boundary conditions and Reynolds number 56
5.3 Swimmers at micro-scale 57
5.3.1 Scallop theorem 57
5.3.2 Micro Organisms 58
5.3.3 Hydrodynamic interactions 60
5.4 Microfluidics Simulations 61
5.4.1 Artificial swimmers 61
5.4.2 Waving sheet 63
5.4.3 Symmetric Purcell swimmer 65
5.4.4 Conclusion 68

V TUNABLE PHOTONIC STRUCTURE 71
6 TUNABLE LCS 73
6.1 Nanoimprinting of metallic structures on top of LCE . . . 73
6.1.1 Introduction 73
6.1.2 E-Beam lithography and Liquid Crystal Elastomers . . . 74
6.1.3 Gold adhesion to other surfaces 75
6.1.4 Metallic nanostructure transfer to LCE 76
6.2 Plasmonic Gratings 78
6.2.1 Introduction 78
6.2.2 General theory diffraction gratings 79
6.2.3 Gratings and Surface Plasmons 80
6.2.4 Gratings fabrication and defects 81
6.3 Tunable gratings 84
6.3.1 Mechanical stretching 84
6.3.2 LCE activation by light 86
Glossary 90

BIBLIOGRAPHY 93

LIST OF FIGURES

Figure 1 Mesogens placement in a Liquid Crystal Elastomer . . . 8
Figure 2 Azobenzene isomerization . . . 9
Figure 3 Liquid Crystal states: isotropic and nematic cases 10
Figure 4 LCE deformation due to the absorption of a photon by azobenzene molecules . . . 10
Figure 5 Absorption spectra of two molecules with azobenzene compounds in methanol . . . 11
Figure 6 Molecules used to fabricate the LCE within this thesis . . . 12
Figure 7 Elastic material - Stress-strain curve . . . 19
Figure 8 LCE deformation: scheme showing the coordinates used for simulations . . . 20
Figure 9 Light evolution in a unaxial LCE . . . 23
Figure 10 Bending radius of two LCE cantilever: uniaxial and hybrid alignment . . . 24
Figure 11 Bending radius of a nano LCE structure when light frequency is comparable . . . 25
Figure 12 Azobenzene cis/trans isomers concentration evolution in time . . . 27
Figure 13 Photocrosslinking example - Cycloaddition of cinnamate . . . 32
Figure 14 Lithography steps showing a positive tone resist 32
Figure 15 Single-photon absorption and Two-photon absorption . . . 33
Figure 16 Photon absorption by a centro-symmetric molecule 34
Figure 17 Direct Laser Writing System . . . 36
Figure 18 Liquid Crystal alignment in a LC cell . . . 38
Figure 19 Van Laar equation for a mixture of two liquid crystal elastomers. . . . 42
Figure 20 Result of swelling on a LCE structure written with DLW . . . 44
Figure 21 Flexibility of LCE written with DLW - soft walls 45
Figure 22 Four LCE rings of diameters $8\mu m$ and $30\mu m$ and height $2\mu m$. a) Four rings before being developed - Inset One ring after being developed imaged by SEM b) and c) the four ring imaged by POM proves that the alignment is following the rubbing direction. . . . 46
Figure 23 Woodpile LCE-structure fabricated via DLW . 47

Figure 24 Lennard Jones potential and force for two distinct particles . . . 53
Figure 25 Scallop theorem . . . 59
Figure 26 Classical motion patterns used by micro organisms . . . 61
Figure 27 Proximity effects due to the micro hydrodynamic interactions . . . 62
Figure 28 Infinite waving sheet (FEM simulation) . . . 65
Figure 29 Finite waving sheet oscillating in a micro-channel (FEM simulation) . . . 66
Figure 30 Volume of water flowing through an inlet - Finite waving sheet case . . . 67
Figure 31 Three-link swimmer . . . 67
Figure 32 Symmetric Purcel Swimmer . . . 68
Figure 33 Volume of water flowing through an inlet - Purcell symmetric swimmer case . . . 69
Figure 34 Laser cutting through the a LCE film . . . 75
Figure 35 Representation of a cell for nano-transfer printing . . . 77
Figure 36 Crosscut microscopy picture showing the LCE and the Polyimide layer after polymerization . 78
Figure 37 Reflection spectrum on a plasmonic grating . . 81
Figure 38 Electromagnetic field in the vicinity of a plasmonic grating . . . 82
Figure 39 Microscopy picture of a gold grating in a LCE film . . . 84
Figure 40 Passive stretching of the liquid crystal. Reflection spectral measurement after strain . . . 85
Figure 41 Scheme of the setup used for reflection measurement . . . 86
Figure 42 Active compression of the liquid crystal. Reflection spectral measurement after strain . . . 87

LIST OF TABLES

Table 1 Parameters used in the following set of simulations . . . 21
Table 2 Concentration of molecules in LCE mixture . . 41
Table 3 Polymerization threshold for different piezo speeds 43
Table 4 Typical Reynolds number for various swimmers in water . . . 60

Table 5 PVA spincoating recipe - 100 nm layer 76

Part I

INTRODUCTION

1

INTRODUCTION

Learn from yesterday, live for today, hope for tomorrow. The important thing is to not stop questioning.

— Albert Einstein

Biotechnology is an emerging market for which people try to produce things at an increasing smaller scale. Among the many active fields, microfluidics, for instance, contains many challenges that physicists are willing to solve. Labs-on-a-chip (LOCs) are widely expected to deliver medical patients from heavy health check-up/analysis. By using a single drop of blood, a LOC should in theory be used as a micro-sized laboratory, where medical checks would be performed with only 50 μL blood. However, these devices are not medicine-specific as they could also help to access new monitoring sensors to detect pollutants or specific chemicals in some fluid. This is only one implementation of a far-reaching technology but many others present challenges and promises for the future.

Reducing size not only means increasing speed and reducing invasive instruments, it is also synonymous with an increase of physical limitations. When it comes to viscosity of fluids for instance, size is a critical factor; fabrication processes are also more difficult. Nanotechnology has historically been focused on 2D and layered structures. Now that Microelectromechanical systems (MEMS) are more and more common for the industry, solutions and techniques for fabricating more complex nano structures are available. Because of their mobile and 3D properties, MEMS inherently offer a bucket of innovation in sensors and actuators, robotics, accelerometers, micro valves, flow controllers, global positioning systems (GPS) component miniaturization.

Similarly, smart polymers received a lot of highlights since the advent of artificial muscles as potential treatment for heavy injuries or as soft actuators for robotic applications. Such materials that can be activated would be a bridge to creating fully soft machines that can operate quickly and with enough strength to perform useful tasks. Actuation of these materials has been shown when using an electric field, a gaz pressure, a motion of ions and a change of temperature. Though most of the efforts have been concentrated on Electroactive polymers (EAP) materials which are controlled by electricity, recent progress have also been made with systems triggered by heat, ions, some chemicals or light.

Developing nano structures and MEMS based on smart materials is challenging but paves the way to active and mobile systems that could be controlled with external stimuli. Systems previously static and inert would gain a lot from the addition of smart materials actuated at the nanoscale. Imagine a micro system with active areas that could

start moving if certain conditions are met. By combining different materials, the system could be in a certain state if and only if the temperature rises above a given threshold and if some chemicals are present in the air or in a fluid.

The present work describes the techniques that have been developed holding these ideas in mind. Liquid Crystal Elastomer (LCE) have been fabricated at a nanoscale and used in combination with plasmonic driven metallic resonators. This work is an attempt to reach active MEMS by using two strategies. Most of the work has been devoted to 3D printing of these active materials. In a second part, metallic nanosystems, fabricated via classical e-beam lithography, were also integrated into active polymers. The reason for this was to offer different alternatives for the miniaturization of light-controlled devices.

The recent advent of `3D printing` for macroscopic objects reflects a new paradigm in the way objects can be built. Instead of simple two dimensional fabrication or carving of a bulk piece of material, a new era has started where objects are built voxel after voxel. This allows the manufacture of more advanced designed tools and to think about more challenging shapes and applications.

In this context, (the technology is still in its early days as this thesis is written), few visionaries are already thinking about active 3D printing. Under the appellation `4D printing` these people envision several implementations, ranging from self-assembled materials to deformable objects [1]. The main objective of this manuscript is to introduce the reader to a fantastic world, where 3D printing meets active materials at the nanoscale. A place where photons are used both for the fabrication and for the actuation of micro sized devices.

Pierre-Gilles de Gennes was the first who predicted the discovery of smart elastomers based on liquid crystals in 1975 [2], but the first synthesis of these active polymers was made in 1991 by Küpfer and Finkelmann [3]. That discovery gave birth to an intense field of research and to numerous polymer actuation mechanisms. Among them, light actuation stands apart. It is the only trigger that can be localized spatially in three dimensions, be remotely controlled, and whose action can be spread over a wide area or restricted to few nanometers (even below the diffraction limit as we will explain here). Plasmonics allows to trigger but also to probe locally the surface of liquid crystal elastomer. The local resonance of electrons in a metallic structure excites photons at the vicinity of its interface.

The thesis will be organized as follows. In this first section, the history and theory behind liquid crystal elastomer will be described. The basic chemical notions will be introduced. In the second section, finite element model simulations will be performed to explain how

light and LCE interact. In the third section, a new fabrication technique based on direct laser writing of azobenzene-containing LCE will be presented. In the fourth section, an application for microfluidics will be detailed. Finally, in the fifth section, a new approach, nanotransfer printing plasmonic structures in a LCE layer, will be showed, together with their optical characterization.

2

LIQUID CRYSTAL ELASTOMERS

2.1 HISTORICAL DEVELOPMENT

Continuo contemplare, omnia mutatione fieri, adsuesce intelligere, nihil neque diligere universitatis naturam atque ea, quae sunt, mutare et nova similia efficere.

— Marcus Aurelius

Responsive materials fall into a class of materials that have the capability to change one or more physical properties upon a change in the environment. In particular, responsive liquid crystal polymers are really interesting materials whose properties on a macroscopic length scale have been intensively studied. Liquid crystal elastomers are rubber-like polymers that respond to external stimuli [4]. They are part of a broad class of Polymer Liquid Crystals (PLCs) which combine the properties of polymers with those of liquid crystals. Their behavior comes from a strong coupling between the internal molecular orientation and macroscopic shape [5]. Thanks to the strength of these materials and to the large forces involved when triggered, they serve for various promising applications such as artificial muscles and actuators [6, 7], lab-on-a-chip devices [8] soft machines [9], microfluidic [10] and biotechnology [11]. The known activation mechanisms span over various stimuli: photomechanical coupling [12, 13], thermal expansion [3], flexoelectricity [14, 15], electrostriction [16], piezoelectricity [17] and various chemical sensing [18, 19, 20].

The first experiments in the nineties [3, 21, 22] were made on heat sensitive materials. However, over the years more and more attention has been given to light sensitive LCE [23, 24, 25, 26] due to the unique functionality of light for remote and spatial control of adaptive structures. The photo-responsivity is created by photo-isomerizable dyes (from the `azobenzene` family) present in the material. When these molecules absorb a photon they can change their own shape (from an elongated `trans-state` to a bent `cis-state`) and thus the molecular order. Usually UV light is used to give rise to a trans-to-cis conversion , while for the reverse process (cis-to-trans) visible light is adopted. The resulting deformation depends on the main orientation of the LCE network and is characterized by volume conservation.

Azo dyes have the advantage that they are non-toxic. Van Oosten et al., in a pioneering study [10], have shown that it is possible to create optically driven artificial cilia of tens of micron in size out of elastomers, by using an inkjet printer technology. Since these materials can be optimized to reach a the time-response in the millisecond range [27], people are now investigating their applications at the micro scale for high-speed actuation.

This is in this context that our work was initiated with the commitment of bringing a new dedicated set of tools to fabricate, model, use

and study light active liquid crystal elastomers. Though these tools might be at an early stage, we believe that they lay the ground for seminal progress about 4D nano printing, biotechnology and nano plasmonic sensing.

2.2 CHEMISTRY

Liquid crystal elastomers incorporate the properties of elastic materials (rubbers), those of liquid crystals and those of active compounds which react to environmental factors such as light [12, 28]. These hybrids show the same mesophases characteristic of ordinary liquid crystals, yet retain many of the useful and versatile properties of polymers. For regular flexible polymers to display liquid crystal characteristics, rod-like or disk-like elements (called `mesogens`) must be incorporated into their chains. The placement of mesogens plays a large role in determining the type of PLC that is formed. Main-chain polymer liquid crystals are formed when the mesogens are themselves part of the main chain of a polymer; side-chain polymer liquid crystals are formed when the mesogens are connected as a side chains to the polymer by a flexible bridge (`spacer`).

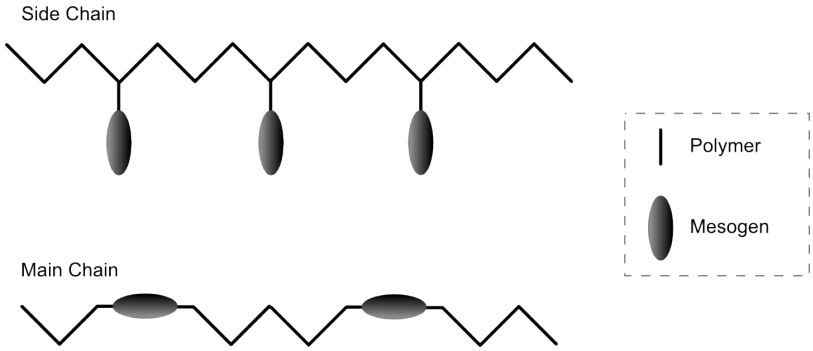

Figure 1: Two mesogen placements. (Top) Side Chain Liquid Crystal. (Bottom) Main Chain Liquid Crystal

In main-chain PLC, the mesogens are generally made up of two or more aromatic rings which provide the necessary restriction on movement that allows the polymer to display liquid crystal properties. The stiffness necessary for liquid crystallinity results from restrictions on resonance and rotation caused by steric hindrance. Another characteristic of the mesogen is its axial ratio that is defined as the length of the molecule divided by the diameter. The flexible group is usually a methylene group in the molecule.

Side-chain PLCs have three major structural components: the backbone, the spacer and the mesogen; usually the backbone consists of a siloxane matrix and the spacer is linked to the mesogen.

To gain the external sensitivity to light, the common strategy is to include azobenzene units in the polymer. Azobenzene is a chemical

compound composed of two phenyl rings linked by a N=N double bond. It is the simplest example of an azo compound. Azobenzene molecules were first described by Mitscherlich in 1856 [29] and are able to undergo a cis-trans isomerization under irradiation with light (see figure 2). This isomerization depends on the wavelength of the excitation light beam and is favored when the polarization of light and the electric dipole moment of the molecule are co-linear [30, 31, 13].

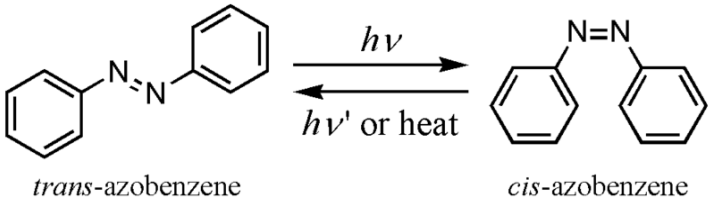

Figure 2: Isomerization of azobenzene. Before excitation, the more stable state is the trans-state (left). When energy is received, the molecule changes shape to go in a second stable state, the cis-state (right). The cis-state is less stable than the trans-state and usually back relaxation occurs after the emission of a photon of a phonon.

The most useful properties of LCs in general are birefringence and long range periodic ordering; these two properties, when they have been understood and controlled electrically, opened a new era in the display industry. In the case of LCEs, the long range order is the prevalent factor. Several ordering phases have been discovered in liquid crystals (nematic, smectic A, smectic C, cholesteric, ...) and this document will concentrate on the main one, nematic, with two distinct alignments: planar uniaxial or hybrid. At high temperatures, the LCs will exhibit no molecular order and will behave as standard liquids, they are said to be in isotropic state. At a lower temperature, before reaching the solid state, the LCs will have an internal order characterized by molecules that have no positional order but tend to point in the same direction (see figure 3): this state is called nematic.

One can define the `nematic director` ($\boldsymbol{n}$; depicted on figure 3) for the average orientation of the monomers. By averaging the angle single rods have related to the nematic director, it is possible to define the `nematic order` Q. If we write P_2 the second Legendre polynomial and θ the angle between a rod and the nematic director $\boldsymbol{n}$, then we have :

$$Q = \langle P_2(cos\theta)) \rangle = \left\langle \frac{3}{2} cos^2\theta - 1/2 \right\rangle \tag{1}$$

With this definition Q equals to 1 for a perfect nematic order and to 0 for a random order (isotropic state). When azo dyes are added to an LCE, the trans-state version of the molecule aligns according to the mesogenic host material and the order is defined by the host.

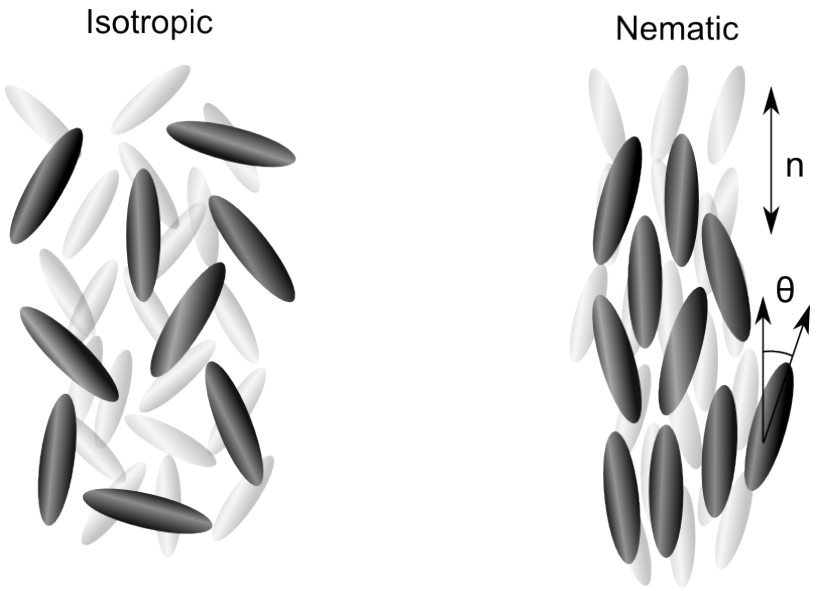

Figure 3: Two different Liquid Crystal states. (Left) When no order is present, the state is called isotropic. (Right) Orientation but not positional order, the state is called nematic. One can define the `nematic director` (n) as the average orientation of the monomers.

However, when the dye is activated and isomerized, the bent cis-state decreases the order of the mesogenic host, thereby causing a macroscopic shape change of the material (see figure 4). Azo-containing LCE have been investigated quite extensively in the last decades and the behavior of these materials can be quite different (a nice review has been published in 2003 [32], which covers many aspects about their fabrication and applications).

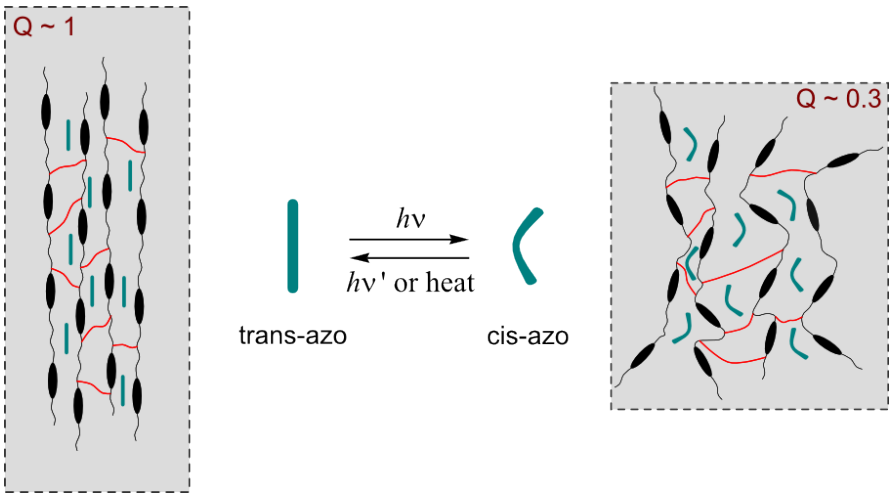

Figure 4: If an azobenzene is embedded in a LCE host, its activation with a photon will decrease the nematic order

A liquid crystal elastomeric mixture usually contains LC monomers, crosslinkers and photoinitiator molecules to start a polymerization.

The addition of azobenzene dyes could be done chemically (the dye is covalently bonded to the polymer) or by embedding the molecules within the host; there is actually three techniques used to add photochromic dyes to a LCE network.

The first approach consists in using a photochromic compound within the initial polymer mixture, the dye will be a `dopant` within the host. It is the easiest fabrication method. The second method is the most efficient but is also more complicated to achieve chemically: the molecules are engineered such that the dye is part of the final polymer (covalently bonded). In this configuration, the isomerization changes directly the matrix. This is the solution being used here (see molecules on figure 6)). Finally, the last method is the less efficient but could be used in very specific situations (when fabrication constraints do not allow the first two techniques): the dye is incorporated by infiltration after the polymerization, it is weakly attached to the network and its action is limited. The fabrication of LCE films will be described concretely later in sections 4.3.1 and 6.1.

The absorption of a photon in azobenzene molecules usually takes place in the UV region. However, it is possible to add chemical groups to the molecule to change the electron donor/acceptor properties and to shift the absorption [33, 34]. A push-pull molecule is characterized by an electron-withdrawing substituent on one side of the double bond and an electron-donating substituent on the other side which makes the π bond very polarized. As seen on figure 5, the absorption shift allows people to use azo-molecules that absorb green laser (532 nm) radiation. For a comprehensive understanding and analysis of the absorption of azobenzene, we refer the reader to [35] and [36].

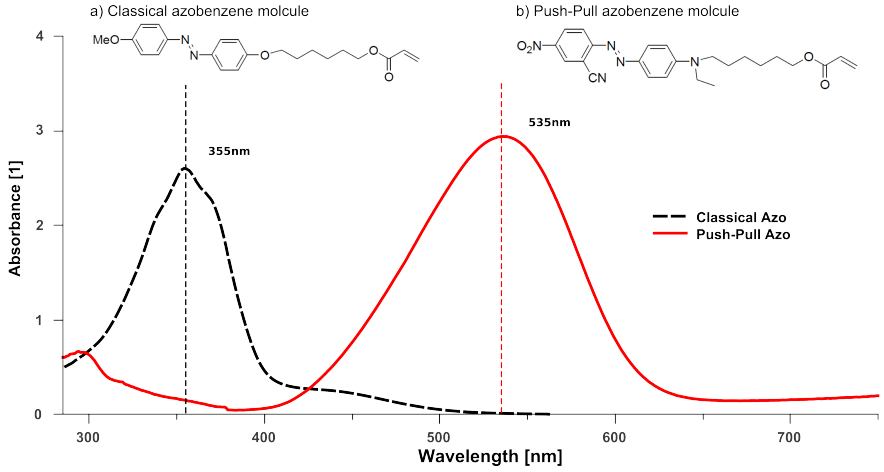

Figure 5: Absorption spectra of two molecules with azobenzene compounds in methanol. a) Classical azobenzene molecule: absorbs in the UV. b) Push-Pull azobenzene molecule: has been engineered to absorb in the visible.

The photoinduced response of azo molecules to irradiation varies a lot from one molecule to the other. These response times span from

20 ns to 200 μs [37, 38, 39]. Ikeda et al. also investigated the response times of the dye within a LCE [40] and found that it is in the range of 100 μs.

So far, the fabrication of liquid crystal elastomers have been done mostly on macroscopic samples. Reaching a lower scale has been done only recently with the progress in inkjet printing or laser writing. In this thesis we describe how to improve the fabrication at the micro and nanoscale with direct laser writing technologies and how to analyze it with plasmonic tools. In addition to that, a simulation framework is presented to allow the modeling of the interaction between electro magnetic field and liquid crystal elastomers.

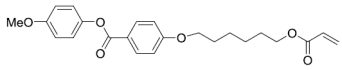

(a) Liquid Crystal

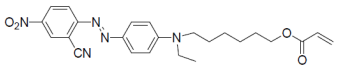

(b) Azobenzene compound

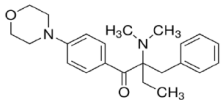

(c) Photoinitiator

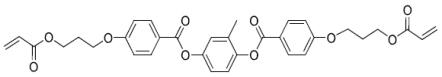

(d) Liquid Crystal Crosslinker

Figure 6: Molecules used to fabricate the LCE within this thesis. (a) Liquid Crystal mesogen (Developed within the LENS group) (b) Azobenzene compound (Developed within the LENS group) (c) Photoinitaitor (Sigma-Aldrich) (d) Liquid Crystal cross-linker (Synthon Chemicals)

Part II

SIMULATION OF LIQUID CRYSTAL ELASTOMERS AT THE NANOSCALE

When an electromagnetic wave interacts with a structure whose size is similar to its wavelength, many non intuitive events occur. Propagation of photons through a layer of liquid crystal elastomer and therefore intensity might not be correctly approximated via classical absorption laws. Simulation of the Liquid Crystal Elastomers dynamics using Finite Element Method is a great tool to understand and to reproduce the activation and deformation of an active polymer network by electromagnetic waves.

3 LCE SIMULATIONS

On ne peut se passer d'une méthode pour se mettre en quête de la vérité des choses.

— René Descartes

Recent progress on LCE synthesis and micro-patterning has opened the way to the development of nano-structured optically-controlled smart devices. As we will describe in chapter 4 dedicated to direct laser writing, small features down to 300 nanometers could be fabricated with this material. On the other side, LCE could also be used as a host for other elements, such as metallic gratings or nanoantennas, whose properties are revealed when an electromagnetic field excites them at the good wavelength. Such interactions are strongly dependent on sizes and are deeply relying on the Maxwell equations. Therefore a convincing modeling of the interactions at the nanoscale involves this set of classical electrodynamics equations.

In this section a `finite element model` that couples structural mechanics to electromagnetic wave propagation is developed. This provides a solid simulation framework that can be used to calculate the deformation of small (micrometer-size) LCE structures in response to illumination, where the light intensity attenuation is non-exponential due to wave diffraction and interference. This is illustrated by showing that a simple approximation of light absorption cannot account for the deformations in structures smaller than five times the wavelength. The photochromic response is analyzed for different alignment configurations and the evolution of the deformation is tracked.

3.1 INTRODUCTION

The initial experiments in the nineties [3, 21, 22] revealed a rich portfolio of properties for the fabricated films: stripe domains formation, super-elasticity, shape-memory. The modeling of such materials received many inputs over the years with techniques spanning over Monte Carlo simulations on lattice [41], elastic energy derivation [42], finite element methods [43, 44] and molecular dynamics[45].

As the attention was growing about light sensitive LCEs, groups started to model the interaction between photon absorption and LCE [23, 24, 25, 26]. To understand this mechanism, it is essential to understand that azobenzene molecules play a major role in the deformation (see previous section 2). After the isomeric shape change resulting from the absorption of a photon (the molecules go from an elongated to a bent conformation) , the molecular order changes. Following the internal molecular change, the whole material changes macroscopically, with the constraint of volume conservation. The deformation will depend on the difference of orientation between the initial and

final state. This liquid crystal orientation can be different in space and for the same crystalline state, several alignments can appear. In this thesis we will only describe the planar uniaxial and hybrid alignments (see figure 18 on page 38 for an illustration of the alignment).

So far, modeling studies have considered the exponential attenuation of the light intensity in the material for slab geometries [46, 47], yet for more complex shapes or structures whose sizes are of the order of the wavelength, wave interferences and scattering phenomena could be taken into account. Consequently, here a finite element method is used to build a versatile framework in which the propagation of light within the material follows the Maxwell equations and where the dynamics of the dyes isomerization is taken into account. This toolbox intends to be used when light absorption cannot be approximate with Beer Lambert law, typically when LCE structures size are below five times the wavelength. The development of new fabrication techniques [48, 49, 10] indeed allows for the creation of micro sized light-activated devices which cannot be modeled with existing methods.

3.2 GOVERNING EQUATIONS

Classical liquid crystals can be described as fluids made of stiff rod / disk-like molecules that show a long range orientation order. An elastic energy function is used to quantify the liquid crystal constitutive behavior where incompressibility is assumed. The presented model is based on a simplified energy function with a reduced set of variables to account for the effect of light on the internal strain.

3.2.1 *Structural Mechanics: Finite Strain Theory*

Deformation ($\boldsymbol{F}$) in structural mechanics represents the transformations of a body under the effect of forces, loads or internal stresses (see section 3.2.2).

$$\boldsymbol{u}(\boldsymbol{X},t) = \boldsymbol{x}(\boldsymbol{X},t) - \boldsymbol{X} \tag{2}$$

$$\nabla_x \boldsymbol{u} = \nabla_x \boldsymbol{x} - \boldsymbol{I} \tag{3}$$

$$\nabla_x \boldsymbol{u} = \boldsymbol{F} - \boldsymbol{I} \tag{4}$$

where $\boldsymbol{u}(\boldsymbol{X},t)$ is the displacement of the material point initially located in point $\boldsymbol{X}$ after time t in a Lagrangian description. The material deformation gradient tensor $\boldsymbol{F}$) is a second-order tensor that characterizes the local deformation at a material point with position vector $\boldsymbol{X}$.

The strain $\boldsymbol{\epsilon}$ is a tensor related to the deformation F by the following equation in the Lagrangian description :

$$\boldsymbol{\epsilon} = \frac{\delta}{\delta \boldsymbol{X}}(\boldsymbol{x} - \boldsymbol{X}) = \frac{1}{2}\boldsymbol{F}^T\boldsymbol{F} - \boldsymbol{I} \tag{5}$$

The main problem of representation with the deformation gradient tensor is that it is rotation-dependent. Since a pure rotation should not induce any stress on a deformable body, various rotation-independent deformation tensors have been introduced in mechanics. The simplest ones are the right Cauchy-Green ($\boldsymbol{C}$) and its inverse, the left Cauchy-Green ($\boldsymbol{D}$) deformation tensor which physically represent the square of local change in distances due to deformation :

$$\boldsymbol{C} = \boldsymbol{F}^T\boldsymbol{F} = \boldsymbol{U}^2 \tag{6}$$

Finally, as invariants of the Cauchy-Green tensors are often used for deriving the strain energy density function of a system, their definition is often presented with the eigenvalues of the Cauchy-Green tensor (I_1,I_2,I_3):

$$\hat{I}_1 = tr(\boldsymbol{C}) = \lambda_1 + \lambda_2 + \lambda_3 \tag{7}$$

$$\hat{I}_2 = \frac{1}{2}[(tr\boldsymbol{C})^2 - (tr\boldsymbol{C^2})] = \lambda_1^2\lambda_2^2 + \lambda_2^2\lambda_3^2 + \lambda_3^2\lambda_1^2 \tag{8}$$

$$\hat{I}_3 = det(\boldsymbol{C}) = \lambda_1\lambda_2\lambda_3 \tag{9}$$

3.2.2 *Stress and Linear Elastic deformations*

When a body is subject to internal forces (such as gravity, pressure, heat expansion or similar forces), the stress quantifies the action of particles within the material on neighboring particles. Stress is defined on a point and its unit is the pascal ($1Pa = 1Nm^{-2}$). If a force of amplitude $1N$ is applied normally or parallel to a $1m^2$ surface, it would produce a stress of magnitude $1Pa$ (see chapter 2 of [50] for a more complete description about stress).

When a solid material is under the action of a deformation, molecular forces will tend to restore the body to its original undeformed state therefore generating an internal `elastic stress`. If the material is soft, and if the deformation changes in time, a `viscous stress` will be the result. The combination of elastic and viscous stresses is generally described under the term `mechanical stresses`.

In continuum mechanics, simple stresses could be described by scalars or vectors depending on the situation. They are classified into one of the following categories uniaxial normal stress, simple shear stress or isotropic normal stress. However, in general a body will be

under the action of several stresses at the same time and the description is only possible with a tensor that reflects the combination of these combined stresses.

The Cauchy Stress Tensor σ, also called true stress tensor or simply `stress tensor`, is a second order tensor that completely defines the internal stresses at a point inside a continuum body :

$$\sigma = \begin{bmatrix} \sigma_{11} & \sigma_{12} & \sigma_{13} \\ \sigma_{21} & \sigma_{22} & \sigma_{23} \\ \sigma_{31} & \sigma_{32} & \sigma_{33} \end{bmatrix} \tag{10}$$

For small deformations, the Cauchy stress tensor is one of the main tool for stress analysis in the theory of linear elasticity [51, 52]. Elasticity is considered linear when the applied deformations are small and when the material is subject to infinitesimal strains only. When this criteria is met, the stress depends linearly on the applied strain and the constitutive equation is called the `Hooke's law` :

$$\sigma = \boldsymbol{C} : \boldsymbol{\epsilon} \tag{11}$$

where $\boldsymbol{C}$ is the stiffness tensor (four order tensor) and $\boldsymbol{\epsilon}$ the infinitesimal strain. In linear elasticity, the strain-displacement relation is given by :

$$\boldsymbol{\epsilon} = \frac{1}{2}\left[\nabla \boldsymbol{u} + (\nabla \boldsymbol{u})^T\right] \tag{12}$$

However, for big deformations, the linear assumption does not hold and the Hooke's law is not valid anymore. A material is often characterized by a `stress-strain curve` in continuum mechanics (see figure 7). It is unique for each material and it reveals many properties of a material such as the `Young modulus` (or Tensile Modulus or Elastic Modulus) which relates to the stiffness of an elastic material. The Young modulus represent the slope of the linear part on the stress-strain curve.

3.2.3 *Hyperlastic materials*

The Hooke's model is not suitable for the kind of materials which show a hyperelastic behavior, different from the elasto-plastic or the linear elastic ones. Rubbers are usually considered as non-hookean materials because their elasticity depends on temperature and loading rate.

To better understand the hyper-elastic model we have to introduce the `strain energy` (U) which is a very important characteristic of

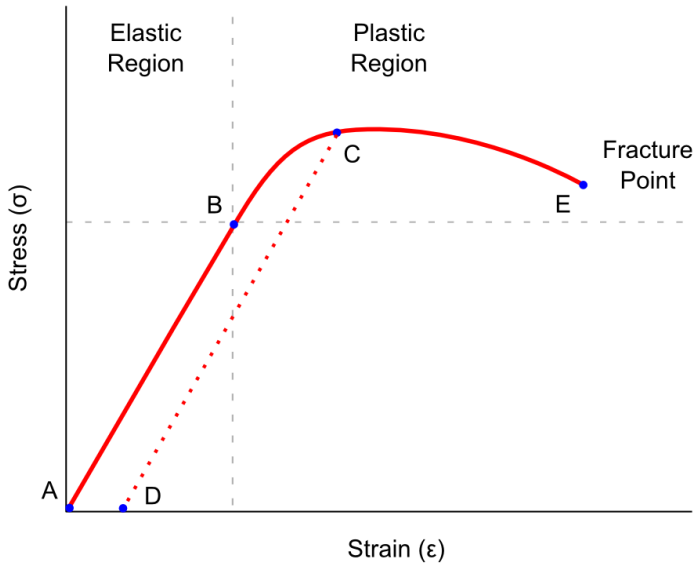

Figure 7: Stress-Strain curve for an elastic material. Within the elastic region, if the material is elongated from (A) to (B) and then released, no irreversible deformation will be created. However, if the elongation continues into the plastic region (C), then after the release of the strain, a macroscopic deformation will be stored internally. This plastic deformation is irreversible (D). Finally, if the strain is too large, the material will break (C).

many materials and represents the energy stored by a system under a deformation.

$$U = \int W(\boldsymbol{\epsilon}, x) dV \tag{13}$$

where W stands for the `strain energy density function` which depends on the deformation tensor $\boldsymbol{F}$ via the strain $\boldsymbol{\epsilon}$ and (in case of inhomogeneous material) on the position inside the continuum ($\boldsymbol{x}$).

Several phenomenological descriptions, and hence models, for hyperelastic materials exist [42]. Among them we chose the neo-Hookean model, a special case of the Mooney-Rivlin one, to better simulate the behavior of liquid crystal elastomers. A neo-Hookean solid is a hyperelastic material model which can be used to predict the nonlinear stress-strain behavior of materials undergoing large deformations.

The neo-Hookean model is based on the statistical thermodynamics of cross-linked polymer chains and is usable for plastic and rubber-like substances. Cross-linked polymers act in a neo-Hookean manner because the polymer chains can move relative to each other in the beginning, when a stress is applied, and at a certain point the chains result stretched to the maximum allowed by the covalent cross links,

and this causes an increase in the elastic modulus of the material. Here we assume the incompressibility of the material :

$$J = \det(\mathrm{F}) = 1 \tag{14}$$

which results in the nearly incompressible version of W for a neo-Hookean model :

$$W = \frac{1}{2}\mu\left(\hat{I}_1 - 3\right) + \frac{1}{2}\kappa\left(J_{el} - 1\right)^2 \tag{15}$$

where μ is the shear modulus, $\hat{I}_1$ is the first invariant of the left Cauchy-Green deformation tensor for incompressible materials, κ is the bulk modulus, and J_{el} stands for the elastic part of the deformation gradient.

In the case of small deformations and if the sample has a length much larger than the width, it has been shown [46] that the behavior of a photo-responsive elastomer can be described by a 2D analysis of the strains in the cross-section of the film. This assumption however prevents us to describe ribbons formation [53] or torsional responses [54].

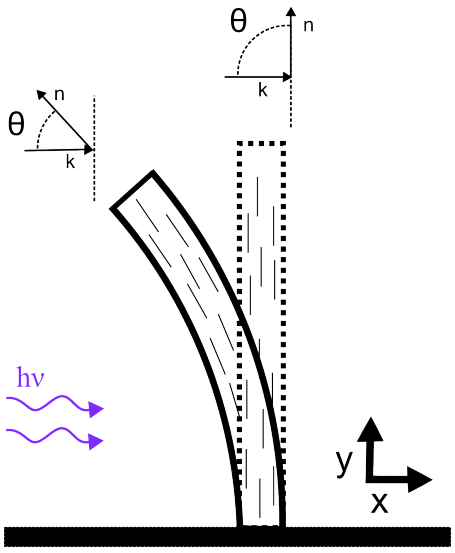

Figure 8: When light is absorbed by one side of a LCE beam, a gradient of strain is created (it could be due to gradient of light absorption or to a pre-alignment). θ is the angle between the wavevector k and the LC director n.

Light absorption can be approximated as an exponential in the case of large structures and low intensity (`Beeer-Lambert approximation law`). Using the coordinates from figure 8 the intensity (I) at distance x is given by :

$$I(x) = I_0 \exp\left(-\frac{x}{d}\right) \tag{16}$$

$$d = \frac{d_{azo}}{\varphi} \tag{17}$$

where I_0 is the intensity of the incoming light, φ is the mole fraction of azobenzene, d the absorption length of azobenzene, d_{azo} is the absorption coefficient for the azobenzene, φ is the dye molar fraction and x is taken in the beam referential. Here we assume that the azobenzene dye is the only absorbing species.

However, when the wavelength becomes similar to structural features of the studied system, or if the intensity is too high, the previous assumption does not stand. The intensity of light will depend on the amplitude of the EM wave (E), governed by the standard Maxwell equations :

$$I(x) \propto \frac{cn\epsilon_0}{2} \mid E(x)^2 \mid \tag{18}$$

In the case of elastic deformations, the response function linking strain to the deforming stress is the `compliance tensor` of the material. In analogy, the correlation between the absorbed light and the induced strain is called `photo-compliance` (P, with unit cm^2/W) [55]. The LCE is considered as transverse isotropic material due to the long rod like molecules of Liquid Crystal. As a reference, we used the values from Table 1 which could be adapted to fit different materials.

Name	**Symbol**	**Value**	**Unit**
Young Modulus Parallel	$E_{\parallel}$	1.3	GPa
Young Modulus Perpendicular	$E_{\perp}$	0.6	GPa
Photocompliance Parallel	$P_{\parallel}$	1.7	cm^2/W
Photocompliance Perpendicular	$P_{\perp}$	-0.7	cm^2/W
Azobenzene Absorption Length	d_{azo}	$0.5e^{-6}$	m^{-1}
Mole fraction of azobenzene	φ	0.05	1

Table 1: Parameters used in the following set of simulations

In the case depicted by figure 8, the strain produced by photon absorption along the y-direction dominates the deformation. The contribution along the other directions can be neglected since the width of the cantilever is small in comparison with its length. For the approximation of a 2D system, the value of ϵ_y component is enough.

Keeping this in mind and the previous assumptions (transverse isotropy, bi-dimensional analysis, and symmetric deformations around the director), the light induced strain can now be defined :

$$\epsilon_{y,light} = \epsilon_{\parallel} cos^2\theta + \epsilon_{\perp} sin^2\theta \tag{19}$$

where θ is the angle between the local director at position $\boldsymbol{r}$ in the system, and :

$$\epsilon_{\parallel}(\boldsymbol{r}) = \varphi P_{\parallel} I(\boldsymbol{r}) \quad (20)$$
$$\epsilon_{\perp}(\boldsymbol{r}) = \varphi P_{\perp} I(\boldsymbol{r}) \quad (21)$$

The total stress hence comes from the internal strain and the light induced strain :

$$\sigma = E\left(\epsilon_0 + \epsilon_{light}(I)\right) \quad (22)$$

This stress can then be used in 15 to get the internal energy.

3.3 EXPONENTIAL APPROXIMATION LIMITS

To compare different deformation cases the bending radius has been chosen as a figure of merit since it has a physical meaning. When considering an exponential absorption within the material, in the case of uniaxial LC alignment an analytical expression for the bending radius has been derived by VanOosten in [47] :

$$r = \frac{\varphi x^3}{6 I_0 P d \left(-2d + 2de^{-\varphi x/d} + \varphi x(1 + e^{-\varphi x/d})\right)} \quad (23)$$

This approximation stands for a Beer Lambert law of absorption within the media and for a fixed azobenzene absorption. In practice, once the dye is excited, its absorption coefficient changes, therefore the photocompliance is a dynamical variable (see next section 3.4).

If you consider a beam of LCE, an anisotropic deformation will favor a bending or a twisting. If light is sent with normal incidence to a uniaxially aligned LCE, the light absorption along the thickness results in a higher intensity on the side facing direct illumination, and a lower one at the back. Therefore, more dyes will undergo isomerization and thus a gradient of deformation will occur along the thickness. If the dyes are aligned parallel the y-direction, this gradient of deformation will lead to a bending toward the light (see figure 9).

Azobenzene dyes can be engineered so that they absorb differently, either spectrally or in amplitude. On figure 9d one can see that the effect of light absorption by the dye (molar absorptivity) is an effective parameter and can be optimized to increase a bending.

The resulting deformation is also different if one studies the case of a planar uniaxial alignment or an hybrid alignment. For an hybrid alignment, the deformation will always be favored in the same direction if the excitation light comes from the left or the right. In the opposite, the deformation of a uniaxially aligned sample will depend on the illumination side: the sample will bend toward the light

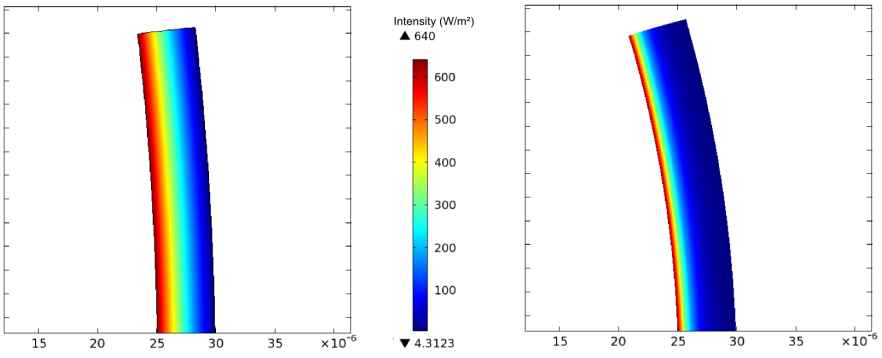

(a) Absorption length: d=6μm

(b) Absorption length: d=1μm

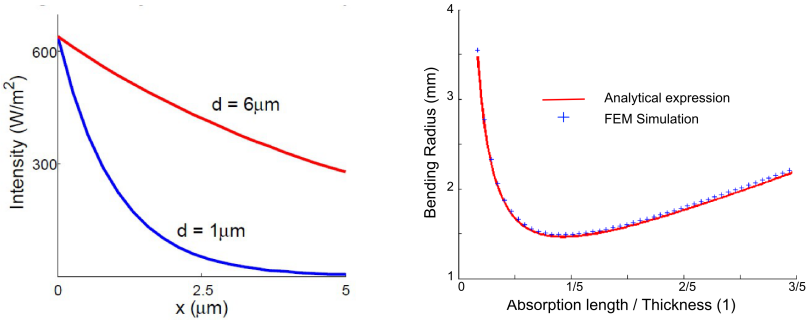

(c) Light absorption (Beer Lambert law)

(d) Bending radius simulation and analytic expression

Figure 9: The deformation of a LCE beam depends on the light intensity gradient in the sample. On the pictures above, light comes from the left side and gets absorbed as it propagates through a uniaxially aligned LCEs with different absorption lengths. (a) When light can propagate easily through the material, the deformation is similar from both sides, therefore, the shape change (the beam gets thicker and shorter) is not noticeable. (b) When light is absorbed effectively, a strong gradient is created along the x-direction, and the contraction along the y-direction is bigger at the left side than at the right side. (c) Light intensity through thickness when absorption follows Beer-Lambert law. (d) Evolution of the bending radius when simulated via a FEM method and analytical expression 23.

because of a gradient in isomerization of the dyes. One can use these features purposely for the design of devices which need a predetermined movement or a movement depending on its relative position to light.

Figure 10 shows that, when the absorption length is smaller than the structure thickness (when light does not propagate deep in the material), the bending radius for uniaxial and hybrid alignments are similar. However, when the absorption length is higher and more light penetrates into the material, the contraction is reduced for uniaxial while it gets stronger in the case of splay alignment (resulting

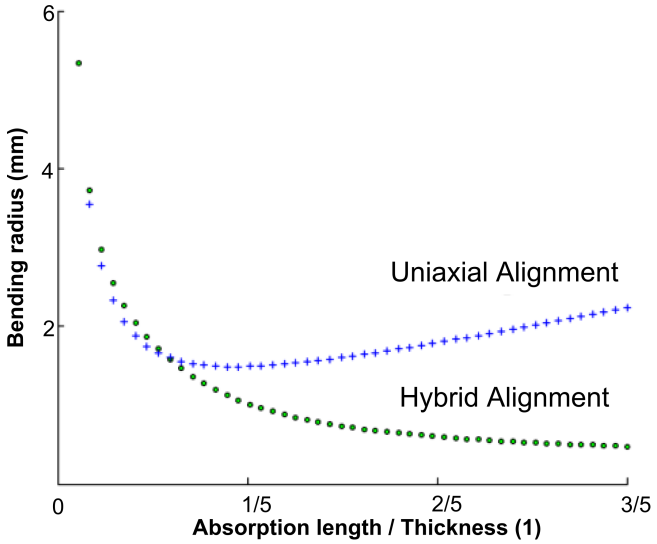

Figure 10: Uniaxial versus hybrid - Bending Radius. Depending on the absorption length of the dye (dye concentration is fixed), the deformation is different. For an hybrid alignment, the less the dye absorbs, the more deformed will be the resulting structure. However, for a uniaxial alignment the situation is different: for low optical absorption, the bending will be quite limited. The is an extremum in the function that is reached where the deformation will be limited.

in a smaller bending radius). This is a consequence of the internal alignment of the dyes.

As more light enters in both cantilevers, more dyes are excited. In the case of uniaxial alignment, this results in a widening and shortening of the whole cantilever (see picture 9a for a reference). On the contrary, for hybrid alignments, the dyes located at the front and back face are perpendicular to each other. So, while they receive a similar amount of energy, they tend to deform in a different manner which contribute to a different deformation at the front and at the back. If the front extends in x and contracts along y, then it will be the opposite at the back (and reciprocally).

When the structure typical size gets comparable with the wavelength of the excitation beam, optical effects such as internal reflections and interferences occur. Therefore the internal intensity cannot be approximated with the Beer Lambert law anymore and using the Maxell Equations turns out to be necessary.

Discrepancies occur with a stronger intensity for longer absorption length (figure 11). Indeed, low absorption increases the thin-film interferences created by multiple boundary reflections. These interferences are at the mechanism that allows photonic crystals to exhibit really powerful optical characteristics [56].

For physical structures whose size is of the order of the micron, the wave nature of light is more obvious than ever and needs to be

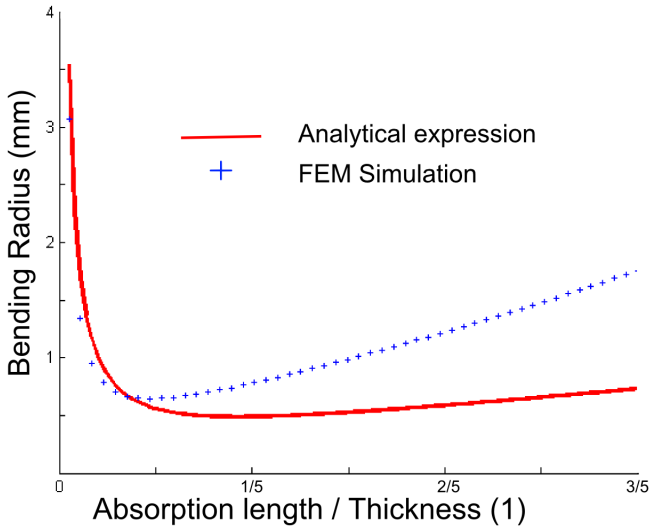

Figure 11: As the wavelength of the exciting light becomes comparable to the structure, internal reflection changes the absorption inside. Hence the bending behavior is different than the analytical case which takes into consideration an exponential decay of light intensity. (Here $\lambda = thickness/3$)

considered to fully account for intensity within the matter. A flat cantilever can then be subject to interference effects when the excitation wavelength is a multiple of its thickness. This kind of effects could be interesting when the dynamics of structure is considered. Because a system could shift its optical band gap during the deformation, a system allowing light propagation initially, could change into a mirror after the change of shape resulting from the isomerization of azobenzene. This is the reason why including the dynamics of the isomerization into the simulations is an important key.

3.4 DYNAMICAL DEFORMATION

The isomerization of azobenzene dyes is a dynamical process which depends on the excitation intensity. At rest state, a molecule can absorb a photon and be switched from trans-state to cis-state with some probability which can be expressed by a time rate called Γ: excitation rate. An excited state can then go back from cis-state to trans-state after some time called τ: relaxation time. Since the strain is only created by the molecules in cis-state configuration, equation 20 becomes :

$$\epsilon_{light} = P(x)\varphi n_c(I(x), t) \tag{24}$$

where n_c is the concentration of dyes in excited state. The time evolution of the two isomers is directed by :

$$\frac{\delta n_t}{\delta t} = -\Gamma I(x,t) n_t + \frac{n_c}{\tau} \tag{25}$$

where n_t is the fraction of dye in trans-state, I the intensity, Γ is the excitation rate, and τ the back-relaxation time. If we assume the intensity to be constant in time ($I(x,t) = I(x,0)$), since $n_c = 1 - n_t$, the system has an exact solution and if we write $\alpha = \Gamma I(x,0)\tau$ we have the following :

$$n_t(x,t) = \frac{1 + \alpha e^{-t(\alpha+1)/\tau}}{\alpha + 1} \tag{26}$$

However this approximation works for very high or low value of the absorption length since the intensity varies with the absorption length which is proportional to the concentration of dye. In addition to that, as the absorption from the two isomers is slightly different, the absorption length becomes a dynamical variable too :

$$d(t) = d_c n_c(t) + d_t n_t(t) \tag{27}$$

where d_t and d_c are the absorption length of azobenzene in trans-state and cis-state respectively.

In the following simulations we assume d_c equal to zero in order to reflect the fact that during the cis-trans transition the absorption band shifts and the dye does not absorb in the same band anymore.

Following the dynamical isomerization helps to understand some effects like oscillations [27]. The initial intensity (time $t = 0$s) shows a steeper slope than the stationary one (time $t = 10$s): as the time is evolving, a relaxation in the bending occurs. For low intensities (see figure 12a), this evolution is monotonous which leads the cantilever to slowly relax.

However, for high power (see figure 12b), the absorbed intensity , for intermediate times (times between $t = 0.8$s and $t = 1$s) is higher than the stationary result (time $t = 10$s). This leads to a steeper absorption for the second half of the cantilever and therefore a higher gradient. This transient relaxation cannot only account for continuous oscillations (which are created when the bending of a cantilever is such that the back face becomes the front face), but it can give a kick in such oscillations.

Hence the concentration of azobenzene dyes should be taken into consideration when simulating the deformation of a LCE cantilever. The back-relaxation induced by the cis-to-trans isomerization would be a key for bistable applications. Building a photonic crystal that allows and prevent periodically light could be fabricated by methods such as direct laser writing.

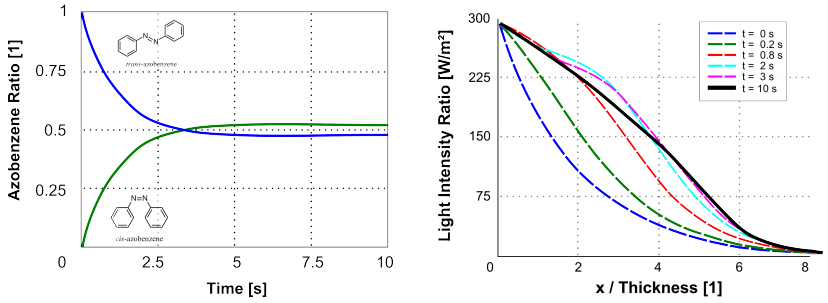

(a) α = 0.6

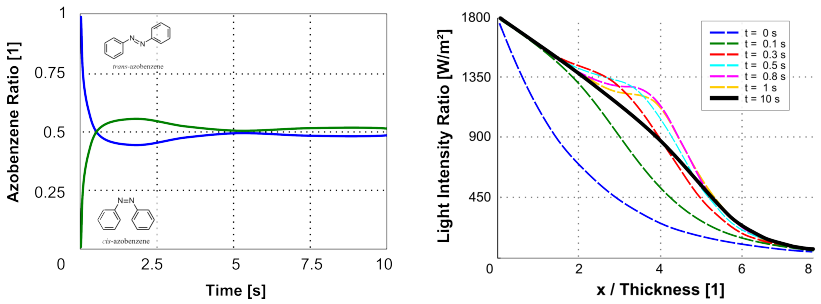

(b) α = 0.1

Figure 12: The initial intensity has an impact on the evolution of the isomerization. (Left) the concentration of trans- and cis- azobenzene in the middle of a 5μm thick cantilever is shown. (Right) The light intensity profile through the cantilever thickness is shown, varying in time. (a) For a low intensity (I_0=300W/m^2), the trans to cis evolution is slow and highly damped, it quickly reaches its stationary level. (b) For a high intensity, the isomerization is quicker and thus includes a quicker relaxation. Damped oscillation are visible in the cantilever response. The light intensity also shows a transient behavior where the light gradient is changing in time.

Part III

LASER WRITING ON LIQUID CRYSTAL ELASTOMERS

The fabrication of micro sized LCE structures is possible through the use of direct laser writing. Resolution down to 300nm can be reached, and the light-activation property of the material is conserved. In this section we explain how to fabricate light-tunable liquid crystal via Two-Photon lithography.

4

DIRECT LASER WRITING

Quand un bon sculpteur modèle des corps humains, il ne représente pas seulement la musculature, mais aussi la vie qui les réchauffe.

— *Auguste Rodin*

The advent of two-photon absorption (2PA) physics over the last 20 years has facilitated many applications among which 3D optical data storage [57, 58], lithographic microfabrication [59, 60, 61, 62, 63] and imaging [64, 65]. The fact that the 2PA activation by a tightly focused laser in an active material is subject to three dimensions (3D) confinement has far-reaching applications and explains why the interest in this technique is important.

This chapter is dedicated to the lithographic fabrication using 2PA, most commonly known as `direct laser writing`. After a general presentation describing the theory for standard photoresists, we introduce the specific case of light-activated LCE.

4.1 PRINCIPLES OF LASER WRITING

Realizing three dimensional structures at a micro metric scale has not been accessible until the nineties. In 1997, Kawata developed a method based on non linear absorption of a laser in a photo-resist [61]. The principles of two photon lithography are similar to classical photo-lithography. An interesting history of two-photon photopolymerization has been written by Sun and Kawata [66].

4.1.1 *Photolithography*

Classical photo-lithography is also called UV lithography or `optical lithography` and the name describes a process during which a photon is used to initiate the polymerization of a resist. The use of absorbing masks allows users to spatially engineer the polymerization. The regions located under the mask will not receive enough energy and only the regions which are not covered by the mask are exposed and thus polymerized. The resulting pattern is then developed by the use of chemicals which will remove either the exposed resist (in the case of `positive resist`) or the non exposed resist (case of `negative resist`).

A photoresist is a polymeric coating that is designed to change properties upon exposure to light. For most photoresists, a photo crosslinking occurs (see figure 13). When polymer chains are linked together by `cross-links`, they lose their ability to move as individual polymer chains. Liquid monomers, where the chains can freely move around, will be turned into a gel or a solid after cross-linking.

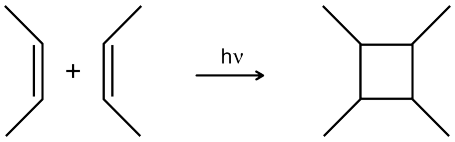

Figure 13: Photocrosslinking example - Cycloaddition of cinnamate

After the exposition, depending on the family of resist used, the application of a `developer` will wash away either the exposed or the unexposed regions selectively. When the exposed region is removed by the developer (i.e., exposure makes the photoresist more soluble), the process is called `positive tone`, and when the developer leaves the irradiated region behind (i.e., irradiation makes the photoresist less soluble), the process is called `negative tone`.

The exposition is usually done with UV or deep-UV light and spatially restricted by `UV masks` placed on top of the sample. The area located bellow the masks is covered and protected from UV radiation, and therefore the resist does not undergo crosslinking. With photolithography, a resolution of 1 micrometer could be achieved, and only two dimensional structures can be fabricated in one single step. The most obvious advantage of the technique is that the exposure time is really short, typically of the order of seconds, and that it allows to write structures over large areas.

As most common micro-electronic devices use semi-conductors or metals, a last step is often performed after the development. Two options are possible here. The first one implies that an `oxide` was present below the resist. `Etching` is applied on the whole sample during a fixed time, long enough to remove the remaining coated resist and the oxide which was not protected. A different solution is to evaporate a metal/oxide on the sample, and then to remove the resist by `lift-off`. The complete process is illustrated on figure 14.

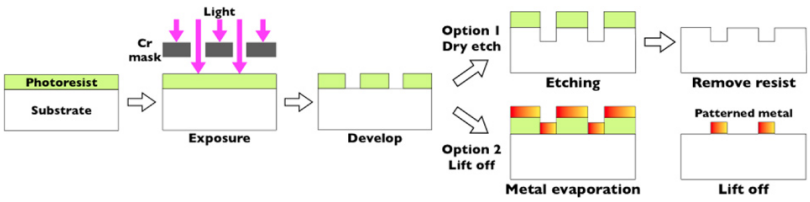

Figure 14: Lithography steps showing a positive tone resist. (Top) Etching (Bottom) Lift-off (reproduced from [67])

To reach the third dimension, people use multi-steps lithography. The process involves several coating - exposition - development - etching // evaporation + lift-off steps and a careful design to get simple layered structures is required. The resulting procedure is thus longer and critical. Any mistake in one of the steps makes the sample useless.

Using `non-linear effects` opens a new dimension and allows for a better resolution. However, since the exposure is made voxel by voxel in space, the exposure time is increased considerably.

4.1.2 *Two-photon absorption*

Basically 2PA lithography is done by focusing infrared light into a photoresist and if the intensity is high enough, two virtual UV photons are absorbed by the material and polymerization can occur. This process is called two-photon absorption and is due to non linear optical effects.

Predicted theoretically in 1931 by Göppert-Mayer [68], the 2PA process has only been observed experimentally in the sixties [69, 70, 71, 72]. Since multiple photons absorption requires a high-intensity electromagnetic field, the invention of the laser had a great impact on this field. For a long time, few dyes with sufficiently large cross sections were known, and therefore few consideration was given to the topic in the early years.

Although, lasers were not formally invented until 1969, Bell Labs was testing masers in 1958, which were only capable of short pulses of intense electromagnetic radiation. In 1961 Kaiser and Garret reported the first two-photon absorption of a compound. They used the new laser technology to excite CaF_2Eu^{2+} with both red and blue light to induce a two photon transition.

In general a molecule can be excited from its electronic ground state (g) to an excited state (e) by absorbing one photon which energy should be equal to the energy difference between g and e (see left-side of figure 15). Basically, 2PA means that a molecule will absorb two photons instead of only one to reach an excited state. As shown on picture 15, in the case of degenerate 2PA (one wavelength) two photons of the same energy excite the molecule at the frequency half of the one normally required.

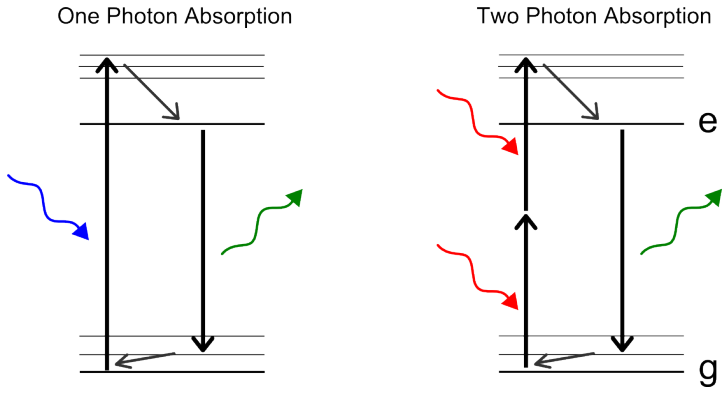

Figure 15: Single photon absorption (left) and Two photon absorption (right) for a non-centrosymmetric molecule

Different variations of this process exist. The 2PA process can occur with two photons of different wavelengths if their energy sum up to the required excitation energy. More than two photons at a time could be absorbed; in general people refer to this process as multiple-photon absorption (MPA).

In the case of `centrosymmetric molecules` the energy required for an absorption may be different for 1PA or 2PA [71]. In these systems, the lowest excited state (e) is only allowed for one photon absorption. Two-photon absorption only occurs at more energetic levels (e') (see picture 16).

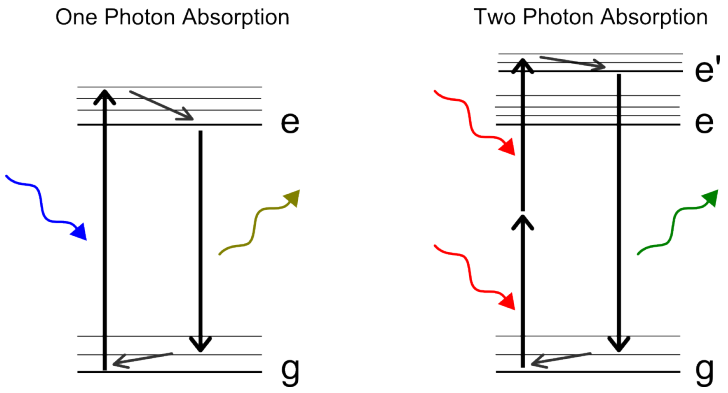

Figure 16: Single photon absorption (left) and Two photon absorption (right) for a centrosymmetric molecule

4.1.3 *Two-photon lithography*

Two-photon lithography is used because the process scales quadratically with the intensity of the excitation light. Therefore, by choosing the correct photoinitiator and by tuning the exposure time, it is possible to polymerize only a limited region of space. If the intensity is increased, more initiators will absorb two photons and thus the polymerization will occur in a bigger area. However, it exists a higher limit for the excitation above which laser induced breakdown (damage) will occur.

In the case of one-photon absorption, the probability for a molecule to absorb an incoming photon scales linearly with the intensity of the excitation beam:

$$ {}^1n = \sigma(\nu) N_g \frac{I}{h\nu} \tag{28} $$

where ${}^1n$ is the number of molecules excited by 1PA per unit time and unit volume, σ is the cross-section of the molecule at frequency ν, N_g is the density of molecules in the ground state g, I is the intensity of the excitation beam and $h\nu$ is the energy of a photon.

When two photons are absorbed, the number of excited molecules becomes proportional to the square of the excitation intensity.

$$ {}^2n = \frac{1}{2}\delta(\nu) N_g \left(\frac{I}{h\nu}\right)^2 \tag{29} $$

where ${}^2n$ is the number of molecules excited by 2PA per unit time and unit volume, δ is the cross-section of the molecule at frequency ν.

This intensity dependence and the fact that the light intensity of focused laser beam decreases as the square of the distance from the focus explain why polymerization can be triggered with a high-spatial resolution in three dimensions. The required energy to achieve 2PA accessible in the vicinity of the focus is thus available in a much narrower region (proportional to r^{-4}) than in the case of standard absorption (proportional to r^{-2}).

Using longer wavelengths also enables polymerization in thicker materials since these frequencies are less capable of being absorbed by one-photon absorption. A higher intensity can therefore be achieved deeper in the material.

The 2PA process requires molecules with large absorption cross sections and high light intensities offered typically by `femtosecond lasers`. An important amount of publications exists regarding the study of the former and we refer the reader to the comprehensive review written by Rumi et al. [73].

When using a negative-tone resist, the area which is subject to 2PA will get polymerized or cross-linked, and thus will become less soluble in a developer. Developing the sample will therefore remove the non-exposed regions from the substrate. The resolution depends not only on the power at the focus and the absorption cross-section of the photoinitiator, but also by the type of chemical reaction. A large cross-section will reduce the exposure time and photon flux needed.

A standard direct laser writing setup (figure 17) involves a femtosecond pulsed laser sending the excitation beam through an high numerical aperture (NA) objective (typically over NA=1). Either the sample or the objective is mounted on a moving piezo-stage. The process is sequential, each step consists of positioning the objective or the sample at the desired (x, y, z) position. Then a shutter is open to let the laser expose the desired voxel for a certain time. The `exposure dose` should be precisely calibrated beforehand to get over the `polymerization threshold` and to avoid the `laser-induced breakdown` (chemical bond breaking due to the incoming intensity absorbed).

Several connected voxels are then exposed on the sample on a predefined way. Because of the non linear nature of the 2PA, voxels can be exposed deep in the sample without exposing the underlying regions. Therefore, complex 3D structures can be designed. Free standing structures can be created, but they need to be enclosed or attached to the substrate to survive the development process. After the exposition, the sample is developed with solvents.

Typically for an objective with NA=1.45 and an excitation wavelength of 800 nm, the waist of the beam at the focus will be of the order of 250 nm. Here, the voxel with enough intensity will in gen-

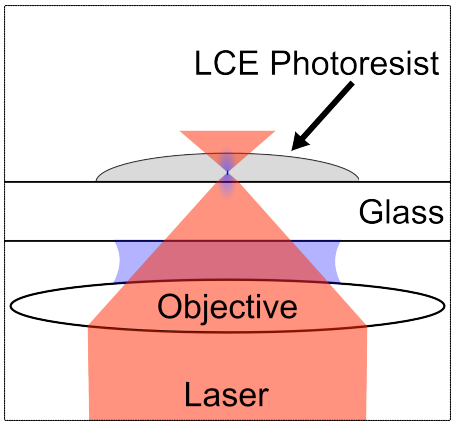

Figure 17: Direct Laser Writing System

eral be an ellipsoid with a short radius of 50 nm (along x and y) and long radius of 150 nm (along z). Considering that a high intensity needs to be achieved, only a limited region of the space will be be subject to 2PA but since polymerization does not stop after the first absorption of a photon, the exposed region strongly depends on the material used. Commercially available resist prepared for direct laser writing (Nanoscribe GmbH) are said to have a 150 nm resolution.

4.2 LASER WRITING ISSUES IN LCES

When using direct laser writing for the fabrication of LCE it is necessary to cope with the specificity of this material. Liquid crystals will intrinsically form micro domains which increase the scattering: a good control and homogenization is thus required before any writing. In addition to that, the light absorption of azobenzene dyes may compete with the one from photoinitiators used in the mixture. These dyes can not only absorb most of the energy, reducing the efficiency of the polymerization, but also be destroyed by intense beam, therefore preventing the LCE to be activated by light later on.

Liquid crystals are usually prepared in a `liquid crystal cell`. It consists of two substrates (which could be glass slides) separated by micro sized spacers inside which the liquid crystal is infiltrated (taking advantage of the small gap and capillarity forces). The surfaces of the cell can be coated with different coatings to create various control over the LC (most frequently for alignment reasons). With conductive layers, for instance, an electric field can be applied to change the alignment the liquid crystals inside the cell. A general overview of the alignment techniques could be found in [74].

4.2.1 *Problems due to the LC*

To get a fully functional LCE, the material has to be polymerized in the nematic state, when the long molecules are aligned uniformly along a common axis. To align these molecules several strategies can be chosen among which a good control of the temperature is always required. The first step is thus to implement a temperature controlled environment where the 2PA will occur.

Getting the liquid crystal material to the nematic state does not help the incident beam to penetrate deeper in the material. Indeed, since liquid crystals are birefringent, the field-induced director axis reorientation imparts a large phase change on the optical field traversing the film: it could be a pure phase modulation a phase retardation or a polarization rotation depending on the alignment of the directors.

For liquid crystal molecules without a proper alignment, the nematic ordering has a very short distance and numerous clusters exists called domains. These domains scatter the light really strongly and can inhibit the 2PA after few microns. However at the isotropic state, light scattering is suppressed dramatically since the domains and therefore the birefringence disappear.

A uniform and large-scale alignment (several microns at least) is thus more than preferred. Several environmental parameters are generally used: geometric constraints, electric and magnetic fields. The geometric effect requires a pre-treatment done on the surface of the LC cell while the electric field uses a conductive layer and the magnetic field does not depend on a specific LC cell treatment.

The mechanism for the surface alignment resulting from mechanical rubbing has never been completely understood. The most common explanations are that the long liquid crystal molecules will align with the grooves made on the surface to reduce the potential energy, or that electric charges created by the rubbing will force the molecules to follow the rubbing direction.

The mechanical alignment of a LC cell is a common technique [75, 76, 77] widely used in the display industry. The LC cell is coated on both inner sides with a polymer (usually Polyvinyl alcohol (PVA) or Polyimide (PI)) which can be either mechanically rubbed or tropically polymerized. The rubbing is done with a clothe after the spinning and curing of the polymer on both surfaces. In a second step, both substrates are assembled ensuring that the rubbed surfaces face each other. The alignment of the rubbing can be parallel, anti-parallel or perpendicular depending on the desired LC alignment (see figure 18 left and center). For certain polyimide molecules, the resulting orientation is perpendicular to the surface. When this coating is used on one side in combination with a planar one at the other side, the molecules gradually twist from a planar to vertical alignment. The LCE is said to be in an hybrid alignment (see figure 18 right).

In the case of an electric alignment, the LC cell is coated with Indium tin oxide (ITO), a transparent conductor, or with a very thin layer of any conductive metal: the substrates act as electrodes. Before the application of an electric field, the orientation of the liquid crystal molecules is determined by the alignment at the surfaces of the substrate. The application of an electric field will change the alignment

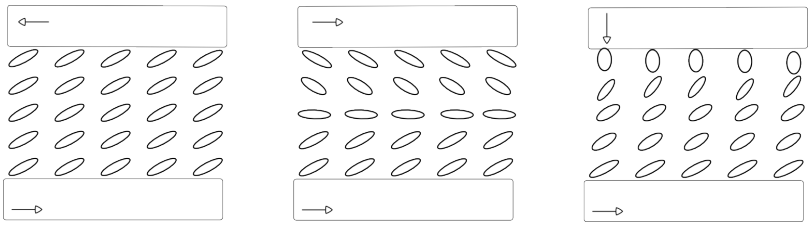

Figure 18: Alignment of LCs depends on the rubbing direction made on the LC cell. For an anti-parallel rubbing (left) the alignment is parallel (planar uniaxial). For a parallel rubbing (center) the alignment is planar. For a planar alignment one side and a perpendicular on the other side (right), the alignment is hybrid.

of molecules located in the center of a LC cell since they are more free to move and have a tendency to align with the current. By starting with various rubbing directions it is therefore possible to align locally the molecule before starting any polymerization.

Finally, in the presence of a strong magnetic field, Liquid Crystal (LC) are known to align with the field during the isotropic to nematic phase change. The alignment only occurs during the phase transition and has not been observed at a fixed temperature. The domains align parallel to the applied magnetic field: the rotation induced by the field during the phase transition depends on the field strength. Smaller domains need a higher field to align than bigger ones and switching off the field leads to a slow disorientation of each domain. The magnetic field also helps the domains to grow bigger (polydomain can become monodomain) and more quickly. This method has the advantage of being really versatile and any orientation can be prepared allowing enormous applications for LCE fabrication via laser writing. Nonetheless, this method requires two phase changes (nematic to isotropic and then the opposite) every time a new orientation is required; this leads to overwhelming long processes.

So far, only mechanical rubbing has really been investigated in the context of laser writing of LCE (but the use of a magnetic field for the macroscopic fabrication of LCE has already been investigated by Keller [78, 79]). However, the potential of magnetic alignment during the writing process would benefit from deeper investigations. In theory, the alignment can be decided in advance for each voxel before the polymerization after a cycle of phase-change. This path of research could lead to very precisely designed functional structures.

4.2.2 *Problems due to the azobenzene*

As described in the chapter dedicated to the chemistry of LCE (2.2), an azobenzene unit can be included in a polymer by three different means: it could be chemically attached to the macromolecules of the polymer, it could be a dopant within the polymer matrix and finally it

could be weakly attached via non-covalent interactions. In the case of the first two methods, the dye is already present during the polymerization, while in the last one, the dye is included after polymerization.

When the azobenzene is included only after the polymerization, it is not really important to care about conflicting absorption within the mixture. On the contrary, if the photochromic dye is present during the polymerization, some precautions regarding the optical absorption of the other compounds need to be taken. Indeed, if the dye is present during the laser-writing process, many competitive events can occur, reducing both the polymerization efficiency and the dye lifetime. First the dye can absorb the excitation beam (either one-photon absorption (1PA), 2PA or both [80]) and get destroyed by the intensity of the field. Second, the radicals being released by the photoinitiator can be incorporated by the dye which is therefore subject to bleaching [81]; since the radicals are not used for polymerization anymore, the efficiency drops. The dye bleaching, or `photobleaching`, is a photochemical destruction of the fluorophore: the light activation of the material cannot be undertaken after bleaching.

A first attention needs to be given to one-photon absorption process. This is not so critical given that classical direct laser-writing uses an excitation beam in the Near-Infrared (NIR) region and the fact that most organic materials emit and interact with light in the UV and visible regions but not in the NIR region. Attention needs to be paid only if the laser used for the 2PA process is in the visible.

For the two-photon absorption process, the problem is more likely to occur since most azobenzene dyes and most photoinitiators absorb in the UV. A competition will occur between the two molecules. Two solutions exist to circumvent this. The first one is to be sure that the 2PA cross-section of the photoinitiator is much larger than the one of the dye for the wavelength corresponding to the 2PA. The second one is to have the dye and the photoinitiator absorption peaks non overlapping. Several photoinitiators are commercially available and very efficient for 2PA. The dye can also be precisely engineered to absorb at a wavelength closer to the visible.

In particular, a push-pull mechanism is characterized by an electron-donor group on one side of the double-bond and by an electron-withdrawing group on the other side. It results in a strongly asymmetric electron distribution, which modifies the optical properties. In particular, it shifts the absorption spectra to the visible (that is the strategy being used here, see figure 5 on page 11). An azobenzene containing a push-pull electronic configuration is likely to absorb more in the visible region and less in the UV, therefore reducing the 2PA cross-section in the region of the excitation beam.

4.3 LASER WRITING OF LCES

Using light-driven LCE containing azobenzene dyes is a rather new approach towards photo-robotics and photo-mechanical systems. Several macroscopic devices have been reported to date: motors [9], inchworm walkers [82], hinges [83]. Recently, much attention has been focused on micro-fluidic and micro-robotics systems since LCEs optomechanical response makes it possible to control micrometers-scale systems with light: artificial cilia [10], fibers [79, 84], surface topologies [85], and switchable microarrays [86, 87]. Although fabrication with laser writing of LCE-based structures has already been reported by Keller and Dorkenoo [49], the material they used does not contain a photoisomerizable dye and the resolution of the resulting structure is of the order of $20\mu m$.

The method presented here explains how to prepare and fabricate light sensitive micro scale structures. It takes advantage of the laser writing technique to polymerize liquid crystal elastomers in a desired way while keeping the light sensitive compounds active. Still in its early days, the technique could potentially opens new perspectives for self tuned optical devices, active photonic crystal or bi-stable plasmonic structures.

4.3.1 *LCE preparation*

Several arbitrary choices have been taken here regarding the fabrication and other parameters can be used for different purposes and situations. Here, the liquid crystal mixture is containing the azobenzene as one of its compounds; this leads to a higher deformation but creates polymerization problems as explained in section 4.2.2. The alignment of LC is made by surface rubbing. The reasons for this are simplicity and time. A magnetic field can finely control the alignment of LC but the field has to be applied during a phase change, so a precise alignment scheme would require many heating/cooling steps.

The main element of the preparation is the LCE mixture which contains a photoinitiator (1%), an azobenzene dye (1%), a crosslinker (from 20 % to 30%) and a LC monomer (from 70% to 80%) (see table 2).

The compounds are dissolved in dichloromethane or toluene and stirred for some hours until the solvent gets totally evaporated. It is really important to be sure that the LCE does not contain remaining solvent. This would later lead to the creation of bubbles in the material during the 2PA polymerization (see picture 20). A solution for that is to prepare the mixture without using a solvent. The resulting problem is that the mixing between different molecules will not be really efficient. If a solvent is used, a great care should be given to

Compounds	Type	Concentration range
Irgacure 369	Photoinitiator	1%
MCL35	Azobenzene dye	1%
LC5	Crosslinker	20%-30%
LC6	Liquid crystal	70%-80%

Table 2: Concentration of molecules in LCE mixture

the evaporation before infiltration of the LC cell. Once in the cell, the solvent can still evaporate but will create many internal voids which will decrease the quality of the polymerized material.

4.3.2 *Transition temperature*

The phase transition temperatures of LCE monomer mixtures depends on the various concentrations used. These transitions in LC remain difficult things to predict. Standard LC usually have at least three phases: from the more stable to the less stable there is crystalline (K), nematic (N) and isotropic (I) transition.

The `mesogenic temperature` range of a liquid crystal mixture is important since the physical properties will be less sensitive to temperature change if the mixture is processed far from the `clearing point`. For a single type of molecule this range is usually limited. For example, 5CB (a common commercial LC) melts at 24°C degrees and clears at 35.3°C degrees. In order to work with convenience, it is better to have a low melting temperature (to avoid freezing of the device at room temperature) and a high clearing point (to reduce fluctuations of the physical properties).

To increase the range, the standard method is to mix different liquid crystals. When several compounds are mixed, their nematic-isotropic temperature is linear proportional to the molar concentration. However, the evolution of the clearing temperature is not following a simple trend. An Eutectic mixture is defined by the mixture of several chemical compounds that solidifies at a lower temperature than any other composition made up of the same ingredients. The melting temperature could often be described by the Schroder - Van Laar equation [88, 89] (see figure 19).

$$T_i = \frac{\delta H_{f_i}}{\delta H_{f_i}/T_{f_i} - Rln(X_i)} \tag{30}$$

where T_i is the nematic to isotropic transition temperature of the element i, δH_{f_i} the fusion enthalpy, T_{f_i} the melting point, R, the gas constant, and X_i the molar fraction.

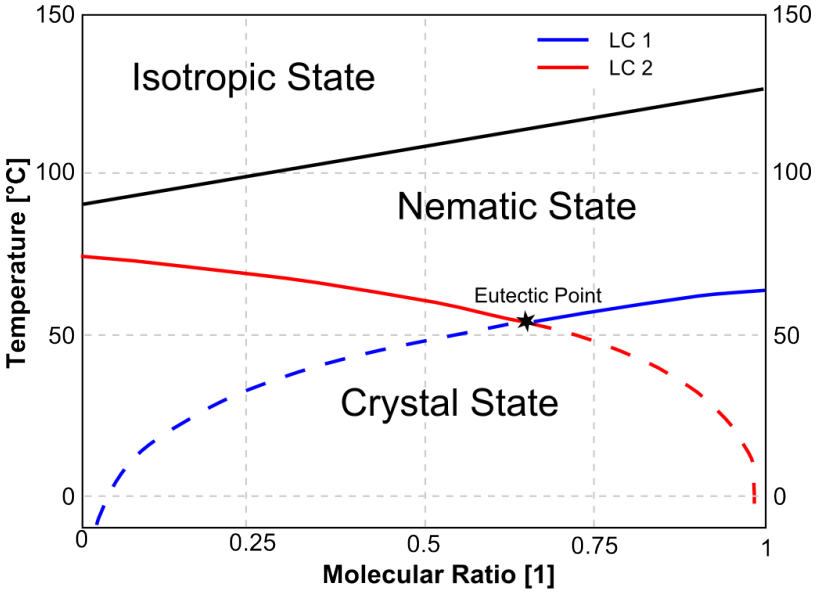

Figure 19: Van Laar equation for a mixture of two liquid crystal elastomers.

Depending on the liquid crystal molecules in use, the concentration between them can vary at the eutectic mix. The application described here has been made with 70% of monomeric LC and 30% crosslinker LC. The transition temperature has been confirmed by Polarized Optical Microscopy (POM) and the mixture lies in the nematic state between 35°C degrees and 55°C degrees.

4.3.3 *Cell preparation*

The LC cell should allow the alignment of the LCE before polymerization, but also has to be opened after the 2PA process to develop the non-polymerized parts. For that reason the LC cell is made out of two glass slides coated with 100 nm of PVA. The two glass slides are rubbed with a clothe after a short curing at 80°C degree for 120 seconds. A 45μ m aluminum foil is used as a spacer between the two glass slides and some glue is used to keep the assemble. Depending on the desired alignment, the two glass slides are faced such that the rubbing made on the PVA is parallel, anti-parallel or perpendicular (see figure 18).

The LCE mixture is infiltrated in the LC cell in the isotropic state at 130°C degrees in several steps. Each step consists in placing a drop of melted LCE at the edge of the cell and waiting until it gets infiltrated inside. When the cell is completely filled, the temperature is decreased to 60°C degrees at any arbitrary rate, then decreased to 45°C degrees at a rate of 1°C /min (a slow ramp is required to help the mesogen alignment).

In order to heat the system during the direct laser writing, a heating chamber has been fabricated to allow a fine tuning of the sample

temperature. Since the heat is transferred to the objective (in contact with the sample via immersion oil), a lot of heat is lost. A heating ring can be placed on the objective to compensate the losses. The heating cycle has thus to be adjusted so that both heating source provides a similar temperature.

4.3.4 *Direct Laser Writing parameters*

The laser power used for the 2PA needs to be finely adjusted so that it is higher than the `polymerization threshold` but below the `laser induced breakdown`. The polymerization threshold is characterized by the `laser illumination dose`.

Determining the correct dose makes it easier to use the optimum exposure time and power for a given resist. The calibration has to be done for each new mixture since the concentration of photoinitiator may vary slightly, thus changing the probability of a photon being absorbed. The dose is simply the light intensity times the exposure time.

$$Dose(mJ/cm^2) = Intensity(mW/cm^2) \times Exposure\ time(s) \quad (31)$$

In our experiment, the laser delivers 130 fs pulses with a 100 MHz repetition rate, circuly polarized and the beam power was measured before the microscope objective (100x, 1.4 NA Oil Objective). The sample position is controlled by a piezo stage and the required laser power to achieve polymerization was depending on its actuation speed. In table 3 the required powers for different speeds are given.

4.3.5 *Direct Laser Writing evolution*

After the exposition, the polymerized material has a different refractive index, which makes it visible even before the development. It is thus possible to monitor the process while writing. The polymerization is a dynamical process: once a photon is absorbed a polymerization starts and implies several monomers which will be bonded together during the reaction. The Kinetic chain length of a polymer is the average number of monomer units consumed for each radical

Piezo Speed (μm/s)	**Laser Power** (mW)
15	1.8
30	2.3
60	3

Table 3: Polymerization threshold for different piezo speeds

initiator that begins the polymerization. This number has a great significance on the properties of the final polymer. As the chain becomes longer, its `viscosity`, its `glass-transition temperature` and its `stiffness` increases. Without the presence of inhibitors, a polymerization will only stop when two chains encounter. The kinetics of the whole process depends strongly on the concentration of photoinitiators, the concentration of inhibitors and the laser intensity.

Another phenomenon can be observed with LCEs when they are subjected to laser writing. After a full line is written on the substrate, the material exhibits a process similar to an anisotropic swelling. It is characterized by a deformation which appears on polymerized lines: before this effect occurs, a polymerized line will appear straight with no geometrical defect. After few seconds, the line will slowly deform and get curly (see figure 20), the visible dynamics of the process occurs in 30 seconds approximately. This swelling is more effective when the lines are written perpendicularly to the rubbing made on the closest substrate. The deeper one writes in the resist, the less curly the lines appear. The swelling will also be less important for higher laser intensities (probably because the stiffness is higher and prevent further deformation).

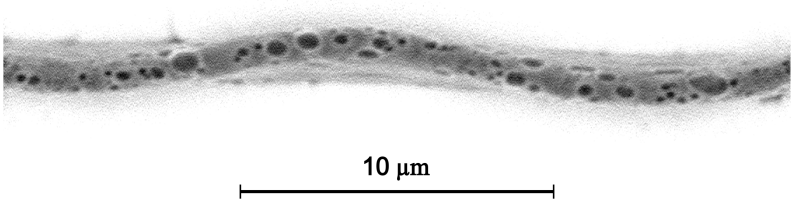

Figure 20: This structure has been developed and shows the effect of the curling induced swelling. A lot of holes are also present which are the results of the evaporation of solvent and/or a laser induced breakdown during the writing. As the bottom sides of the LCE line is fixed to the glass substrate, swelling only occurs on the top area.

The swelling effect may be the result of two simultaneous processes. The first one is due to a slow polymerization: even after the creation of the radicals, the polymerization could continue and if the kinetic is slow, the polymerization will stop after few seconds or minutes. Since the LC monomers are aligned along the rubbing on the surface, this slow polymerization is likely to occur preferentially in this direction. Another less controllable source of swelling could be due to the penetration of non-polymerized monomers in the polymerized matrix due to the molecular structure affinity by `absorption`.

This effect of absorption is more obvious when the polymerized region is not in direct contact with the substrate. Indeed, when the laser writing occurs at the surface (within the first micrometer), no de-

formation of the structure is visible , whereas when the laser writing occurs deeper in the material, the deformation is clearly noticeable. This is a proof that a volume change and not a surface change is happening in the material. The amplitude of the swelling could be reduced by increasing the intensity of the illumination beam, which however also reduces the resolution and can lead to laser induced destruction of the material.

After these preliminary studies, a power of 4 mW, and the writing speed of 60 μ m/s have been chosen for stable fabrication processes.

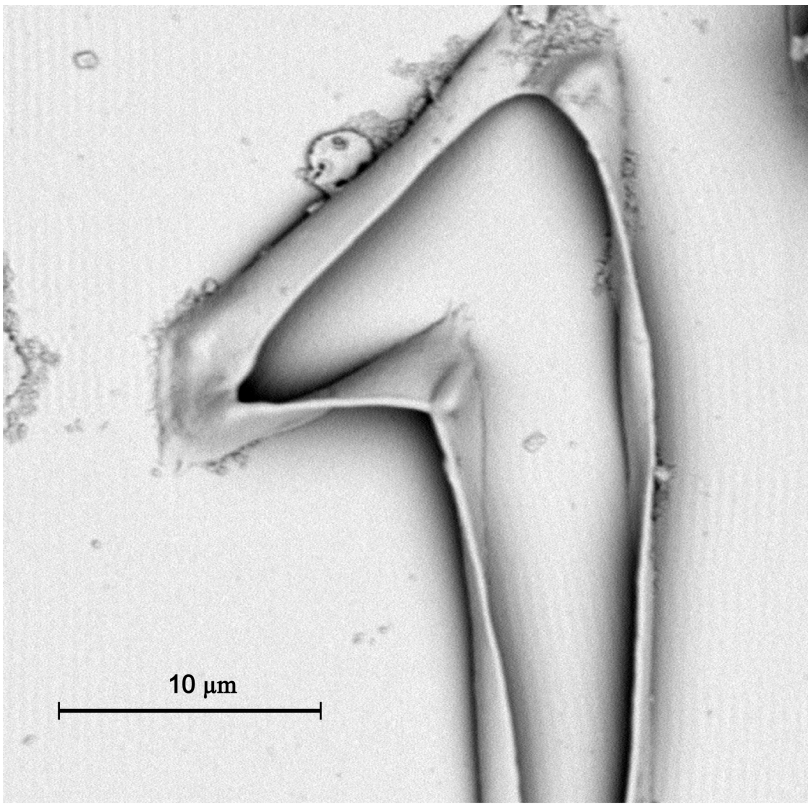

Figure 21: During development the structure can be very flexible and needs to be processed with care. Here, the structure has been developed too quickly. The walls are curled because of the stress induced by the developing solvents

4.3.6 *LCE development*

During the development, the molecules that have not been polymerized are washed away with a solvent. Typically the structures were developed in a pre-bath of PGMEA or NMP for 15 minutes then in a bath of isopropanol for another 10 minutes. During this process the material will shrink, therefore the swelling problem mentioned earlier will be slightly reduced. The fact that structures initially get swollen

and that during the development it shrinks, makes that objects are fabricated with less reproducibility.

Since the LCE is similar to a rubber it is very flexible during the development and it is important to use solvent with low vapor pressure and high boiling temperature so that the designs are not damaged by a too effective solvent (see figure 21).

4.3.7 *Experimental Results*

Two-photon absorption polymerization was induced by a focused laser beam from a 780 nm femtosecond laser in a commercial DLW workstation (Photonic Professional, Nanoscribe GmbH). The laser delivers 130 fs pulses with a 100 MHz repetition rate. The laser beam was circularly polarized and focused with a 100x, 1.4 NA Oil Objective (Zeiss, Plan Apochromat). The sample position was controlled by a 3D piezo translation. After laser writing, the cell was opened and the structure was developed according to the process described in the previous section.

A serie of `LCE rings` have been fabricated with the diameters ranging from 8 to 30 μ m and the same height of 2 μ m (see Figure 22). The rings maintain the round shape and flat surface (see the SEM image in the inset of 22 a), and the molecular orientation along the cell rubbing direction (22 b-c).

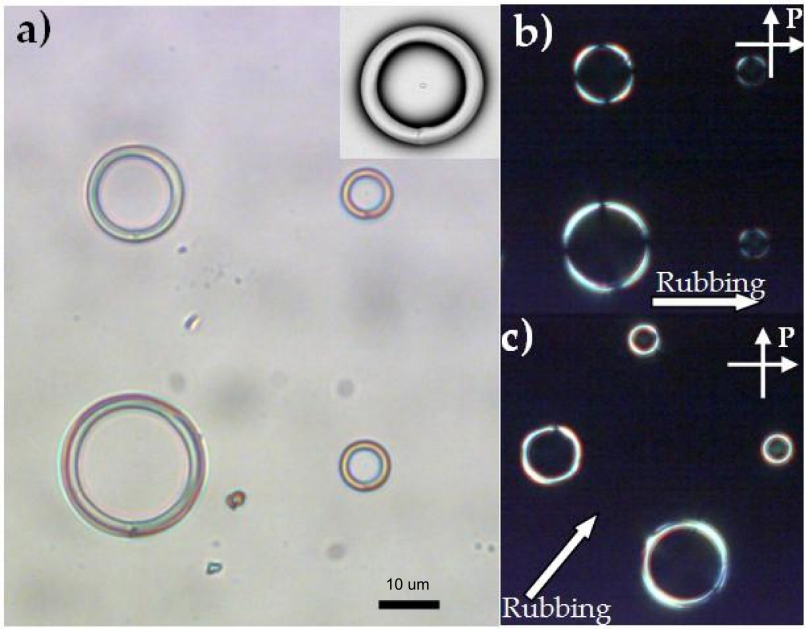

Figure 22: Four LCE rings of diameters 8μm and 30μm and height 2μm. a) Four rings before being developed - Inset One ring after being developed imaged by SEM b) and c) the four ring imaged by POM proves that the alignment is following the rubbing direction.

A $50 \times 50\mu$ m, 4 layers `woodpile structure` has been also fabricated demonstrating advanced 3D fabrication capabilities (see figure 23). The woodpile has a pitch of 5 μm and each layer has a 1.3 μm thickness. POM photographs reveal molecular orientation in each single log within the woodpile structure (see figure 23 b and c).

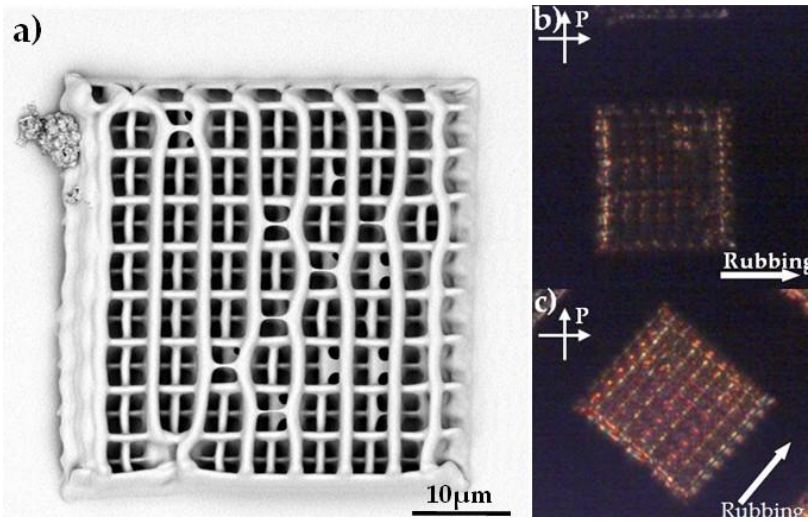

Figure 23: A $50 \times 50\mu m$ woodpile structure made in LCE via Direct Laser Writing. (a) SEM picture of the woodpile (b) and (c) POM picture showing the LC alignment

Part IV

LIQUID CRYSTAL ELASTOMER AND MICRO FLUIDIC

Liquid Crystal Elastomers are soft actuators that could be remotely activated, in air or in a fluid. Their properties could be used to fabricate micro swimming devices propelled by a light beam. This section explains the limitations occurring in a fluid at a micro scale, and simulates the swim of two embodiments which could potentially be created via Direct Laser Writing.

5

MICROFLUIDICS OF MEMS

Never confuse Motion with Action

— Benjamin Franklin

Since LCEs are considered as artificial muscles and because the ratio between light intensity and shape-change is important, a good application for these materials would be to replicate the motion of micro organism at a micrometer scale. Understanding the motion of micro organisms is not intuitive and different approaches coexist: the main ones come from the area (how does an algae swim ?) and the fluids mechanics (what is the optimal motion in the microscale world ?).

5.1 INTRODUCTION

Swimming at a very small scale (typically micrometers), is not really an intuition-driven process. Indeed, the physics in action there, has no obvious comparison to our macroscopic world: the friction forces dominate the kinetic ones and forbid classical movement's patterns.

To get an idea of such a viscosity at a macroscale, one should imagine how difficult it would be to swim in a corn sirup's pond. One will try to breaststroke and will hardly move. In fact one will go back and forth, following one's arm movement, and stays, even after a long time, at the same position. If you are at a surface of a solid surface you could easily crawl, but if you are underwater, there is no easy way to swim in the classical human fashion.

In the first section of this chapter we will describe the constitutive equations of motion for microfluidics. The following section will allow the reader to understand why a kinetic based swim cannot work at the microscale and what solutions have been found in Nature to allow micro-organisms to move. The fastest (and probably one of the best) strategy is to use what Nature came up to after billions of trials and errors. A short review about micro-swimmers is made in the second part of this chapter. Finally two artificial swimmers are analyzed by the mean of finite element method simulations.

5.2 FLUID MECHANISMS AT SMALL SCALE

5.2.1 *General Properties*

This section is partly based on the book from Nguyen and Wereley [90].

To understand the motion of objects in a fluid, it is first important to understand what is a fluid. A typical definition is given by R. Fox in [91]

> A fluid is a substance that deforms continuously under the application of shear (tangential) stress, no matter how small that stress may be.

A fluid could be a liquid or a gas for instance. Because a fluid is continuously deforming, a good description of its overall movement is given by a `flow`. The features of a fluid and its flow can be organized in distinct categories ([92]) :

Fluid

- `Transport properties` such as viscosity, thermal conductivity, and diffusivity
- `Thermodynamic properties` such as pressure, temperature, and density
- `Miscellaneous properties` such as surface tension, vapor pressure, and surface accommodation coefficients

Flow

- `Kinematic properties` such as linear and angular velocity, vorticity, acceleration, and strain rate

Computationally one can model a fluid with two different approaches. The first one considers the fluid as a collection of particles, and is required in the case of nanoscale descriptions: `molecular description`. The second one considers the fluid as a continuum and is mainly used for macroscale applications: `continuum description`. Since this work is focused on objects whose typical size is above 10 microns, we decided to use the continuum description and the Navier-Stokes equations (see section 5.2.2).

5.2.1.1 *Molecular Description*

An accurate model of the interaction of two simple, non-ionized, non-reacting molecules is given by the Lennard-Jones potential :

$$V_{ij}(r) = 4\epsilon \left[c_{ij} \left(\frac{r}{\sigma} \right)^{-12} - d_{ij} \left(\frac{r}{\sigma} \right)^{-6} \right] \tag{32}$$

where r is the distance separating the molecules i and j, c_{ij} and d_{ij} are parameters particular to the pair of interacting molecules, ϵ is a characteristic energy scale, and σ is a characteristic length scale.

The term with the r^{-12} dependence is a phenomenological model of the pairwise repulsion that exists between two molecules when they are brought very close together. The term with the r^{-6} dependence is a mildly attractive potential due to the `Van der Waals force` between any two molecules.

The force between two molecules can then be derived from the potential:

$$F_{ij}r = \frac{\partial V_{ij}(r)}{\partial r} \tag{33}$$

If m is the mass of a single molecule, the period of oscillation in the Lennard-Jones potential is given by :

$$\tau = \sigma\sqrt{\frac{m}{\epsilon}} \tag{34}$$

On plot 24 one can see the classical attraction/repulsion behavior between two molecules. One important observation to make is that the potential never goes back completely to zero after the minimum. It means that there is always a distant attraction for every couple of molecules. When this condition does not seem to hold anymore, it is possible to use the continuous description to avoid unnecessary computational loads.

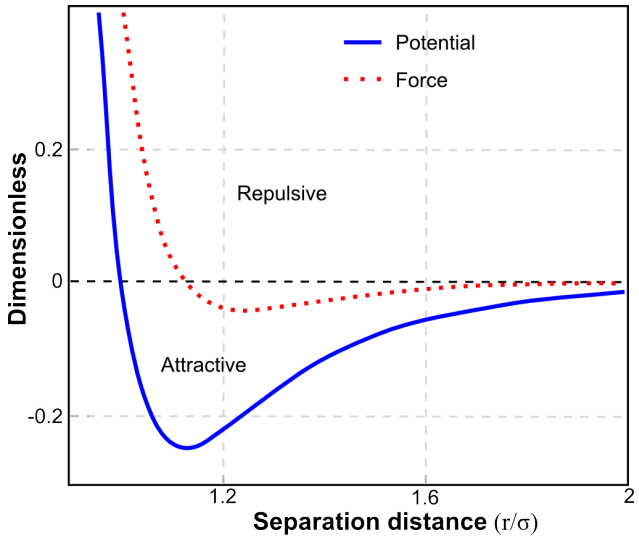

Figure 24: Lennard Jones potential and force for two distinct particles

5.2.1.2 *Continuous Description*

The study of fluid mechanics (at conventional, macroscopic length scales) generally proceeds from the assumption that the fluid can be treated as a continuum. All quantities of interest such as density, velocity, and pressure are assumed to be defined everywhere in space and to vary continuously from point to point within a flow. This concept is reflected in the equation of continuity which describes the conservation of mass while a given quantity is transported. The case of incompressible flow refers to the simplest case in which the material

density is constant within each infinitesimal volume. For an incompressible fluid the divergence of the fluid velocity is zero, which gives the following equation of continuity :

$$\frac{\delta \rho}{\delta t} + \nabla \cdot (\rho v) = 0 \tag{35}$$

with t the time, $\rho(x,t)$ the fluid density and $v(x,t)$ the Eulerian velocity.

If the molecules of a fluid are closely packed relative to the length scale of the flow, the continuum assumption is very likely to be valid. If the molecules are sparsely distributed relative to the length scale of the flow, assuming continuity of fluid and flow properties is probably a dangerous approach. However, even at microscopic length scales, there can still be many thousands of molecules within a length scale significant to the flow. For example, a 10-μm channel will have approximately 30,000 water molecules dispersed in it, enough molecules to consider the flow as continuous.

According to random process theory, in order to get reasonably stationary statistics, i.e. less than 1% statistical variations, 10^4 molecules must be used to compute an average value.

The `transport quantities` such as viscosity and diffusivity must also be continuous in order for the fluid to be treated as a continuum. The analysis of the transport quantities is somewhat different from that of the point quantities where a certain number of molecules were required in order for the property to be treated as continuous. For the transport quantities to behave continuously, it is important that the fluid molecules interact much more often with themselves than with flow boundaries. As a somewhat arbitrary criterion, one can choose the measurement volume to be a cube whose sides are 10 times as large as the molecules-interaction length scale.

For a gas, the best estimate of an interaction length scale is the displacement distance, also known as the mean free path, which is on the order of 100 nm. For a liquid, the molecules are essentially in a continual state of collision or interaction, so their displacement distance is not a good estimate of how many interactions will be present in some cube of space. Their molecular diameter is a much better estimate.

Approximately we have the following length scale limit for the continuous description of a fluid (see page 17 in [90] for more details) :

$$L_{gas} = 1\ \mu\text{m} \tag{36}$$

$$L_{liquid} = 10\ \text{nm} \tag{37}$$

5.2.2 *Navier-Stokes Equation*

The continuous description is based on the well known `Navier-Stokes equation` which derives from three constituting equations. In addition to the conservation of mass (continuity equation - see equation 35) and the energy conservation, the Newton's second law (momentum equation) is also used to derive the equation :

$$\rho \frac{Dv}{Dt} = \nabla \cdot \sigma + \rho f \tag{38}$$

where v is the velocity,ρ is the density, σ the stress tensor and f the external body force per unit mass.

In continuum mechanics, a Newtonian fluid is a fluid whose viscous stress is proportional to the strain rate. Water is a typical example of an incompressible Newtonian fluid. For an incompressible Newtonian fluid, the Navier-Stokes equations are :

$$\rho \left(\frac{\delta v}{\delta t} + (v \cdot \nabla) v \right) = -\nabla p + \mu \nabla^2 v + \rho f \tag{39}$$

$$\nabla \cdot v = 0 \tag{40}$$

with $\rho(x,t)$ is the fluid density, $v(x,t)$ is the Eulerian velocity and μ the dynamic viscosity.

A detailed discussion about the Navier Stokes Equations may be found in many fluid mechanics manuscripts [90, 93, 94].

5.2.3 *The Stokes Equations*

The fluid behavior is completely different from that of gases and is significantly more complex. For instance, in the gas theory, you can use the `Knudsen number` ($K_n = \lambda / L$, where λ is the mean free path and L some length scale characteristic of the flow) to let you know if the fluid will follow the Navier-Stokes equation or not. For liquids, the Knudsen number is not defined. Turning to experimental results do not help either. If one look at the viscosity of a liquid flowing through a channel, if you compare a small scale to a large scale, the viscosity could be either lower, the same or higher. The limit length scale (10 nm) that we gave earlier tells us when the fluids should be considered as continuous, but not the flow.

Indeed the Navier Stokes equations (39) are nonlinear with respect to the speed of the flow and only in exceptional cases will the nonlinear term vanish (for instance for a steady laminar flow between infinite parallel walls). The problem is really hard to solve when the nonlinear term is kept. Hopefully, at very low scale, the viscosity is such that this term could be neglected.

A common practice is to use the `Reynolds number` to decide when to use the Navier-Stokes equations or a linear derivation, the `Stokes Equations`. The Reynolds number is defined by :

$$Re = \frac{\rho V L}{\mu} \tag{41}$$

where V and L are representative values of the speed of the flow and the particle dimensions respectively, ρ is the density of the fluid and μ its dynamic viscosity. The kinematic viscosity is frequently used and is defined by $\nu = \mu/\rho$.

When $Re << 1$ the nonlinear term can be neglected and the class of solvable problems is greatly expanded :

$$-\nabla p + \mu \nabla^2 v = -\rho f \tag{42}$$

$$\nabla \cdot v = 0 \tag{43}$$

The first equation is known as the `Stokes equation` and both equations together are called `creeping flow equations`. They do not contain any inertial effects of the fluid flow and that they are linear in the fluid velocity.

5.2.4 *Boundary conditions and Reynolds number*

The boundary conditions between a solid and a fluid have always been a dilemma within the community. Since 1880 until today, the usual assumptions for macroscale liquids inside a solid container were assumed to be `no-slip boundary condition` (fluid as the same speed as the wall, see equation 44) together with a no-temperature jump condition and a no penetration boundary (normal speed of the fluid is equal at the speed of the wall). For the microscale, the no-slip boundary is questioned. A good review has recently been made on the recent models that could be used [95].

$$u_{fluid} = u_{wall} \tag{44}$$

At the microscale, the requirement for very low Reynolds number is often fulfilled: a microorganism in water will be a good example of a swimming object in a low Reynolds number environment. According to the previous section the interaction between a swimmer and the fluid will be described by the Stokes equation. A physical description of what is a low Reynolds number is therefore useful to better understand the physics at work in such environment.

The Reynolds number was introduced as $Re = \rho VL/\mu$ (equation 41) but a more understandable way to see it is to consider the ratio between inertial forces and friction :

$$Re = \frac{\text{Inertial forces}}{\text{Viscous forces}}$$

When $Re << 1$ the system is dominated by inertia and flows are laminar and less likely to create turbulences. The Reynolds number depends on the typical length scales at stake: V and L, the speed of the flow and the typical size of the swimmer (its widest dimension). If the flow is really slow, a big object could be in the creeping flow regime. Generally very small objects (sub millimeter) will often be in the creeping flow regime.

To illustrate the effect of viscosity on small micro-organisms, think of `E. coli bacteria`. Its typical size is approximately 3μ m and it travels at a speed $v = 30\mu$ m/s approximately. The experienced Re number will be 1.5 10^{-4}. After moving in water, if `E.coli` stops, the coasting distance will be roughly 0.1Å in a time close to a microsecond. This is an important point to keep in mind when reading the coming section about non reciprocal motion: inertia is really negligible at the micro scale.

5.3 SWIMMERS AT MICRO-SCALE

This section exhibits different solutions that Nature founded to propel its various life forms. From bacterias to spermatozoa and algae, different strategies has been selected through evolution. To start with, let's remind the reader that microbes are the smallest living organisms that we know (especially the viruses, smallest members of the family with sizes down to 50 nm).

5.3.1 *Scallop theorem*

Apart from the biological aspect of such study, relying on microscopy to discover the propelling devices ([96, 97, 98]), the physics of swimming requires a great attention. Two seminal works were brought by Taylor [99] and Purcell [100]. Taylor was one of the first to investigate the physical problems related to the propulsion of a small object and Purcell gave a renowned talk about life at low Reynolds number.

As explained in the previous section, the leading parameter for such swimmers is the Reynolds number. At very low scale, when this number is smaller than 1, the viscous force is dominant. The hydrodynamics follows the linear equations of the creeping flow (equations 42 and 43).

In this situation, flows are `laminar` (not turbulent) they occur in parallel layers and there is no lateral mixing. Adjacent layers slide

along each other without any loss of order in the structure. This is a consequence of the time-reversal symmetry of the Stokes equation 42. In layman's terms, time reversal is synonym to the conservation of energy and to a conservation of entropy. Reciprocally, when a flow is `turbulent` there is usually no time reversibility and vortices are created which carry angular and linear momentum, energy and mass.

If time reversal is possible, the energy spent for a trajectory from A to B at an arbitrary pace will be the same as a trajectory from B to A. All paths, from A to B (or from B to A) along the same trajectory are equivalent and do not depend on the speed at which they are taken. The initial state A is found to be exactly the same after a path from B to A.

This fact has an important corollary named after Purcell as the `Scallop theorem`: if a swimmer deforms in time-reversible way, then no net propulsion can be achieved in a low Reynolds context. A scallop is a bivalve mollusk that propels by actively opening and closing its shell. The motion involves two states: open shell (A) closed shell (B) and is time-reversible. The scallop performs a net motion only because of inertia. In a low Reynolds environment, the scallop could not propel, it would always come back to its original position.

The name Purcell gave to his theorem is irrelevant because scallops use jet propulsion (as many sea mollusks like octopuses or squids). However, figure 25 describes the idea Purcell had in mind during his conference. The main effect here is due to inertia: while the opening is done slowly to prevent motion, the closing is done quickly to create kinetic forces.

Therefore, according to this theorem, a reciprocal pattern movements (one that can be time-reversed) cannot work. Object or organisms with one degree of freedom can only produce a reciprocal motion and this is why Purcell suggested a simplistic 2 degrees-of-freedom swimmer that the community called the `Purcell swimmer` [101, 102, 103]. Though it has only two hinges, its motion pattern is not the most intuitive one.

5.3.2 *Micro Organisms*

In water, the Reynolds number of swimmers greatly depends on their size and swimming speed. For most of the organisms we know, this parameter is greater than 1. However, for micro organisms, it typically ranges below 10^{-4} (see table 4).

To counter this limitation, organisms had to find solutions to move in this environment. The most famous examples are the rotation of an helical flagella, used for instance by the bacterium Eschericha Coli, or the oscillation of periodic waves over the cilia that cover the surface of the cell.

In the recent years, many new discoveries were made about the motion of micro organisms or cells. This is the result of improving visualization methods (such as fluorescent microscopy) [104] or the ability to use an optical trap to measures swimming forces [105, 106, 107] at the micro scale. This set of tools allowed for a better understanding of the biological mechanisms and the forces in action. A comprehensive review of micro organisms motion in fluids have been written by Lauga and Powers in 2009 [108].

The basic elements of motion in micro organisms are based on long flexible appendages called flagella or cilia [98]. Though the two organelles are similar structurally, the beating pattern of the flagella is usually planar and similar to a propagating wave, whereas the beating pattern of cilia is more complicated and have 3D features. Cilia often exhibit power and recovery stroke. These appendages can also be rotated by motors located in the cell wall and lead to helical motion pattern (see figure 26).

Many micro organisms can swim forward and backward by reversing their flagella motion pattern. The flagellum is constituted by a micro-tubules cytoskeleton. The diameter of the flagellum is of the order of 20 nanometers for bacteria and 200 nm for eukariotic organ-

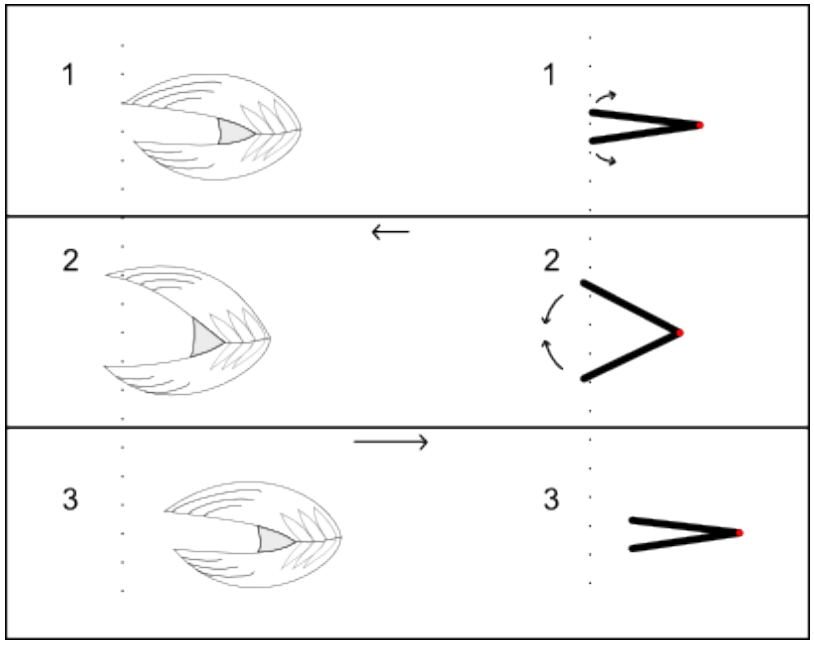

Figure 25: Sketch of the scallop theorem as described by E.M. Purcell initially. Since the scallop has only one degree of freedom (red hinge) it can only propel by creating kinetic energy in a turbulent flow. In (1) the scallop is initially closed and will slowly open its shell. This slow motion will move the scallop toward the left until it reaches state (2). At this point, the scallop quickly closes its shell, producing a strong turbulent flow, which will bring the scallop to the right (3).

Swimmer	Typical size (m)	Re number
Dolphin	3	10^7
Human	2	10^4 — 10^5
Jellyfish	0.2	10^3
Goldfish	0.05	10^2
Plankton	10^{-3}	10
Micro Organism	10^{-6}	10^{-5} — 10^{-4}

Table 4: Some examples for typical Reynolds numbers of various swimmers in water. The viscosity of water is $\mu \approx 10^{-3}$ Pa s. Typical swimming velocities are used.

isms and its length ranges from some dozens of nanometers to some millimeters [109]. The rotational or waving frequency of flagella vary but some organisms achieve roughly a resulting propulsion speed of 60 body lengths per second: E.Coli has a 1 μm diameter body and can propel at 30 μm/s [110] with a 100 Hz rotation speed while for Streptococcus an actuation frequency of 320 Hz have been observed [111].

5.3.3 *Hydrodynamic interactions*

In addition to other classical forces, immersed objects in a fluid experience `hydrodynamics interactions`. These interactions are the result of a flow created when an object moves in a fluid. This flow propagates through the fluid and other particles are therefore also affected.

The hydrodynamic interactions are long range interactions in a low Reynolds environment. Hence, swimmers are strongly affecting and affected by other objects, even when they are located far from the swimmer.

The result is that `collective swimming` is a frequent event at the nanoscale [108]. Two swimmers on a converging course will likely adopt the same direction as a result of the creeping flow equation [112]. For instance above a critical sperm density, spermatozoa have been observed to swim in cooperation [113].

Collective swimming also induces a beating synchronization for cilia: two nearby cilia will beat synchronously and in the same direction. On a large scale a `metachronal wave` is created: a traveling wave is propagating at the surface of the organism [114, 115].

Collective swimming receives a great attention nowadays in terms of observations or simulations [116, 117] since it cannot be neglected at the micro scale. The presence of a metachronal wave is responsible for the motion of the organism since it enhances the velocity and efficiency of liquid transport compared to a single cilia (see figure 27a).

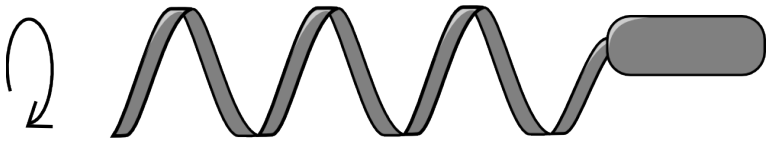

(a) Helicoid motion pattern

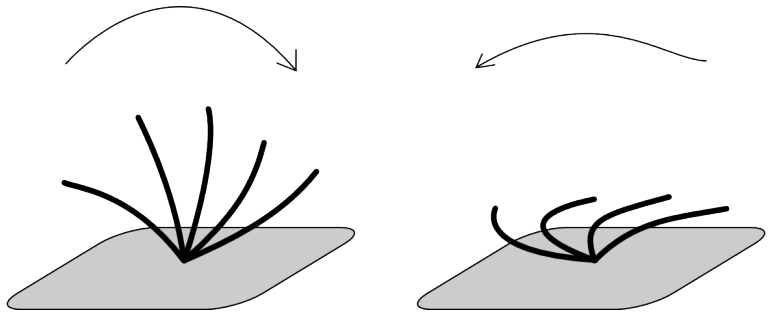

(b) Cilia

Figure 26: Motion patterns frequently used by micro organisms. (a) The corkscrew-like motion pattern. An helix tail is rotated by a motor clockwise or counter-clockwise which allows the organism to propel forward or backward. (b) A cilia (at the surface of larger organisms) performs a whip-like beating cycle. (Left) During the "power" step, the flagellum is stiff and stay linear. (Right) During the "recovery" step the flagellum is flexible and comes back to the initial position. This cycle produces a net transport of fluid parallel to the surface.

Another striking effect is the fact that swimmers interact with solid walls or boundaries as well. Boundaries affect the locomotion in three main aspects. The first one is the change of speed near a wall, which could be compensated by an increase of swimming power [118, 119]. The second effect is a change of trajectory and is more obvious for organisms with helical flagella: their trajectory changes from linear to circular near a surface [120, 121]. The third effect is a reorientation of the swimmer which will get the swimmer to swim parallel to the wall in certain case or to hit the wall in other cases [122, 123].

5.4 MICROFLUIDICS SIMULATIONS

5.4.1 *Artificial swimmers*

In 1951, Taylor [99] was one of the first who suggested a motion mechanism and to derive the resulting speed and direction. He analyzed the propulsion of an infinite plane sheet which lateral displacement was governed by a sinusoidal wave (see section 5.4.2). The conference talk Purcell held in 1976 [100] introduced the topic to a broad audience and presented the various problems present at a small physical scale. The non-reciprocity (scallop) theorem is one of them (see previous section 5.3.1), but swimmers also have to swim in a given di-

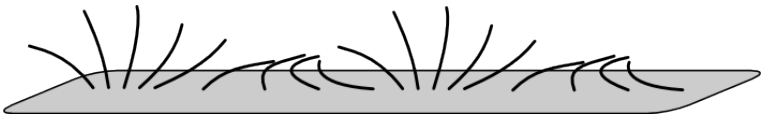

(a) Metachronal wave

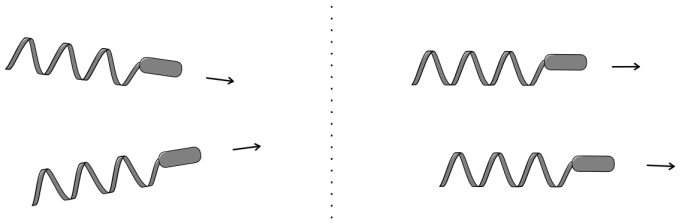

(b) Collective swimming

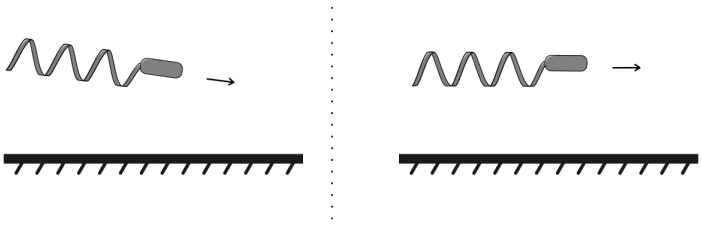

(c) Swimming near a wall

Figure 27: Proximity effects due to the micro hydrodynamic interactions. (a) Vicinal cilia will oscillate in coordination with a small phase difference. This lead to the creation of a metachronal wave. (b) Two swimmers in a colliding trajectory will adopt the same trajectory and swim together, and in phase. (c) A swimmer close to a wall will rotate to swim parallel to the wall.

rection against their environment and taking into account diffusivity: sometime it is better not to swim and to wait until diffusion brings you where you have an energy source (light or nutrients).

Many attempts where made in the field of modeling, theory and in experiments to produce artificial swimmers. Bioengineering and nanofabrication progresses have been enabling a completely new area of research. Several designs have been proposed and modeled and some of them have been tested. These designs fall into three categories. Deformable swimmers with a fixed number of degrees of freedom form the first group. The classical example was given by Purcell during his talk as a three-linked swimmer (a symmetric version will be described in section 5.4.3). The second category gathers swimmers with various parts which distance varies in time and phase over time; the shape of the various parts is also subject to change in some cases. The last category mimics nature and congregates swimmers with continuous degrees of freedom and continuous actuation

mechanisms. Bacteria with an oscillating cilia or rotating helical flagella are obvious representatives.

To create artificial structures that can perform micro robotic tasks in liquids has proven not to be easy and have mainly be investigated for magnetic field dependent swimmers [124, 125]. Some solutions involve DNA binding of magnetic particles to create a artificial flagellum [126]. Initial promising results were obtained for microscopic swimmers and propellers [127, 128, 129].

The appealing aspects of the approach described in this manuscript are that one can make much smaller structures and that the energy delivery into the swimmer, as well as its motion control, is done by light. This would allow for the actual physical realization of many of the theoretical micro robotic structures that have been proposed so far, as well as many new designs, should they operate in liquid environments or in air. While self-propulsion in liquids involves issues at low Reynolds number, for dry environments several forces have to be taken into account, including electro-magnetic, Van der Waals forces, and surface effects which dominate over volume effects. For a discussion on these issues, see, for instance [130]. In pioneering work, sub-millimeter moving elements were created, driven by either electro statical forces [131] or magnetic forces [132].

By taking advantage of the LCE properties, an autonomous, remotely controlled and powered device could be created. The highest oscillation frequency of a LCE-based cantilever observed is 270 Hz [133] which is comparable to the actuation frequency of the fastest living micro organism (see section 5.3.2). It is therefore possible to think about light driven micro robots performing tasks in micro channels. The following sections describe two simple models of micro swimmers and compare their swimming efficiency.

5.4.2 *Waving sheet*

One of the first model describing the evolution of organisms at the micro scale was published by Taylor in the fifties [99]. He analyzed the propulsion of an infinitely long planar sheet, oscillating in a transverse way immersed in a viscous fluid. He derived an analytical expression for the speed and discovered that two nearby sheets have to oscillate in phase in order to reduce the dissipated energy.

In the following we consider a sheet which is directed by the following equation:

$$y(x,t) = bsin(kx - \omega t) \tag{45}$$

where $y(x,t)$ is the amplitude at position x and time t, b is the wave amplitude, $2\pi/k$ the wavelength and ω the angular frequency. To

simplify the problem, the amplitude b is assumed to be small compared to the wavelength.

By solving the Stokes equations (42 and 43) and imposing a uniform and laminar flow far from the sheet in addition to the no-slip boundary condition, we get the following velocity U for the swimmer.

$$U = -\frac{1}{2}\omega k b^2 \tag{46}$$

Due to the symmetry of the problem, the speed is collinear with $\boldsymbol{e_x}$ so we get the following speed: $\boldsymbol{U} = -\frac{1}{2}\omega k b^2 \boldsymbol{e_x}$. When the wave propagates to one direction, the flow is following accordingly, but the swimmer propels in the opposite direction. Therefore, a swimmer heading to the left uses a wave that propagates to the right.

Here, the assumption that the wave is perfect and infinite was made. This results in a solution where the Reynolds number is not present, hence in a viscosity independent velocity. However, in practice the wave will strongly depend on the viscosity and the energy used by the swimmer.

A more realistic approach is to consider a finite sheet with a similar swimming behavior. This problem is a simplification of the way a spermatozoon would propagate in a two dimensional environment [134]. To reproduce an feasible object, the swimmer is attached by both ends and starts initially in a flat state. At t=0, it is allowed to deform and a propagating wave is sent through its body via the following equation :

$$y(x,t) = bsin(kx - \omega t)sin(x\pi/L)smooth(t) \tag{47}$$

where L is the separating distance between the two extremities and $smooth(t)$ a smooth step function that reflects a smooth time ramp.

The constraint at both ends could be interpreted as a LCE device attached in a micro channel. When actuated by light in a predetermined fashion, the shape deforms and gets into a wave like object. The sinusoidal control can be done remotely (light is modulated spatially in phase and intensity with an Acousto-optic modulator for instance) or locally by the use of photonic structures

Setting this device in a microchannel would allow to create a light activated micropump. Though there is a net transport of fluid from the left to the right, the simulation shown in picture 29 depicts the velocity of fluid near the device. The total volume (an arbitrary thickness of 1 μm is used for the third dimension) of water passing through the inlet is shown on figure 30.

If the device is not attached and can freely move, it would propel with a velocity proportional to the volume of water passing through the inlet (figure 30). There is indeed a reciprocity between both events as mentioned earlier. The swimmer's velocity is related to the amount

of water encountered along a given path during an oscillation period. Therefore, in the previous example a section of 2.5 μm^2 was analyzed (the cross section is arbitrary selected and forms the inlet), which resulted in a reciprocal speed of 0.17 μs^{-1}.

Nevertheless, getting a free swimmer with an continuously oscillating body might create some issues in terms of fabrication and control with light. The alternative suggested by Purcell (one alternative among many others) offers the advantage that the number of degrees of freedom is finite: therefore actuation can be done step after step.

5.4.3 *Symmetric Purcell swimmer*

The three-link swimmer (figure 31) is the simplest form of swimmer with discrete number of degrees of freedom that could propel (it offers two degrees of freedom).

This model have been investigated [101, 102, 103] and due to the lack of symmetry, a direction for the swimmer is difficult to find a priori. Numerical results indicate that the direction of net translation

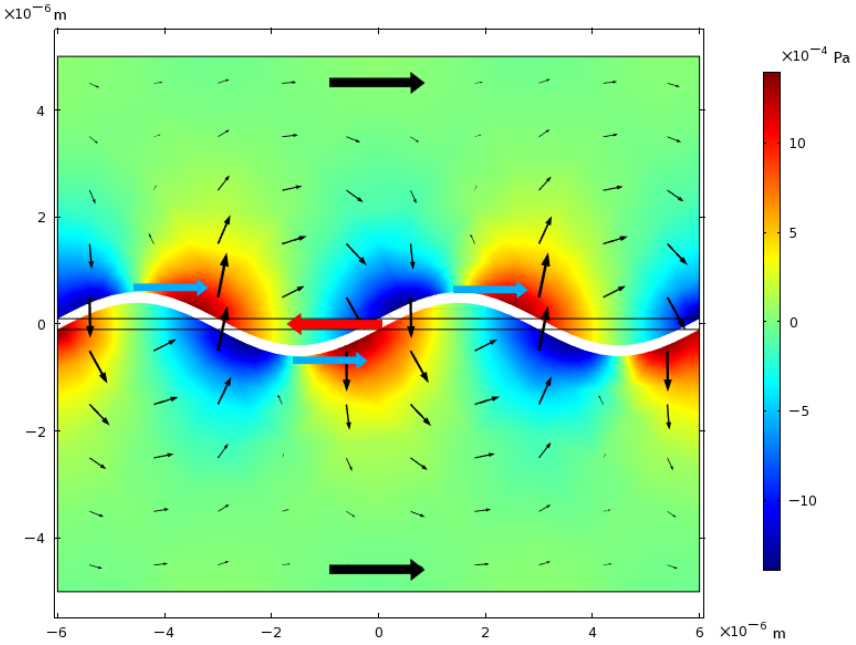

Figure 28: An infinite waving sheet is oscillating with a certain amplitude b, wavelength $2\pi/k$ and frequency ω. The wave propagates from the left to the right (blue arrows) and produces a net transport of fluid (black arrows). This transport becomes negligible in the far field (the two big black arrows show the average transport of fluid in the vicinity of the swimmer and are not scaled, while the small black arrows represent the local transport). As a result, the sheet moves to the left (red arrow). While the wave propagates it changes the pressure applied on the fluid (depicted through the color scale). (FEM simulation)

and the speed of Purcell's swimmer depend on the angular amplitude of the swimming strokes as well as on the relative length of the links [102].

A symmetric version (four-link swimmer) brings in a more intuitive way of understanding the motion. Here the swimmer can open a couple of legs at the same time (he cannot move only one leg). When a couple of legs is open, the drift introduced by a flow on the swimmer is reduced. Therefore, a given sequence of opening and closing legs will create an uneven drag on the device.

However, even if the direction seems to be intuitive to determine before hand, things are not so handy in practice. For motion pattern depicted in figure 32 for instance, the direction depends in fact on the amplitude and phase of the legs openings. This singularity has been reported in the literature [101] and have been independently confirmed here via FEM simulations. A complete investigation about the origin of this effect has yet to been made, but it already reveals the sensitivity of motion at the lower scale.

To reproduce a elastomeric swimmer with characteristic similar to finite waving sheet studied in the previous section FEM simulations have been carried out. The motion pattern follows the figure 32. The swimmer measures 6 μm in length, is 1 μm large and its legs are 1.5 μm long. To understand the efficiency of its strokes, the volume of water flowing around him is plotted on figure 5.4.2.

The volume of water around a fixed swimmer is proportional to the speed of a free swimmer in a fixed container. Therefore, a high volume of displaced water is a value of merit for the swimmer. Different amplitudes give different speeds and directions for this swimmer.

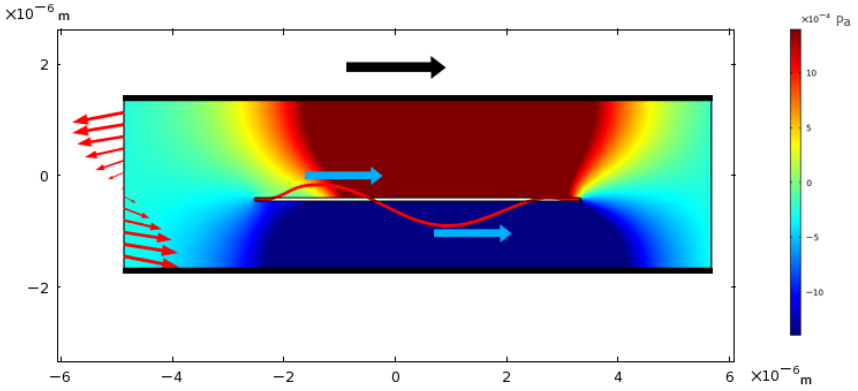

Figure 29: A bounded waving sheet is oscillating with a certain amplitude between two walls. The wave propagates from the left to the right (blue arrows) and produces a net transport of total fluid (black arrow). At the inlet, some fluid enters at the bottom while some fluid escapes at the top (the red arrows shows the velocity of the fluid). While the wave propagates it changes the pressure applied on the fluid (depicted through the color scale). (FEM simulation)

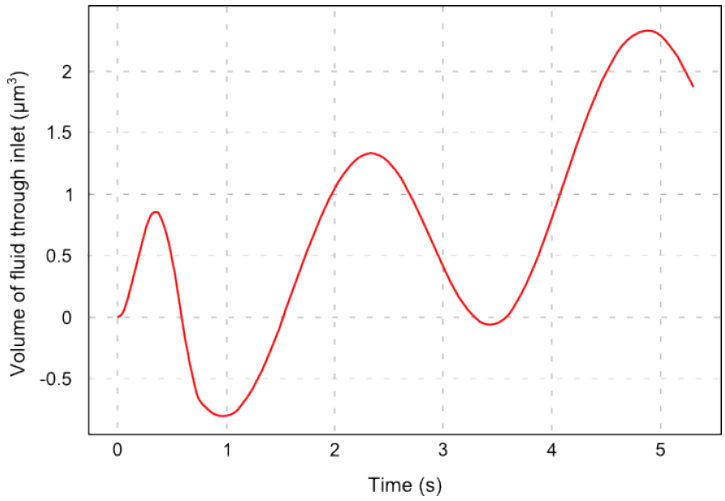

Figure 30: Volume of water flowing through the inlet of a channel for a finite oscillating sheet (ω = 0.5 Hz; b = 0.5 μ m, L = 5 μ m) in function of time.

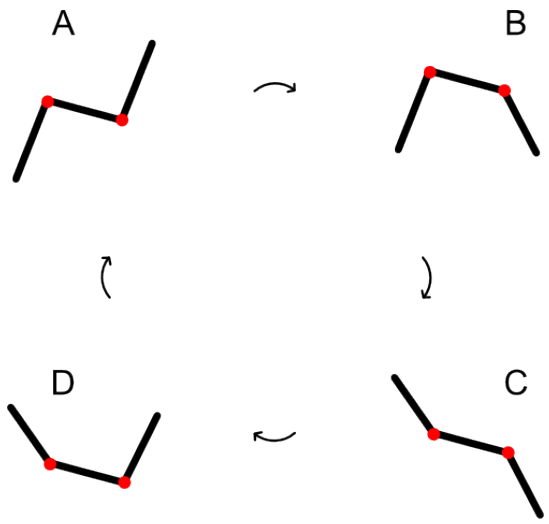

Figure 31: Simple three-link swimmer: the consecutive actuations of the arms cannot be reversed in time (A $\mapsto$ B $\mapsto$ C $\mapsto$ D $\mapsto$ A is different than A $\mapsto$ D $\mapsto$ C $\mapsto$ B $\mapsto$ A).

The ease of fabrication is balanced by a lack of efficiency since this swimmer is an order of magnitude less efficient than the oscillating sheet and by a strong dependence on the amplitude and stroke pattern used during the swim. For a similar amplitude of motion (the amplitude of legs being compared to the amplitude of the waving sheet), the speed of the symmetric swimmer reaches 0.01 μs^{-1} whereas it is 0.17 μs^{-1} for the waving sheet. The obvious drawback of this way of swimming is that the swimmer does two steps forward for one step back, a lot of energy is invested for a motion that brings it in the wrong direction.

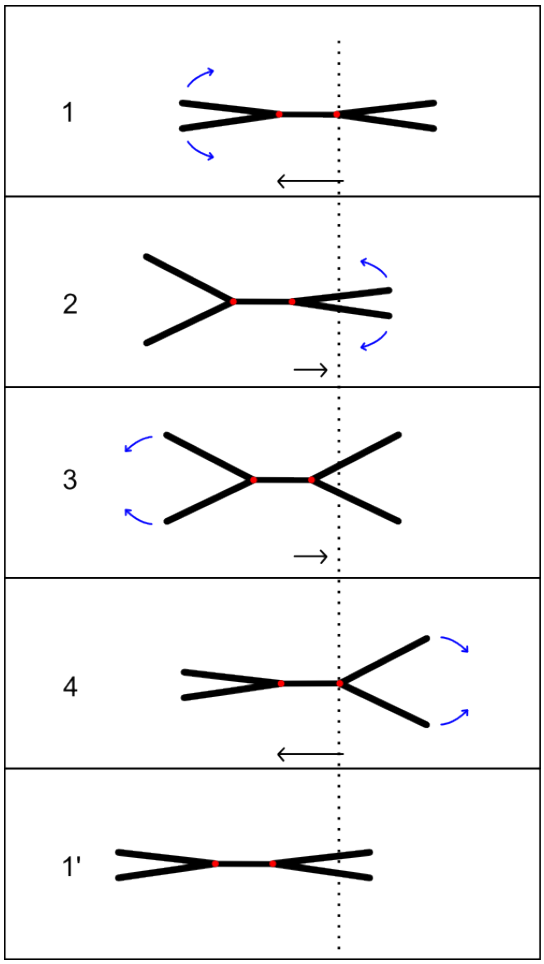

Figure 32: A symmetric Purcell swimmer performing a non-reciprocal motion. Because of symmetry, the object moves on a horizontal line. The black arrows demonstrate that the drift is reduced when legs are open. The motion hence shows a tendency to go to the right (two favored steps: $1 \mapsto 2$ and $4 \mapsto 1'$) rather than to the left (two unfavored steps: $2 \mapsto 3$ and $3 \mapsto 4$).

5.4.4 *Conclusion*

These two examples were modeled in order to understand what would be propulsion of a LCE based micro device in water. As mentioned in the preface, one can think of using bistability to create a micro motor, which in turn would be helpful to rotate, say, an helix.

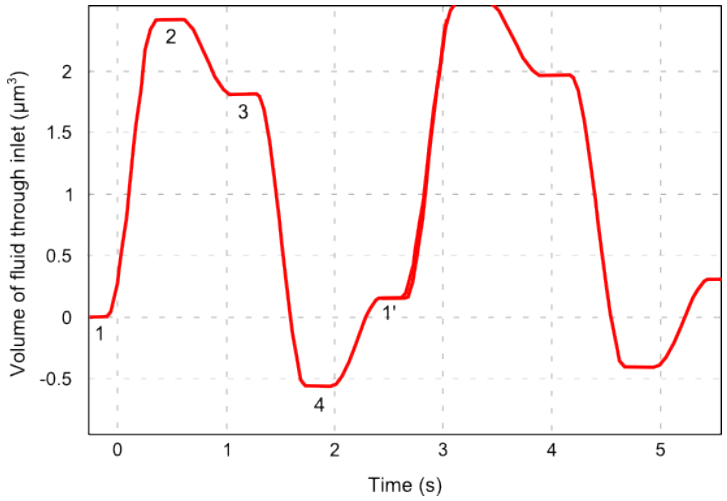

Figure 33: Volume of water flowing through the inlet of a channel for a symmetric Purcell swimmer (ω = 0.5 Hz; b = 0.5 μm) in function of time.

Part V

TUNABLE PHOTONIC STRUCTURE

We fabricate a light tunable plasmonic reflection grating on a liquid crystal elastomer. The azobenzene contained in the elastomer allows for reversible deformations leading to a modified pitch of the LCE embedded metallic structures. When the elastomer is excited, the reflection peak of the structure red-shifts, but when the light is turned off, the material comes back to its original configuration. Tuning plasmons depends on the incoming intensity and the tuning ranges from 0 nm to 100 nm shift with a 2 nm precision.

6 TUNABLE LCS

Everybody has talent, but ability takes hard work

— Michael Jordan

Liquid Crystal Elastomers can be used as micro devices in MEMS, but also to control the position of solid elements embedded at the surface of a material with a nanometric precision. Combining metallic nano structures and LCEs would offer a new capability to the previously static elements. While the fabrication of metallic objects with e-beam lithography is known and controlled, the integration in a bulk LCE is not straightforward. Their integration requires additional fabrication steps.

Getting plasmonic structures on top of a deformable layer brings up a new toolbox for applications which enables tuning of some properties.

6.1 NANOIMPRINTING OF METALLIC STRUCTURES ON TOP OF LCE

6.1.1 *Introduction*

During a classical e-beam lithography process, metallic layers are patterned on top of a non deformable solid substrate like glass or silica. Performing a similar process on a flexible, soft substrate is difficult for several reasons. This difficulties happen during the e-beam patterning but also during the evaporation of metals and from the limited stability to process chemicals (developer, lift-off etc.). A common way to overcome these limitations is to combine soft lithography with e-beam lithography [135, 136]. The various methods could be classified in three categories: printing, replica molding [137] and embossing (nano-imprinting) [138], most of them have been developed in the late nineties.

Replica molding is frequently used and is a process during which a pattern is transfered from a mold into another material (often a liquid which solidifies when in contact with the mold). Embossing is the printing of a pattern by pressing a mold onto a flat surface. Finally, printing is a material transfer from a mold onto a substrate.

Nanotransfer printing allows nanometer features to be transfered into the substrate, but also to control physical properties of this substrate more easily [139]. This fabrication technique is well suited for transferring small gold elements to fagile surfaces like liquid crystal elastomers.

This is the strategy that has been followed in order to embed periodic lines of gold into a free standing layer of liquid crystal elastomer.

While the control over the mesogen alignment cannot be made with a high precision, the position of the embedded elements is quite reliable. Gold, because of good optical properties in the visible and near infrared region, is the metal that has been used for the fabrication of the nanostructures described in this thesis. We will therefore concentrate our description to this material.

The fabrication involves different liquid crystal alignments and therefore different methods to process the samples. After a listing of the possible issues and limitations which could occur from a direct lithography, a solution to transfer nano objects to a LCE film is detailed.

6.1.2 *E-Beam lithography and Liquid Crystal Elastomers*

To get nanometer size active objects, the first idea one could think of, is the application of E-beam lithography (EBL) to polymerize only a small area of LCE. EBL involves the use of electrons to chemically change the properties of a resist. The method is similar to photolithography (see section 4.1.1) but the energy involved by electrons is much larger than in the case of photons. Using electrons to trigger a polymerization in liquid crystal elastomers is feasible in theory but has not been investigated. It is probable that the high energy brought by the electron would damage the polymer network, reducing the hyper-elastic features.

It is also feasible to prepare metallic structures on top of LCE by the use of lithography. However, the low electronic conductivity would increase charging effects in the resist, therefore decreasing the achievable resolution. Another point to take into consideration is that the resist layer needs to be as flat as possible during the exposition to increase the control over the desired geometries. This involves a spin coating of the LCE layer (if used as a resist) and thus prevents a prealignment of the liquid crystal moieties. Finally the development and lift-off processes both involve strong solvents which will probably interact with the LCE material if they don't completely destroy it. In practice this solution is not realistic.

Another more energetic approach when it comes to nanofabrication is called Focused Ion Beam (FIB) milling which is used for ablation. Ions are bombarding a material with the objective of breaking chemical bonds and detach molecules at the focal point. Commercial systems easily reach a sub-10nm resolution.

However, the use of FIB milling on LCEs does not allow such performances. Because of the low electrical conductivity of the material, a strong charging effect prevents reproducible work conditions and good resolution. Localizing a definite position and focusing on the surface becomes really troublesome. In addition to that, as previously said, the high energy brought with ions will most likely limit the me-

chanical properties or destroy the azobenzene dyes withing a certain area near the focus.

A better way to cut a LCE is to use a tightly focused laser beam which will bring enough energy so that it can cut the material (see picture 34). This technique also allows a 3D process. Though this technique does not have a better resolution than photolithography, it offers a simple alternative where activation mechanism is not destroyed.

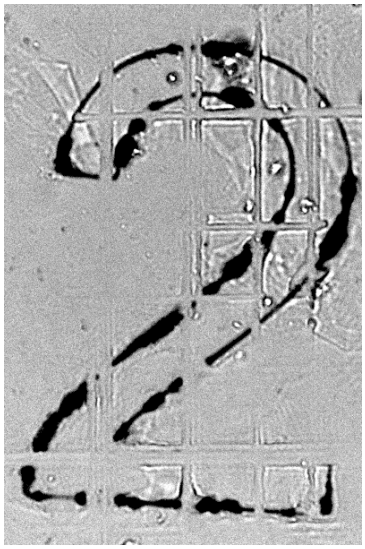

Figure 34: Some lines were removed from a 2μm-thick LCE structure. A 532nm laser was focused through a 100x Objective (NA 1.4) with an incoming power of 24mW. The width of the structure is 10 μm.

Getting a nanostructure together with a LCE material is therefore not easy but could still be achieved with a method similar to `nano-transfer printing`. The method is described in the following section and involves two steps. The first one is a classical e-beam lithography fabrication on a solid substrate, and the second one is very similar to the LCE fabrication where a cell is used to host the LC monomer before polymerization. One glass of the cell is covered by the nano structures which will be embedded in the LCE. This method allows to keep an alignment for the liquid crystal and get high quality metallic elements.

6.1.3 *Gold adhesion to other surfaces*

When gold structures are prepared with e-beam lithography, one of the main issues is their weak adhesion to inert and commonly used glass and silica substrates. The use of adhesion layers like metals such as chromium [140] or polymers such as SU8 [141] is often recommended.

However gold could also be functionalized by the use of self assembled monolayers (SAM) which will increase the anchoring between polymeric materials and functional groups (this is the case for instance of thiols) [142]. This allows to increase the adhesion between gold and a liquid crystal elastomer polymer.

These two properties could be used to transfer gold from an initial layer (like glass) where adhesion is weak to a second one (LCE) where adhesion is promoted through the use of surfactant. In addition to that, if the metallic nanostructures are build on top of a sacrificial layer, the removal from the substrate is further enhanced. Both methods have been used in concert to successfully detach and embed gold patterns into LCE as described below.

6.1.4 *Metallic nanostructure transfer to LCE*

In order to transfer gold from one substrate to another, as previously mentioned, the key step is the use of a PVA sacrificial layer in the e-beam lithography recipe. A 100nm layer is spincoated on top of a ITO coated glass. The adhesion between ITO and PVA could be an issue if the PVA solution is not pure enough and if the spinning rate is not optimized. Any dust or inhomogeneity present in the PVA would lead to a "comet" if the speed is not adjusted. For a PVA solution with 1% concentration we used the recipe described in table 5, followed by a baking step of 5 minutes at 80°C degrees.

Speed (rpm)	Ramp (s)	Dwell (s)
200	0	3
500	3	2
5000	3	10

Table 5: PVA (1% concentration) spincoating recipe - 100 nm layer

PVA is soluble into water but not into MIBK/IPA the developers nor in Dichloromethane, used during lift off to remove the PMMA. However, its chemical structure could be altered when electrons are bombarding its surface. To prevent this molecular change and to keep PVA water-soluble, a 50nm protective layer made of silicon oxide was evaporated on top. This acts as a barrier to prevent electron diffusion through the sacrificial layer.

Then, a 250 nm PMMA layer is spincoated on top and regular e-beam lithography fabrication is pursued. The dose is adjusted to expose the PMMA all way down till the SiO_2 layer. Finally a thermal gold evaporation and lift-off procedure is applied. The final sample has 50 nm thick gold nanostructures laying on a 100 nm PVA layer (itself covered by a thin 50 nm SiO_2 layer). If one would plunge the

sample in water at this moment, the gold would simply be detached from the glass.

Prior to embedding the nanostructure into the LCE, a functionnalization of the gold is made by plunging the sample for 12 hours into thiols (11-Mercaptoundecanoic acid - Sigma Aldrich) dissolved in ethanol. The molecules will cover the gold and help the adhesion with the liquid crystal chains. This substrate is used as one side of the cell in which LCE infiltration will be made.

This cell will host the LCE in isotropic and nematic state before its polymerization. Traditional alignment techniques involve surface treatment of the substrates of the cell (see figure 18) and surfactant coating (the interested reader can discover more in the review about photoalignment techniques from Ishimura [143]). It is usual to treat both sides of the cell, however, in the present situation, only one face can receive a surface treatment. The side which result from EBL cannot be engineered: its surface must be flat for a precise lithography, and in addition it is coated with SiO_2. Therefore, only one side of the cell can be treated, consequently reducing the alignment properties.

However, the second side of the cell can be subject to various actions. To achieve a planar alignment, a PVA layer could be coated on the second substrate and rubbed (see figure 35a). We refer the reader the section 4.2.1 and 4.3.3 for more details about that technique.

To get an homeotropic alignment, a surfactant such as PI is used: on top of a PVA layer, 15 μm photoactivable polyimide (Fujifilm Durimide 7020) is spincoated. This layer is softbaked at 110°C degrees for 5 minutes then photoactivated with UV at 10 mW for 15 minutes: indeed LCE are known to align homeotropically to the PI surface if it has been illuminated long enough by a normally incident beam (see figure 35b).

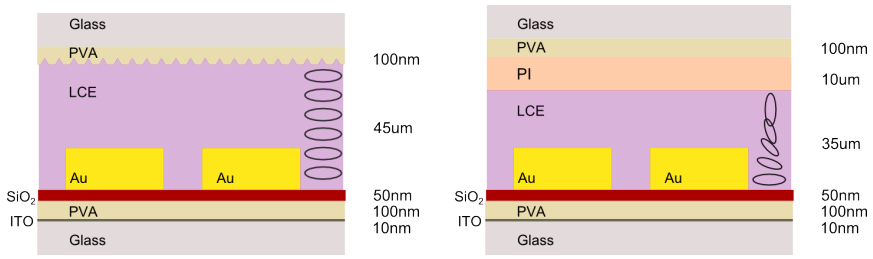

(a) Planar Uniaxial alignment case (b) Hybrid alignment case

Figure 35: Two representations of the cell used for nano transfer printing of gold structures into a LCE layer. (a) By rubbing the surface of the top layer of PVA, a planar alignment is created. (b) By adding a polyimide layer on top, the LC will align perpendicular to the surface.

Similar to section 4.3.3, spacers (45μm) are used between the two glass slides to create the cell. Liquid Crystal Elastomer is then infiltrated in the isotropic state, at 120°C degrees into the cell. To align

uniformly the mesogens, a slow cool down (1°C/min) is necessary until reaching the nematic state at 40°C degrees, temperature at which the sample is kept for 24 hours. UV radiation (10mW) is applied twice, for 2 minutes, first on the side containing the gold structures, then on the opposite side.

The opening the cell is facilitated by the soluble PVA layers. Keeping the sample in warm water (90°C degrees) while applying a gentle shaking for two hours is enough to dissolve most of the sacrificial layers and open the cell with a blade. Removing the polyimide layer is not feasible without the use of strong solvents which would damage the polymeric film, therefore the resulting LCE film is still attached to a polyimide layer of 10 μm (see picture 36).

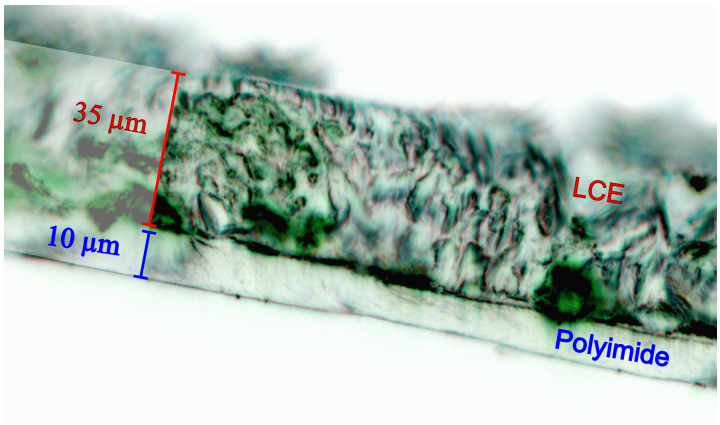

Figure 36: Crosscut microscopy picture showing the LCE and the Polyimide layer after polymerization and removal from the cell. The homogeneous material below is the polyimide (10μm), at the top sits the LCE layer (35μm).

Since the rigidity of this layer strongly affects the deformation, using a thinner layer would be a better strategy. However, surface effects depend on the thickness of the layer to some extent [143], therefore one needs to find a good trade-off between the alignment efficiency and the surfactant thickness.

6.2 PLASMONIC GRATINGS

6.2.1 *Introduction*

Tunable plasmonic devices are widely awaited for many applications due to their ability to selectively work at different wavelengths. Such properties could be useful in different fields such as ultrasensitive Raman and fluorescence sensors [144, 145]. Tuning could be useful if the range is broad enough (more than 50 nm) but also fine enough (down to 5 nm) which is crucial for plasmonic resonances.

People have already suggested several solutions allowing an active tuning of the plasmonics response, either by tuning the plasmonic element itself or by changing the substrate properties. The substrate can be adjusted mechanically [146, 147, 148], electrochemically [149], electronically [150] or optically [151] and modification of the active element can be addressed optically [152] or by infiltration [153]. Another investigated solution uses gold nanoparticles (here the plasmonic device) coated with polymer brushes which are heat activated and change shape[154].

Among these strategies, only a few allow a fine reversible tuning of a plasmonic resonance over a broad range. In this chapter we report on the fabrication of gold nanostructures embedded in a light-active liquid crystal elastomer. When the LCE is illuminated by a laser, the material not only changes its absorption and birefringence properties but also deforms under the internal stress created by the molecular reorganisation. These three effects combine into a highly efficient tuning environment for plasmonic structures. By the use of a remote control (laser light), it is possible to finely modify the distance between different elements and to change the refractive index of the material which results in a large tuning capability.

6.2.2 *General theory diffraction gratings*

Gratings are optical components which use periodic elements to diffract light and produce constructive or destructive interferences. Because of these interferences, for a given wavelength, light intensity will be higher for some selected directions. These special angles depend upon the wavelength hence different colors will propagate differently: the grating is a dispersive element.

The periodic property of a grating may result from one or several properties from the material: transmission, reflection or refraction. For a given angle of incidence, the angles of maximum intensity transmitted from the grating are defined by integer numbers and called `diffraction orders`. The grating equation, known as the `Snell-Descartes law`, gives the angle of maximum reflection for a wave incoming with a certain θ_i angle on the grating [155].

$$d(sin(\theta_i) + \sin(\theta_m)) = m\lambda \tag{48}$$

where θ_i is the incidence angle, θ_m the angle of the m-th order and d is the pitch of the grating.

But gratings at the surface of a metal are also often used to couple a plane wave into Surface Plasmon Polaritons (SPPs). When certain conditions are met, the electrons within the metallic bars are polarized by the incoming wave and enter in resonance. They create a surface

plasmon resonance, which is a collective oscillation of electrons. This effect is used to probe properties of materials at a nanometer scale.

6.2.3 *Gratings and Surface Plasmons*

While Wood was observing the diffraction of a continuous light source through a metallic grating in 1902 [156], he observed in the spectrum what was considered, at the time, as anomalies. For p-polarized light, he was able to find very narrow peaks of minimum illumination. For s-polarized light, however, these effects were not noticeable. The soon called "Wood's anomalies" received a lot of attention since then, and the experiment is considered to be the initiator of the research field studying SPPs.

In 1907, Rayleigh was the first to offer an incomplete explanation for these anomalies [157, 158] followed some years later by a theoretical breakthrough from Fano in 1941 [159]. However the interaction of plasmons and gratings was better understood in the late sixties [160, 161, 162] thanks to the use of lasers and to the production of holographic gratings for scientific purpose. For a deeper insight about Wood's anomalies history, we refer the reader to Maystre [163].

When an incoming wave interacts with a metal, it gives rise to the excitation of the electrons within the metal. For some wavelengths and polarizations, this excitation will be resonant with metallic lines. The result is a surface plasmon (a collective oscillation of electrons) and an increase of reflection for properly designed geometries.

Picture 37 illustrates this. A normal incident plane wave is simulated and interacts with a periodic gold grating. The grating is embedded into a dielectric (LCE) domain and the incoming wave propagates in the air. The simulations have been performed by Jan Renger using a `multiple multipole method` (using OpenMaX software).

When a plane wave hits the grating, several effects occur among which the constructive interference of the scattering by the grating lines which leads to the common diffraction orders. In addition to these events, a Localized Surface Plasmon (LSP) is also created when the light interacts with the metallic structure. The wave vector, the bars width and the refractive index contrast are of particular importance to give rise to a LSP. For an excitation wavelength of 800 nm with normal incidence, a gold line with a 200 nm width will allow the grating to enter in resonance. Different regimes are visible. A plasmon wave is created for a 800nm excitation at the interface between gold and air where the refractive index match the half-lambda resonance condition. In the substrate, the refractive index is of the order of 1.5, the resonant wavelength is blue-shifted to 600 nm.

Depending on the pitch of the grating, these half-lambda dipoles will interact and prevent or enhance light diffraction and reflection. For a pitch of 800 nm, these interactions impact on light propagation

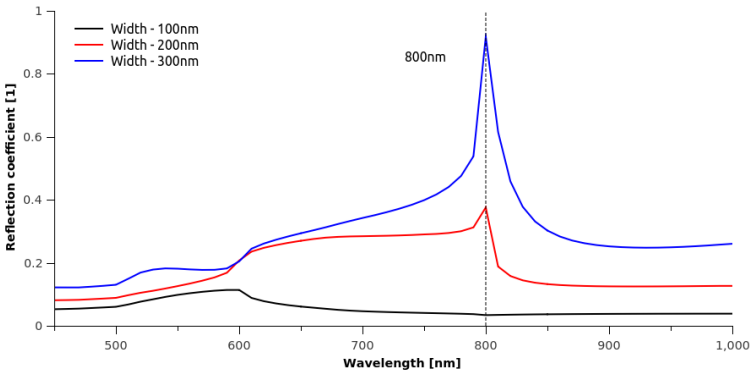

(a) Reflection coefficient - Gold in glass

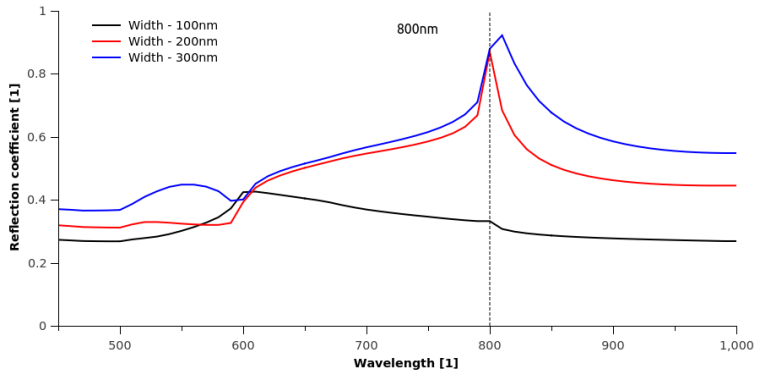

(b) Reflection coefficient - Gold in LCE

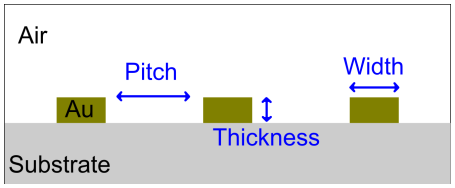

Figure 37: Reflection spectrum of several plasmonic gratings illuminated by a plane wave with normal incidence. The grating pitch is 800nm and has a 50nm thickness. The simulation is made for different line widths. (a) The gold grating is embedded in glass. (b) The gold grating is embedded in LCE.

and lead to a peak of intensity for reflected light. This behavior can be seen on the electromagnetic field observed at the vicinity of the grating on figure 38.

6.2.4 *Gratings fabrication and defects*

Gratings have been fabricated and transfered in a LCE layer in order to control their properties and to change their optical response. The contraction or expansion of the film resulting from a laser illumination would change the distance separating the metallic lines. The

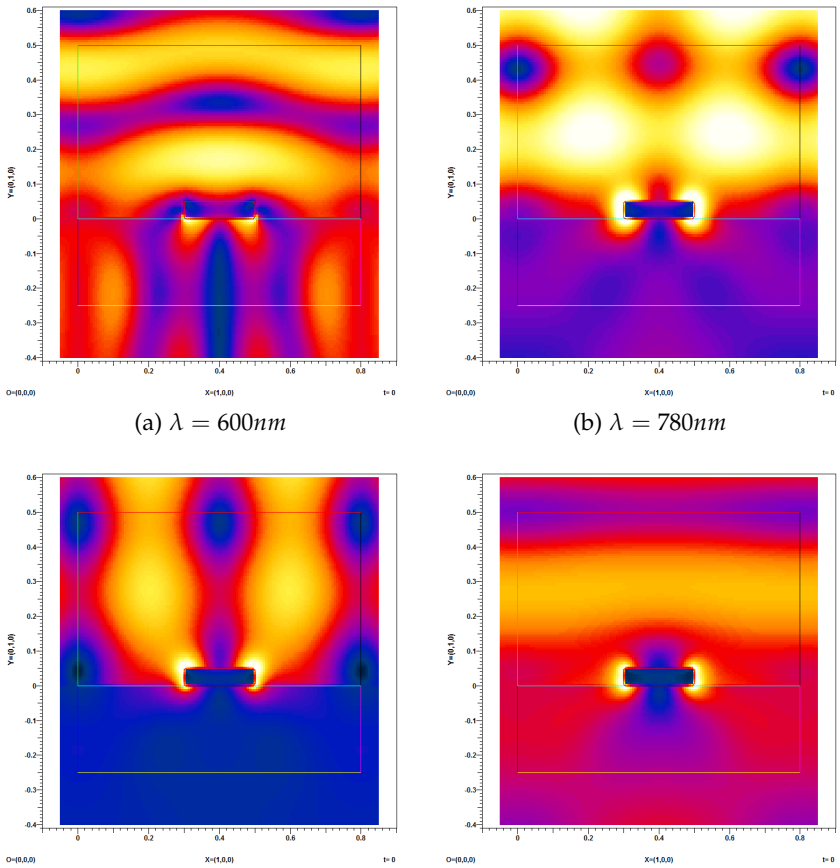

(a) $\lambda = 600nm$ (b) $\lambda = 780nm$

(c) $\lambda = 800nm$ (d) $\lambda = 900nm$

Figure 38: The electromagnetic field is represented in the vicinity of a plasmonic grating. The grating is made out of gold and lays on glass. A normal incident p-polarized wave is interacting with the system for different wavelengths. The pitch of the grating is 800nm and it extends infinitely out of the plane. The color scale represents the intensity of light. (a) When $\lambda = 600nm$ a standing wave is created in the substrate by counter propagating waves. This standing wave impacts on the reflection coefficients. (b) and (c) When $\lambda = 780nm$ and $\lambda = 800nm$ a standing wave is created at the air interface, and again, the reflection coefficients are changed (d) When $\lambda = 900nm$ no resonance occur and light propagate through the interface.

fabrication and transfer of the gratings are critical steps which require a good control.

Following the simulations presented earlier (previous section 6.2.3), gold gratings have been designed and fabricated by electron beam lithography to enter in resonance at 800nm. The initial gratings were made with gold on a sacrificial PVA layer. A surface of 50 microns by 50 microns was covered with lines of 200 nm width, 50 nm thick and with a pitch of 800 nm (see the scheme located at the bottom of figure 37).

These gold structures are latter embedded in the polymeric active host by using nanotranfer printing as described in section 6.1.4: the glass with the gold structure will be used as one side of a cell in which the LCE will be infiltrated prio to polymerization.

Within this cell, two liquid crystal alignments can be prepared. For a planar uniaxial alignment, the second side of the cell is coated with PVA and its surface is mechanically rubbed. (see 35a). In order to get an hybrid alignment, the second side of the cell is coated with polyimide and UV-illuminated for 15 minutes (see 35b).

Finally the cell is open and the film is detached from the solid substrates (see previous section 6.1.4). The resulting sample is a free standing LCE film, with gold gratings embedded in its surface.

Several issues can occur during this process. The most common is caused by a weak adhesion to the LCE substrate. The choice of thiol as SAM to increase adhesion has been driven by empirical observations. However, while most of the gold is transfered using this method, it is frequent to see missing lines of gold in gratings (see figure 39a). This problem does not impact on measurements because it is local: one can always find an area where all the lines have been transfered.

The second issue is due to mechanical stress occurring within the LCE layer during the polymerization and when the cell is opened. Indeed, the polymerization of the film is made in a closed environment and the cross linking density evolves in time until a stationary limit: this can lead to the creation of cracks. Later, when the cell needs to be opened, it is heated to 90°C degrees. The heat expansion can also generate fissures and cracks.

These cracks cannot be avoided with the described methods and are found globally on the samples (see figure 39b). In theory, the signal to noise ratio of the optical measured response is affected, but in practice, the difference between two areas with different crack densities is not noticeable. .

Finally, when the film is detached from the glass substrate and kept at room temperature, it changes shape and is not flat anymore due to internal relaxation. The resulting film is usually curly, and this curling is not homogeneous. Therefore the distance between lines changes slightly when compared to the grating obtained after EBL, and this change might be different at every position. The optical response resulting from this heterogeneity is a broadening of resonance peaks.

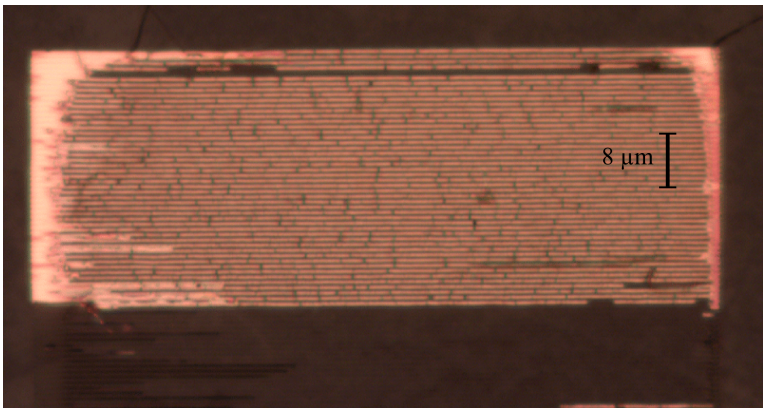

(a) Microscopy picture of a gold grating in a LCE film

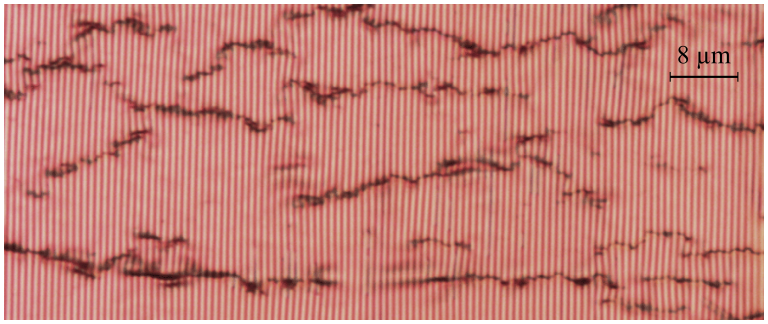

(b) Defect at the surface of the grating after opening the cell

Figure 39: Microscopy picture of a gold grating in a LCE film. (a) Not all the gold is transfered, some lines are missing from the LCE bulk (dark area). (b) During the peel-off the LCE layer from its solid surface, the gold is undergoing a stress that creates fissures along the grating lines.

6.3 TUNABLE GRATINGS

6.3.1 *Mechanical stretching*

As the nanostructures are embedded in a polymer matrix, they are constrained to follow any motion the host will have. Thus, a passive or active deformation will induce a plasmonic detuning because of spatial changes. LCE being hyperelastic by nature, they have a broad elastic range.

It is practically easier to pull a film than to compress it. A mechanical traction on the elastomeric film will tune the grating in various ways depending on its relative orientation to the expansion. During a deformation, the LC director rotates to reduce the strain induced stress [164, 165]. This director change will consequently modify the optical properties of the medium but the stronger effect on the plasmonic grating will come from the spatial spreading.

If the substrate is pulled in such a way that the grating lines are perpendicular to the deformation vector. The pitch between the lines will

increase, they will go away from each other. This leads to a redshift of the optical response (wider pitch corresponds to longer wavelengths). The material can be reversibly elongated while it stays in the elastic region (see figure 7 page 19). Therefore, there is a maximum reversible extension of the grating, noted δ_e.

Reciprocally, if the film is pulled with a deformation vector parallel to the grating lines, then the strain associated to the volume conservation will get the lines closer to each other. It leads this time to a blue shift, because the pitch has decreased. Reversibility considerations also characterize the maximum pitch change due to a contraction δ_c.

For various angles and amplitudes of deformation, the change of pitch will span over $[-\delta_c; \delta_e]$. For the elastomer prepared according to the recipe presented on table 2 (page 41) the maximum reversible elongation of a 45 μm thick film is 10%. Within that elongation, the pitch of the grating can be changed as much as [-10 μm; 50 μm] (see figure 40).

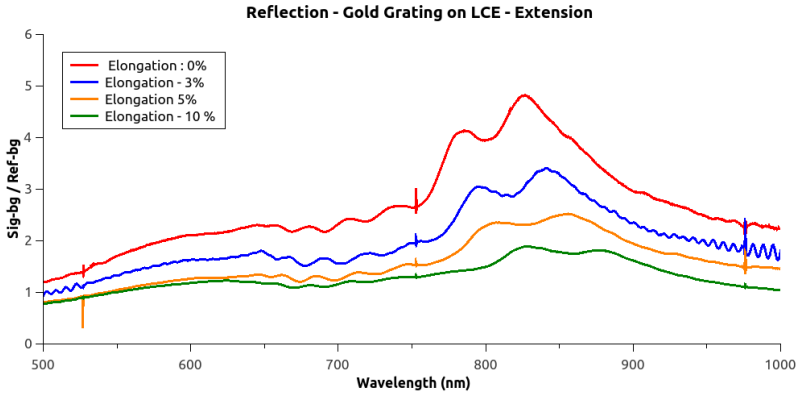

Figure 40: Passive stretching of the liquid crystal. Reflection spectral measurement after strain

The reflection spectrum of a grating submitted to a normal stretching is shown on figure 40. The lines are going away from each other, the pitch is increasing and therefore a redshift is observed. At the same time a broadening of the peak occurs, probably caused by a heterogeneous spreading of the lines. The various polymer chains are entangled differently.

During the expansion (δ_e), the pitch variation (δ_P) is linear and we have approximately the following: $\delta_P = \delta_e/2$. This could be explained by an inhomogeneous pulling. Both sides of the film were glued on a moving slit, so the clamping might be too soft.

This mechanical passive tuning is reversible and reaches a 5% change (a 50 nm shift has been achieved). Even though Baumberg reached a 60% reversible tuning with a different technique [147], the possibilities offered by LCEs go beyond that. The samples prepared and described in this thesis could be extended by only 10%, but with a better control on the fabrication, people are creating LCEs which can

deform up to 500% [5]. Hence, with an better fabrication process it would be theoretically possible to get a very broad reversible tuning.

6.3.2 *LCE activation by light*

The tuning of the grating could also be done by activation of the polymeric host by light. The excitation of the liquid crystal elastomer layer will change the azobenzene molecular conformation, therefore leading to a birefringence change from the host material and to a geometric change. Depending on the LCE alignment and polarization of the incident light relative to the azobenzene electrical dipole moment, the pitch of the structure will be reduced or increased. In a similar fashion as what was just explained, the reflection peak will be red shifted or blue shifted.

A set of experiments has been done on a free standing film. As explained in section 6.1.4, a film is detached from the glass substrate and consequently is not attached anymore to any solid substrate. In order to observe the sample through an inverted microscope this layer is placed on top of an open slit which acts as a support (see pitcure 41).

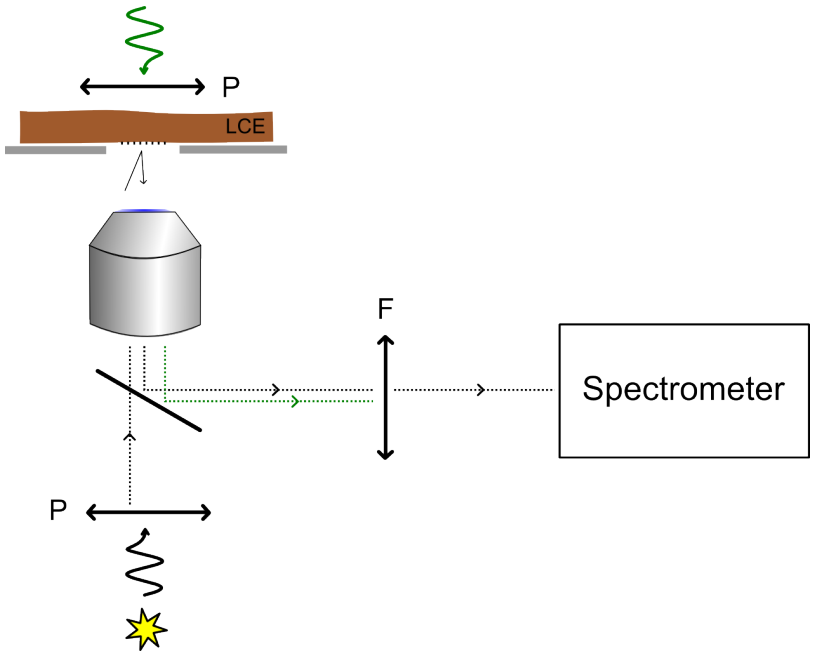

Figure 41: Scheme of the setup used to measure a reflection spectrum. A white light source (bottom) is used to probe the grating in the LCE film. This light is p-polarized. A 532nm exciting beam (top) is used to activate the layer and create a contraction. The reflected light is 532nm-filtered and sent to a spectrometer.

A TM-polarized plane wave is illuminating the structure, and the reflection spectrum is collected by a low-NA 4x objective and sent onto a spectrometer. Excitation of the sample is made in transmis-

sion with a laser. The laser is polarized before illuminating the sample, and filtered before entering the spectrometer. A 10 mW, 532 nm, diode laser was used and the polarization was either parallel or perpendicular to the structures.

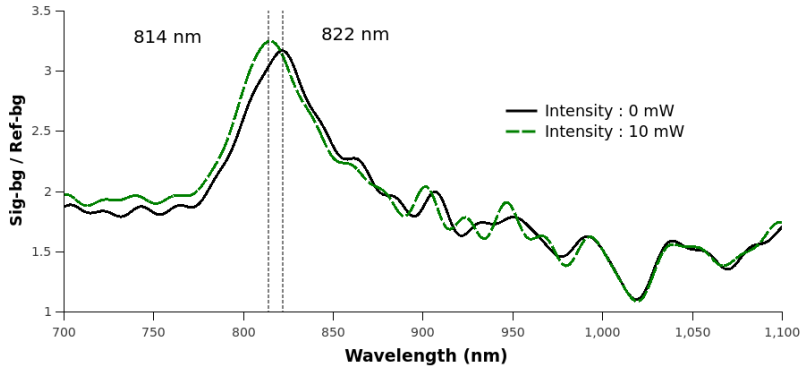

Figure 42: Reflection spectrum showing an active tuning of a plasmonic grating: the metallic lines are observed in reflection and the planar-uniaxial LCE is excited with a p-polarized light.

A first set of measurement have been collected with an excitation light polarized parallel to the structure (TE case), and a second set was collected when this excitation laser was polarized perpendicular to the grating (TM case). Two samples have been prepared and measured: one sample was uniaxially aligned and the other had an hybrid alignment. On each sample, different gratings were present with pitch of 600 nm and 800 nm.

In the prepared samples the azobenzene orientation is perpendicular to the main orientation of the liquid crystals. These liquid crystals being aligned parallel to the grating lines, the dyes are in consequence oriented perpendicular to the grating lines. As the dyes are preferentially excited when the polarization of light is collinear with their dipole moment (see section 2.2), the detuning is polarization dependent.

The detuning observed in figure 42 is only visible when the 532 nm is polarized perpendicular to the grating. The additional peaks appearing above 850 nm are artifacts due to thin-film interferences in this region (the LCE is not absorbing above 700 nm). This mechanism shows that when energy is absorbed by the LCE film, the pitch can be shrunk by 1%.

Sonho que se sonha sozinho é apenas um sonho.
Sonho que se sonha junto é o começo da realidade.

— Hélder Câmara

CONCLUSION

Through this thesis, techniques of micro and nano fabrication involving liquid crystal elastomers have been presented. A micrometer is a useful scale for LCE applications since the current efficiency of material requires a strong focus laser beam. Therefore, working with micrometer scale structures seems to be a fair trade-off between technological and material-wise limitations.

We hope to have convinced the reader that fabrication using direct laser writing (micrometer scale) or nano imprinting (nanometer scale) are feasible and can serve as efficient tools to produce active building blocks for the MEMS industry or more simply to access properties at the nanoscale that have never been reach before.

The current development of 3D printing is not only occurring at the macroscopic scale, but also under a microscope, with environment-sensitive materials. This thesis is an attempt to demonstrate the importance of getting more knowledge about liquid crystal elastomers to perform tasks at the nanoscale. Many challenges remain to operate more accurately and efficiently the material, but great hopes could be founded on it. One can think of building a light powered micro motor (using photonic crystals to reach bistability) and to embed it into any kind of vehicles or robots at scale never achieved yet.

GLOSSARY

3D	three dimensions. 31, 35
1PA	one-photon absorption. 39
2PA	two-photon absorption. 31, 33, 35–37, 39, 42, 43
Acousto-optic modulator	An acousto-optic modulator (AOM), also called a Bragg cell, uses the acousto-optic effect to diffract and shift the frequency of light using sound waves (usually at radio-frequency).. 64
coasting distance	The distance an moving object subjected to inertial forces will keep following after the driving force is removed. 57
EAP	Electroactive polymers. 3
EBL	E-beam lithography. 74, 83
Eutectic mixture	a mixture of several chemical compounds that solidifies at a lower temperature than any other composition made up of the same ingredients. 41
FIB	Focused Ion Beam. 74
incompressible flow	In fluid mechanics or more generally continuum mechanics, incompressible flow reers to a flow in which the material density is constant within a fluid parcel - an infinitesimal volume that moves with the velocity of the fluid. 53
ITO	Indium tin oxide. 37, 76
Kinetic chain length	is the average number of monomer units consumed for each radical initiator that begins the polymerization of a chain and is a more general development of the average degree of polymerization. 43

Lagrangian description	In the Lagrangian description the position and physical properties of the particles are described in terms of the material or referential coordinates and time. In this case the reference configuration is the configuration at $t = 0$. 16
LC	Liquid Crystal. 38, 40, 41
LCE	Liquid Crystal Elastomer. 4, 15, 31, 36–38, 40, 44, 79, 84
LOC	Lab-On-a-Chip. 3
LSP	Localized Surface Plasmon. 80
MEMS	Microelectromechanical systems. 3, 4, 73
mesophase	In physics, a mesophase is a state of matter intermediate between liquid and solid. 8
MPA	multiple-photon absorption. 33
NA	numerical aperture. 35
Newtonian fluid	In continuum mechanics, a fluid is said to be Newtonian if the viscous stresses that arise from its flow, at every point, are proportional to the local strain rate. 55
NIR	Near-Infrared. 39
photoresist	Polymeric coating that is designed to change properties upon exposure to light. 31
PI	Polyimide. 37, 77
PLC	Polymer Liquid Crystal. 7, 8
POM	Polarized Optical Microscopy. 42
PVA	Polyvinyl alcohol. 37, 42, 76
SAM	self assembled monolayers. 76, 83
SPP	Surface Plasmon Polariton. 79, 80
steric hindrance	Steric hindrance occurs when the large size of groups within a molecule prevents chemical reactions that are observed in related molecules with smaller groups. 8
voxel	is small defined region of the space in three dimensions. It is equivalent to a pixel (two dimensions). 4, 35

BIBLIOGRAPHY

[1] Skylar Tibbits. The emergence of "4D printing" | video on TED.com, 4 2013.

[2] PG de Gennes. Entanglements and rubber elasticity. *CR Acad. Sci. Paris B*, 281:101, 1975.

[3] Jürgen Küpfer and Heino Finkelmann. Nematic liquid single crystal elastomers. *Die Makromolekulare Chemie, Rapid Communications*, 12(12):717–726, 1991.

[4] P. G. de Gennes, T. C. Chung, and A Petchsux. Réflexions sur un type de polymères nématiques. *C.R. Acad. Sci. Ser. B*, 281:101–103, 1975.

[5] Mark Warner and Eugene Michael Terentjev. *Liquid Crystal Elastomers*. Oxford University Press, October 2003.

[6] Pierre-Gilles de Gennes. Un muscle artificiel semi-rapide. *Comptes Rendus de l'Académie des Sciences - Series IIB - Mechanics-Physics-Chemistry-Astronomy*, 324(5):343–348, March 1997.

[7] Yue Zhao and Tomiki Ikeda. *Smart light-responsive materials: azobenzene-containing polymers and liquid crystals*. Wiley, Hoboken, N.J., 2009.

[8] Casper van Oosten. *Responsive Liquid Crystal Networks*. PhD thesis, Eindhoven University of Technology, 2009.

[9] Munenori Yamada, Mizuho Kondo, Jun-ichi Mamiya, Yanlei Yu, Motoi Kinoshita, Christopher J. Barrett, and Tomiki Ikeda. Photomobile polymer materials: Towards light-driven plastic motors. *Angewandte Chemie*, 120(27):5064–5066, 2008.

[10] Casper L. van Oosten, Cees W. M. Bastiaansen, and Dirk J. Broer. Printed artificial cilia from liquid-crystal network actuators modularly driven by light. *Nature Materials*, 8(8):677–682, August 2009.

[11] Scott J. Woltman, Gregory D. Jay, and Gregory P. Crawford. Liquid-crystal materials find a new order in biomedical applications. *Nature Materials*, 6(12):929–938, December 2007.

[12] H. Finkelmann, E. Nishikawa, G. G. Pereira, and M. Warner. A new opto-mechanical effect in solids. *Physical Review Letters*, 87(1):015501, June 2001.

[13] Yanlei Yu, Makoto Nakano, and Tomiki Ikeda. Photomechanics: Directed bending of a polymer film by light. *Nature*, 425(6954):145, 2003.

[14] D. Wiant, J. T. Gleeson, N. Éber, K. Fodor-Csorba, A. Jákli, and T. Tóth-Katona. Nonstandard electroconvection in a bent-core nematic liquid crystal. *Physical Review E*, 72(4):041712, October 2005.

[15] J. Harden, B. Mbanga, N. Éber, K. Fodor-Csorba, S. Sprunt, J. T. Gleeson, and A. Jákli. Giant flexoelectricity of bent-core nematic liquid crystals. *Physical Review Letters*, 97(15):157802, October 2006.

[16] W. Lehmann, H. Skupin, C. Tolksdorf, E. Gebhard, R. Zentel, P. Krüger, M. Lösche, and F. Kremer. Giant lateral electrostriction in ferroelectric liquid-crystalline elastomers. *Nature*, 410(6827):447–450, March 2001.

[17] Helmut R. Brand and Harald Pleiner. Piezoelectricity versus flexoelectricity and electrostriction in cholesteric and chiral smectic liquid-crystalline elastomers. *Die Makromolekulare Chemie, Rapid Communications*, 11(12):607–612, 1990.

[18] Kenneth D. Harris, Cees W. M. Bastiaansen, Johan Lub, and Dirk J. Broer. Self-assembled polymer films for controlled agent-driven motion. *Nano Letters*, 5(9):1857–1860, September 2005.

[19] Felix Weiss and Heino Finkelmann. Hexagonal lyotropic liquid crystalline hydrogels : Influence of uniaxial stress and ph value on the anisotropic swelling behavior. *Macromolecules*, 37(17):6587–6595, August 2004.

[20] Felix Kleinschmidt, Markus Hickl, Kay Saalwächter, Claudia Schmidt, and Heino Finkelmann. Lamellar liquid single crystal hydrogels : Synthesis and investigation of anisotropic water diffusion and swelling. *Macromolecules*, 38(23):9772–9782, November 2005.

[21] Jürgen Küpfer and Heino Finkelmann. Liquid crystal elastomers: Influence of the orientational distribution of the crosslinks on the phase behaviour and reorientation processes. *Macromolecular Chemistry and Physics*, 195(4):1353–1367, 1994.

[22] Isabel Kundler and Heino Finkelmann. Strain-induced director reorientation in nematic liquid single crystal elastomers. *Macromolecular Rapid Communications*, 16(9):679–686, 1995.

[23] Timothy J. White. Light to work transduction and shape memory in glassy, photoresponsive macromolecular systems:

Trends and opportunities. *Journal of Polymer Science Part B: Polymer Physics*, 50(13):877–880, 2012.

[24] Hongbo Wang, Kyung Min Lee, Timothy J. White, and William S. Oates. trans-cis and trans-cis-trans microstructure evolution of azobenzene liquid-crystal polymer networks. *Macromolecular Theory and Simulations*, page n/aï¿œn/a, 2011.

[25] C. D. Modes, M. Warner, C. L. van Oosten, and D. Corbett. Anisotropic response of glassy splay-bend and twist nematic cantilevers to light and heat. *Physical Review E*, 82(4):041111, October 2010.

[26] L. Jin, Y. Yan, and Y. Huo. A gradient model of light-induced bending in photochromic liquid crystal elastomer and its nonlinear behaviors. *International Journal of Non-Linear Mechanics*, 45(4):370–381, May 2010.

[27] Timothy J. White, Nelson V. Tabiryan, Svetlana V. Serak, Uladzimir A. Hrozhyk, Vincent P. Tondiglia, Hilmar Koerner, Richard A. Vaia, and Timothy J. Bunning. A high frequency photodriven polymer oscillator. *Soft Matter*, 4(9):1796, 2008.

[28] J. Cviklinski, A. R. Tajbakhsh, and E. M. Terentjev. Uv isomerisation in nematic elastomers as a route to photo-mechanical transducer. *The European Physical Journal E*, 9(1):427–434, December 2002.

[29] E. Mitscherlich. Ueber das stickstoffbenzid. *Annalen der Pharmacie*, 12(2-3):311–314, 1834.

[30] J.F. Rabek. *Progress in Photochemistry and Photophysics*. Photochemistry and Photophysics. CRC Press, 1992.

[31] Almeria Natansohn and Paul Rochon. Photoinduced motions in azo-containing polymers. *Chemical Reviews*, 102(11):4139–4176, November 2002.

[32] Valery Shibaev, Alexey Bobrovsky, and Natalia Boiko. Photoactive liquid crystalline polymer systems with light-controllable structure and optical properties. *Progress in Polymer Science*, 28(5):729–836, May 2003.

[33] H. M. Dhammika Bandara and Shawn C. Burdette. Photoisomerization in different classes of azobenzene. *Chemical Society Reviews*, 41(5):1809–1825, February 2012.

[34] Julia Bahrenburg, Katharina Röttger, Ron Siewertsen, Falk Renth, and Friedrich Temps. Sequential photoisomerisation dynamics of the push-pull azobenzene disperse red 1. *Photochemical & Photobiological Sciences*, 11(7):1210–1219, June 2012.

[35] T. Nägele, R. Hoche, W. Zinth, and J. Wachtveitl. Femtosecond photoisomerization of cis-azobenzene. *Chemical Physics Letters*, 272(5-6):489–495, July 1997.

[36] Thomas Schultz, Jason Quenneville, Benjamin Levine, Alessandro Toniolo, Todd J. Martínez, Stefan Lochbrunner, Michael Schmitt, James P. Shaffer, Marek Z. Zgierski, and Albert Stolow. Mechanism and dynamics of azobenzene photoisomerization. *Journal of the American Chemical Society*, 125(27):8098–8099, July 2003.

[37] ChuanXiang Sheng, Robert A. Norwood, Jiafu Wang, Jayan Thomas, Yinglan Wu, Zhiping Zheng, N. Tabirian, Diane M. Steeves, Brian R. Kimball, and N. Peyghambarian. Time-resolved studies of photoinduced birefringence in azobenzene dye-doped polymer films. *Applied Optics*, 47(28):5074–5077, October 2008.

[38] Igor K. Lednev, Tian-Qing Ye, Ronald E. Hester, and John N. Moore. Femtosecond time-resolved uv-visible absorption spectroscopy of trans-azobenzene in solution. *The Journal of Physical Chemistry*, 100(32):13338–13341, January 1996.

[39] Tatsuya Fujino and Tahei Tahara. Picosecond time-resolved raman study of trans-azobenzene. *J. Phys. Chem. A*, 104(18):4203–4210, 2000.

[40] Takeo Sasaki, Tomiki Ikeda, and Kunihiro Ichimura. Time-resolved observation of photochemical phase transition in polymer liquid crystals. *Macromolecules*, 25(14):3807–3811, July 1992.

[41] P. Pasini, G. Skačej, and C. Zannoni. A microscopic lattice model for liquid crystal elastomers. *Chemical Physics Letters*, 413(4-6):463–467, September 2005.

[42] A. DeSimone and L. Teresi. Elastic energies for nematic elastomers. *The European Physical Journal E*, 29(2):191–204, June 2009.

[43] W S Oates and H Wang. A new approach to modeling liquid crystal elastomers using phase field methods. *Modelling and Simulation in Materials Science and Engineering*, 17(6):064004, September 2009.

[44] Yoshiki Sawa, Kenji Urayama, Toshikazu Takigawa, Antonio DeSimone, and Luciano Teresi. Thermally driven giant bending of liquid crystal elastomer films with hybrid alignment. *Macromolecules*, 43(9):4362–4369, 2010.

[45] Alexey V. Lyulin, Muataz S. Al-Barwani, Michael P. Allen, Mark R. Wilson, Igor Neelov, and Nicholas K. Allsopp. Molecular dynamics simulation of main chain liquid crystalline polymers. *Macromolecules*, 31(14):4626–4634, July 1998.

[46] D. Corbett, C. L. van Oosten, and M. Warner. Nonlinear dynamics of optical absorption of intense beams. *Physical Review A*, 78(1):013823, July 2008.

[47] Casper L. van Oosten, Daniel Corbett, Dylan Davies, Mark Warner, Cees W. M. Bastiaansen, and Dirk J. Broer. Bending dynamics and directionality reversal in liquid crystal network photoactuators. *Macromolecules*, 41(22):8592–8596, November 2008.

[48] H Zeng, J Hua, JC Lavocat, C Parmeggianni, and D Wierma. High resolution 3d direct laser writing for liquid crystalline elastomer micro structures. *Advanced Materials*, 2013.

[49] Emel Sungur, Min-Hui Li, Gregory Taupier, Alex Boeglin, Michelangelo Romeo, Stï¿œphane Mery, Patrick Keller, and Kokou D. Dorkenoo. External stimulus driven variable-step grating in a nematic elastomer. *Optics Express*, 15:6784–6789, May 2007.

[50] Arno Zang and Ove Stephansson. *Stress Field of the Earth's Crust*. 2010.

[51] Martin Howard Sadd. *Elasticity theory, applications, and numerics*. Elsevier Butterworth Heinemann, Amsterdam; Oxford, 2005.

[52] S. P Timoshenko and J. N Goodier. *Theory of elasticity. 3rd ed.* Mcgraw-Hill, 1970.

[53] Yoshiki Sawa, Fangfu Ye, Kenji Urayama, Toshikazu Takigawa, Vianney Gimenez-Pinto, Robin L. B. Selinger, and Jonathan V. Selinger. Shape selection of twist-nematic-elastomer ribbons. *Proceedings of the National Academy of Sciences*, 108(16):6364–6368, April 2011. PMID: 21464276.

[54] Jeong Jae Wie, Kyung Min Lee, Matthew L. Smith, Richard A. Vaia, and Timothy J. White. Torsional mechanical responses in azobenzene functionalized liquid crystalline polymer networks. *Soft Matter*, 9(39):9303–9310, September 2013.

[55] C. L. van Oosten, K. D. Harris, C. W. M. Bastiaansen, and D. J. Broer. Glassy photomechanical liquid-crystal network actuators for microscale devices. *The European Physical Journal E*, 23(3):329–336, July 2007.

[56] John D Joannopoulos, Steven G Johnson, Joshua N Winn, and Robert D Meade. *Photonic crystals*. Princeton University Press, Princeton, 2008.

[57] James H. Strickler and Watt W. Webb. Three-dimensional optical data storage in refractive media by two-photon point excitation. *Optics Letters*, 16(22):1780–1782, November 1991.

[58] Dimitri A Parthenopoulos and Peter M Rentzepis. Three-dimensional optical storage memory. *Science*, 245(4920):843–845, August 1989. PMID: 17773360.

[59] George Witzgall, Rutger Vrijen, Eli Yablonovitch, Vinh Doan, and Benjamin J. Schwartz. Single-shot two-photon exposure of commercial photoresist for the production of three-dimensional structures. *Optics Letters*, 23(22):1745–1747, November 1998.

[60] R. A. Borisov, G. N. Dorojkina, N. I. Koroteev, V. M. Kozenkov, S. A. Magnitskii, D. V. Malakhov, A. V. Tarasishin, and A. M. Zheltikov. Fabrication of three-dimensional periodic microstructures by means of two-photon polymerization. *Applied Physics B*, 67(6):765–767, December 1998.

[61] Shoji Maruo, Osamu Nakamura, and Satoshi Kawata. Three-dimensional microfabrication with two-photon-absorbed photopolymerization. *Optics Letters*, 22(2):132–134, January 1997.

[62] En-Shinn Wu, James H. Strickler, W. R. Harrell, and Watt W. Webb. Two-photon lithography for microelectronic application. In *Proc. SPIE 1674, Optical/Laser Microlithography V*, volume 1674, pages 776–782, 1992.

[63] Brian H. Cumpston, Sundaravel P. Ananthavel, Stephen Barlow, Daniel L. Dyer, Jeffrey E. Ehrlich, Lael L. Erskine, Ahmed A. Heikal, Stephen M. Kuebler, I.-Y. Sandy Lee, Dianne McCord-Maughon, Jinqui Qin, Harald Rockel, Mariacristina Rumi, Xiang-Li Wu, Seth R. Marder, and Joseph W. Perry. Two-photon polymerization initiators for three-dimensional optical data storage and microfabrication. *Nature*, 398(6722):51–54, March 1999.

[64] W Denk, J H Strickler, and W W Webb. Two-photon laser scanning fluorescence microscopy. *Science (New York, N.Y.)*, 248(4951):73–76, April 1990. PMID: 2321027.

[65] Stefan W. Hell, Steffen Lindek, and Ernst H.K. Stelzer. Enhancing the axial resolution in far-field light microscopy: Two-photon 4Pi confocal fluorescence microscopy. *Journal of Modern Optics*, 41(4):675–681, 1994.

[66] Hong-Bo Sun and Satoshi Kawata. Two-photon photopolymerization and 3d lithographic microfabrication. In *NMR - 3D - Analysis - Photopolymerization*, number 170 in Apvances in Polymer Science, pages 169–273. Springer Berlin Heidelberg, January 2004.

[67] Nathan C. Lindquist, Prashant Nagpal, Kevin M. McPeak, David J. Norris, and Sang-Hyun Oh. Engineering metallic nanostructures for plasmonics and nanophotonics. *Reports on Progress in Physics*, 75(3):036501, March 2012.

[68] Maria Göppert-Mayer. Uber elementarakte mit zwei quantensprungen. *Annalen der Physik*, 401(3):273–294, 1931.

[69] W. Kaiser and C. G. B. Garrett. title = Two-Photon Excitation in CaF_2:Eu^{2+},. *Physical Review Letters*, 7(6):229–231, September 1961.

[70] P. M. Rentzepis and Yoh-Han Pao. LASER INDUCED OPTICAL SECOND HARMONIC GENERATION IN ORGANIC CRYSTALS. *Applied Physics Letters*, 5(8):156–158, October 1964.

[71] W. Martin McClain. Two-photon molecular spectroscopy. *Accounts of Chemical Research*, 7(5):129–135, May 1974.

[72] W L Peticolas. Multiphoton spectroscopy. *Annual Review of Physical Chemistry*, 18(1):233–260, 1967.

[73] Mariacristina Rumi, Stephen Barlow, Jing Wang, Joseph W. Perry, and Seth R. Marder. Two-photon absorbing materials and two-photon-induced chemistry. In Seth R. Marder and Kwang-Sup Lee, editors, *Photoresponsive Polymers I*, pages 1–95. Springer Berlin Heidelberg, Berlin, Heidelberg, 2008.

[74] Ata Saeed Rasha Mohamed Alla. *On the Control of Nematic Liquid Crystal Alignment*. PhD thesis, University of Gothenburg, May 2013.

[75] Dwight W Berreman. Solid surface shape and the alignment of an adjacent nematic liquid crystal. *Physical review letters*, 28:1683–1686, 1972.

[76] Martin Schadt, Hubert Seiberle, and Andreas Schuster. Optical patterning of multi-domain liquid-crystal. *Nature*, 381:16, 1996.

[77] Martin Schadt, Klaus Schmitt, Vladimir Kozinkov, and Vladimir Chigrinov. Surface-induced parallel alignment of liquid crystals by linearly polymerized photopolymers. *Japanese Journal of Applied Physics*, 31(part 1):2155–2164, 1992.

[78] Hong Yang, Axel Buguin, Jean-Marie Taulemesse, Kosuke Kaneko, Stéphane Méry, Anne Bergeret, and Patrick Keller. Micron-sized main-chain liquid crystalline elastomer actuators with ultralarge amplitude contractions. *Journal of the American Chemical Society*, 131(41):15000–15004, October 2009.

[79] Jawad Naciri, Amritha Srinivasan, Hong Jeon, Nikolay Nikolov, Patrick Keller, and Banahalli R. Ratna. Nematic elastomer fiber actuator. *Macromolecules*, 36(22):8499–8505, November 2003.

[80] Leonardo De Boni, Lino Misoguti, Sergio C. Zï¿œlio, and Cleber R. Mendonï¿œa. Degenerate two-photon absorption spectra in azoaromatic compounds. *ChemPhysChem*, 6(6):1121–1125, June 2005.

[81] K. M. Dyumaev, A. A. Manenkov, A. P. Maslyukov, G. A. Matyushin, V. S. Nechitailo, and A. M. Prokhorov. Dyes in modified polymers: problems of photostability and conversion efficiency at high intensities. *Journal of the Optical Society of America B*, 9(1):143–151, January 1992.

[82] Munenori Yamada, Mizuho Kondo, Ryo Miyasato, Yumiko Naka, Jun-ichi Mamiya, Motoi Kinoshita, Atsushi Shishido, Yanlei Yu, Christopher J. Barrett, and Tomiki Ikeda. Photomobile polymer materials-various three-dimensional movements. *Journal of Materials Chemistry*, 19(1):60–62, December 2008.

[83] Maika Moua, Ryan R. Kohlmeyer, and Jian Chen. Wavelength-selective, IR light-driven hinges based on liquid crystalline elastomer composites. *Angewandte Chemie*, pages na–na, 2013.

[84] Taiki Yoshino, Mizuho Kondo, Jun-ichi Mamiya, Motoi Kinoshita, Yanlei Yu, and Tomiki Ikeda. Three-dimensional photomobility of crosslinked azobenzene liquid-crystalline polymer fibers. *Advanced Materials*, 22(12):1361–1363, 2010.

[85] Axel Buguin, Min-Hui Li, Pascal Silberzan, Benoit Ladoux, and Patrick Keller. Micro-actuators: When artificial muscles made of nematic liquid crystal elastomers meet soft lithography. *Journal of the American Chemical Society*, 128(4):1088–1089, February 2006.

[86] Nï¿œria Torras, Kirill E. Zinoviev, Jaume Esteve, and Antoni Sï¿œnchez-Ferrer. Liquid-crystalline elastomer micropillar array for haptic actuation. *Journal of Materials Chemistry C*, 1(34):5183–5190, August 2013.

[87] Zeng Yan, Xinming Ji, Wei Wu, Jia Wei, and Yanlei Yu. Light-switchable behavior of a microarray of azobenzene liquid crystal polymer induced by photodeformation. *Macromolecular Rapid Communications*, 33(16):1362–1367, 2012.

[88] Johannes Jacobus Laar. *Sechs vorträge über das thermodynamische potential und seine anwendungen auf chemische und physikalische gleichgewichtsprobleme*. F. Vieweg und sohn, 1906.

[89] JJ Van Laar. Einiges über dampfspannungen von einheitlichen stoffen und von binären gemischen. dampfdrucke von quecksilber und graphit. *Zeitschrift für anorganische und allgemeine Chemie*, 171(1):42–60, 1928.

[90] Nam-Trung Nguyen and Steven T. Wereley. *Fundamentals and Applications of Microfluidics*. Artech House (Integrated Microsystems Series), 2006.

[91] R. W. Fox and A. T. McDonald. *Introduction to Fluid Mechanics*. New York: Wiley, 1999.

[92] G. K. Batchelor. *An Introduction to Fluid Dynamics*. Cambridge University Press, 2000.

[93] John Happel and Howard Brenner. *Low Reynolds number hydrodynamics: with special applications to particulate media*, volume 1. Springer, 1965.

[94] L. D Landau and E. M Lifshitz. *Fluid mechanics*. Elsevier/Butterworth-Heinemann, Amsterdam, 2004.

[95] Eric Lauga, Michael P Brenner, and Howard A Stone. Microfluidics: The no-slip boundary condition. *cond-mat/0501557*, January 2005. Chapter 19 in: Handbook of Experimental Fluid Dynamics, C. Tropea, A. Yarin, J. F. Foss (Eds.), Springer, 2007.

[96] J. Gray and G. J. Hancock. The propulsion of sea-urchin spermatozoa. *Journal of Experimental Biology*, 32(4):802–814, December 1955.

[97] C Brennen and H Winet. Fluid mechanics of propulsion by cilia and flagella. *Annual Review of Fluid Mechanics*, 9(1):339–398, 1977.

[98] James Lighthill. Flagellar hydrodynamics. *SIAM Review*, 18(2):161–230, April 1976.

[99] Geoffrey Taylor. Analysis of the swimming of microscopic organisms. *Proceedings of the Royal Society of London. Series A. Mathematical and Physical Sciences*, 209(1099):447–461, November 1951.

[100] E. M. Purcell. Life at low reynolds number. *AIP Conference Proceedings*, 28(1):49–64, December 1976.

[101] J. E. Avron and O. Raz. A geometric theory of swimming: Purcell's swimmer and its symmetrized cousin. *New Journal of Physics*, 10(6):063016, June 2008.

[102] L. E. Becker, S. A. Koehler, and H. A. Stone. On self-propulsion of micro-machines at low reynolds number: Purcell's three-link swimmer. *Journal of Fluid Mechanics*, 490:15–35, 2003.

[103] Daniel Tam and A. E. Hosoi. Optimal stroke patterns for purcell's three-link swimmer. *Physical Review Letters*, 98(6):068105, February 2007.

[104] Linda Turner, William S. Ryu, and Howard C. Berg. Real-time imaging of fluorescent flagellar filaments. *Journal of Bacteriology*, 182(10):2793–2801, May 2000. PMID: 10781548.

[105] Rachel Patton McCord, John N. Yukich, and Karen K. Bernd. Analysis of force generation during flagellar assembly through optical trapping of free-swimming chlamydomonas reinhardtii. *Cell Motility and the Cytoskeleton*, 61(3):137–144, 2005.

[106] Tadir Y, Wright Wh, Vafa O, Ord T, Asch Rh, and Berns Mw. Micromanipulation of sperm by a laser generated optical trap. *Fertility and sterility*, 52(5):870–873, November 1989. PMID: 2680630.

[107] Suddhashil Chattopadhyay, Radu Moldovan, Chuck Yeung, and X. L. Wu. Swimming efficiency of bacterium escherichiacoli. *Proceedings of the National Academy of Sciences*, 103(37):13712–13717, September 2006. PMID: 16954194.

[108] Eric Lauga and Thomas R Powers. The hydrodynamics of swimming microorganisms. *Reports on Progress in Physics*, 72(9):096601, September 2009.

[109] Frederick C Neidhardt, John L Ingraham, and Moselio Schaechter. *Physiology of the bacterial cell: a molecular approach*. Sinauer Associates, Sunderland, 1990.

[110] Graeme Lowe, Markus Meister, and Howard C. Berg. Rapid rotation of flagellar bundles in swimming bacteria. *Nature*, 325(6105):637–640, February 1987.

[111] Guanglai Li and Jay X Tang. Low flagellar motor torque and high swimming efficiency of caulobacter crescentus swarmer cells. *Biophysical journal*, 91(7):2726–2734, October 2006. PMID: 16844761.

[112] Erik Gauger. Hydrodynamics of nanomachines in biology, 2005.

[113] Ingmar H. Riedel, Karsten Kruse, and Jonathon Howard. A self-organized vortex array of hydrodynamically entrained sperm cells. *Science*, 309(5732):300–303, July 2005. PMID: 16002619.

[114] Shay Gueron and Konstantin Levit-Gurevich. Energetic considerations of ciliary beating and the advantage of metachronal coordination. *Proceedings of the National Academy of Science*, 96:12240–12245, October 1999.

[115] Boris Guirao and Jean-François Joanny. Spontaneous creation of macroscopic flow and metachronal waves in an array of cilia. *Biophysical Journal*, 92(6):1900–1917, March 2007.

[116] Jens Elgeti. *Sperm and Cilia Dynamics*. text.thesis.doctoral, Universität zu Köln, 2006.

[117] Nariya Uchida and Ramin Golestanian. Synchronization and collective dynamics in a carpet of microfluidic rotors. *Physical Review Letters*, 104(17):178103, April 2010.

[118] David F. Katz. On the propulsion of micro-organisms near solid boundaries. *Journal of Fluid Mechanics*, 64(01):33–49, 1974.

[119] A. J. Reynolds. The swimming of minute organisms. *Journal of Fluid Mechanics*, 23(02):241–260, 1965.

[120] Eric Lauga, Willow R. DiLuzio, George M. Whitesides, and Howard A. Stone. Swimming in circles: Motion of bacteria near solid boundaries. *Biophysical Journal*, 90(2):400–412, January 2006.

[121] Willow R. DiLuzio, Linda Turner, Michael Mayer, Piotr Garstecki, Douglas B. Weibel, Howard C. Berg, and George M. Whitesides. Escherichia coli swim on the right-hand side. *Nature*, 435(7046):1271–1274, June 2005.

[122] Jens Elgeti, U. Benjamin Kaupp, and Gerhard Gompper. Hydrodynamics of sperm cells near surfaces. *Biophysical Journal*, 99(4):1018–1026, August 2010.

[123] D. M. Woolley. Motility of spermatozoa at surfaces. *Reproduction*, 126(2):259–270, August 2003. PMID: 12887282.

[124] Peer Fischer and Ambarish Ghosh. Magnetically actuated propulsion at low reynolds numbers: towards nanoscale control. *Nanoscale*, 3:557–563, 2011.

[125] Samuel Sanchez, Alexander A. Solovev, Stefan M. Harazim, and Oliver G. Schmidt. Microbots swimming in the flowing streams of microfluidic channels. *Journal of the American Chemical Society*, 133(4):701–703, February 2011.

[126] Remi Dreyfus, Jean Baudry, Marcus L. Roper, Marc Fermigier, Howard A. Stone, and Jerome Bibette. Microscopic artificial swimmers. *Nature*, 437(7060):862–865, October 2005.

[127] Li Zhang, Jake J. Abbott, Lixin Dong, Bradley E. Kratochvil, Dominik Bell, and Bradley J. Nelson. Artificial bacterial flagella: Fabrication and magnetic control. *Applied Physics Letters*, 94(6):064107, February 2009.

[128] Soichiro Tottori, Li Zhang, Famin Qiu, Krzysztof K. Krawczyk, Alfredo Franco-Obregó, and Bradley J. Nelson. Magnetic helical micromachines: Fabrication, controlled swimming and cargo transport. *Advanced Materials*, 24(6):811–816, 2012.

[129] Ambarish Ghosh and Peer Fischer. Controlled propulsion of artificial magnetic nanostructured propellers. *Nano Letters*, 9(6):2243–2245, June 2009.

[130] M. Sitti. Micro- and nano-scale robotics. In *American Control Conference, 2004. Proceedings of the 2004*, volume 1, pages 1–8 vol.1, 2004.

[131] B.R. Donald, C.G. Levey, C.D. McGray, I. Paprotny, and D. Rus. An untethered, electrostatic, globally controllable MEMS microrobot. *Microelectromechanical Systems, Journal of*, 15(1):1–15, 2006.

[132] Chytra Pawashe, Steven Floyd, and Metin Sitti. Modeling and experimental characterization of an untethered magnetic microrobot. *The International Journal of Robotics Research*, 28(8):1077–1094, August 2009.

[133] Svetlana Serak, Nelson Tabiryan, Rafael Vergara, Timothy J. White, Richard A. Vaia, and Timothy J. Bunning. Liquid crystalline polymer cantilever oscillators fueled by light. *Soft Matter*, 6(4):779–783, February 2010.

[134] Ahmet Fatih Tabak. *Simulation based experiments of traveling-plane-wave-actuator miropumps and microswimmers*. Thesis, 2007.

[135] S. R. Quake. From micro- to nanofabrication with soft materials. *Science*, 290(5496):1536–1540, November 2000.

[136] Marc A. Unger, Hou-Pu Chou, Todd Thorsen, Axel Scherer, and Stephen R. Quake. Monolithic microfabricated valves and pumps by multilayer soft lithography. *Science*, 288(5463):113–116, April 2000. PMID: 10753110.

[137] Younan Xia and George M. Whitesides. Soft lithography. *Angewandte Chemie International Edition*, 37(5):550–575, 1998.

[138] Mingtao Li, Jian Wang, Lei Zhuang, and Stephen Y. Chou. Fabrication of circular optical structures with a 20 nm minimum feature size using nanoimprint lithography. *Applied Physics Letters*, 76(6):673–675, February 2000.

[139] Byron D. Gates, Qiaobing Xu, Michael Stewart, Declan Ryan, C. Grant Willson, and George M. Whitesides. New approaches to nanofabrication : Molding, printing, and other techniques. *Chemical Reviews*, 105(4):1171–1196, April 2005.

[140] R. Audino, G. Destefanis, F. Gorgellino, E. Pollino, and S. Tamagno. Interface behavior evaluation in gold/chromium, gold/titanium and gold/palladium/titanium thin films by means of resistivity and stylus measurements. *Thin Solid Films*, 36:343–347, 1976.

[141] Maria Nordström, Alicia Johansson, Encarnacion Sánchez Noguerón, Bjarne Clausen, Montserrat Calleja, and Anja Boisen. Investigation of the bond strength between the photo-sensitive polymer SU-8 and gold. *Microelectronic Engineering*, 78-79:152–157, March 2005.

[142] Ronald P. Andres, Jeffery D. Bielefeld, Jason I. Henderson, David B. Janes, Venkat R. Kolagunta, Clifford P. Kubiak, William J. Mahoney, and Richard G. Osifchin. Self-assembly of a two-dimensional superlattice of molecularly linked metal clusters. *Science*, 273(5282):1690–1693, September 1996.

[143] Kunihiro Ichimura. Photoalignment of liquid-crystal systems. *Chemical Reviews*, 100(5):1847–1874, May 2000.

[144] Jeffrey N. Anker, W. Paige Hall, Olga Lyandres, Nilam C. Shah, Jing Zhao, and Richard P. Van Duyne. Biosensing with plasmonic nanosensors. *Nature Materials*, 7(6):442–453, June 2008.

[145] E. C. Le Ru, P. G. Etchegoin, J. Grand, N. Félidj, J. Aubard, and G. Lévi. Mechanisms of spectral profile modification in surface-enhanced fluorescence. *The Journal of Physical Chemistry C*, 111(44):16076–16079, November 2007.

[146] Fumin Huang and Jeremy J. Baumberg. Actively tuned plasmons on elastomerically driven au nanoparticle dimers. *Nano Letters*, 10(5):1787–1792, May 2010.

[147] Mathias Kolle, Bo Zheng, Nicholas Gibbons, Jeremy J. Baumberg, and Ullrich Steiner. Stretch-tuneable dielectric mirrors and optical microcavities. *Optics Express*, 18(5):4356–4364, March 2010.

[148] Andreas Kontogeorgos, David R. E. Snoswell, Chris E. Finlayson, Jeremy J. Baumberg, Peter Spahn, and G. P. Hellmann.

Inducing symmetry breaking in nanostructures: Anisotropic stretch-tuning photonic crystals. *Physical Review Letters*, 105(23):233909, December 2010.

[149] Yann R. Leroux, Jean Christophe Lacroix, Kathleen I. Chane-Ching, Claire Fave, Nordin Félidj, Georges Lévi, Jean Aubard, Joachim R. Krenn, and Andreas Hohenau. Conducting polymer electrochemical switching as an easy means for designing active plasmonic devices. *Journal of the American Chemical Society*, 127(46):16022–16023, November 2005.

[150] Johann Berthelot, Alexandre Bouhelier, Caijin Huang, Jérémie Margueritat, Gérard Colas-des Francs, Eric Finot, Jean-Claude Weeber, Alain Dereux, Sergei Kostcheev, Hicham Ibn El Ahrach, Anne-Laure Baudrion, Jérome Plain, Renaud Bachelot, Pascal Royer, and Gary P. Wiederrecht. Tuning of an optical dimer nanoantenna by electrically controlling its load impedance. *Nano Letters*, 9(11):3914–3921, November 2009.

[151] Vincent K. S. Hsiao, Yue Bing Zheng, Bala Krishna Juluri, and Tony Jun Huang. Light-driven plasmonic switches based on au nanodisk arrays and photoresponsive liquid crystals. *Advanced Materials*, 20(18):3528–3532, 2008.

[152] A. V. Krasavin, A. V. Zayats, and N. I. Zheludev. Active control of surface plasmon-polariton waves. *Journal of Optics A: Pure and Applied Optics*, 7(2):S85, February 2005.

[153] Francesca Intonti, Silvia Vignolini, Francesco Riboli, Margherita Zani, Diederik S. Wiersma, Laurent Balet, Lianhe H. Li, Marco Francardi, Annamaria Gerardino, Andrea Fiore, and Massimo Gurioli. Tuning of photonic crystal cavities by controlled removal of locally infiltrated water. *Applied Physics Letters*, 95(17):173112, October 2009.

[154] Hélène Gehan, Claire Mangeney, Jean Aubard, Georges Lévi, Andreas Hohenau, Joachim R. Krenn, Emmanuelle Lacaze, and Nordin Félidj. Design and optical properties of active polymer-coated plasmonic nanostructures. *The Journal of Physical Chemistry Letters*, 2(8):926–931, April 2011.

[155] E. Popov. *Gratings: Theory and Numeric Applications*. Popov, Institut Fresnel, 2012.

[156] R.W. Wood. XLII. on a remarkable case of uneven distribution of light in a diffraction grating spectrum. *Philosophical Magazine Series 6*, 4(21):396–402, 1902.

[157] Lord Rayleigh. Note on the remarkable case of diffraction spectra described by prof. wood. *Philosophical Magazine Series 6*, 14(79):60–65, 1907.

[158] Lord Rayleigh. On the dynamical theory of gratings. *Proceedings of the Royal Society of London. Series A*, 79(532):399–416, August 1907.

[159] U. Fano. The theory of anomalous diffraction gratings and of quasi-stationary waves on metallic surfaces (sommerfeld's waves). *Journal of the Optical Society of America*, 31(3):213–222, March 1941.

[160] A. Hessel and A. A. Oliner. A new theory of wood's anomalies on optical gratings. *Applied Optics*, 4(10):1275–1297, October 1965.

[161] Ye-Yung Teng and Edward A. Stern. Plasma radiation from metal grating surfaces. *Physical Review Letters*, 19(9):511–514, August 1967.

[162] R. H. Ritchie, E. T. Arakawa, J. J. Cowan, and R. N. Hamm. Surface-plasmon resonance effect in grating diffraction. *Physical Review Letters*, 21(22):1530–1533, November 1968.

[163] Daniel Maystre. Theory of wood's anomalies. In Stefan Enoch and Nicolas Bonod, editors, *Plasmonics*, number 167 in Springer Series in Optical Sciences, pages 39–83. Springer Berlin Heidelberg, January 2012.

[164] E. M. Terentjev P. Bladon. Deformation-induced orientational transitions in liquid crystals elastomer. *J. Phys. II France*, 4:75–91, 1993.

[165] G. R. Mitchell, F. J. Davis, and W. Guo. Strain-induced transitions in liquid-crystal elastomers. *Physical Review Letters*, 71(18):2947–2950, November 1993.

COLOPHON

This document was typeset with LaTeX using the typographical look-and-feel `classicthesis` developed by André Miede, and has slightly been modified by the author. The template is available for both LaTeX and LyX:

http://code.google.com/p/classicthesis/

Final Version as of December 29, 2013 (`classicthesis` version 1.3).

Hermann Zapf's Palatino and Euler type faces (Type 1 PostScript fonts URW Palladio L and FPL) are used. The "typewriter" text is typeset in Bera Mono, originally developed by Bitstream, Inc. as "Bitstream Vera". (Type 1 PostScript fonts were made available by Malte Rosenau and Ulrich Dirr.)